UNIVERSITY OF PARDUBICE

FACULTY OF CHEMICAL TECHNOLOGY

Doctoral Dissertation

2018 **Ing. Abraham Kabutey**

UNIVERSITY OF PARDUBICE
FACULTY OF CHEMICAL TECHNOLOGY

ENVIRONMENTAL ASPECTS OF SELECTED ELECTROCHEMICAL AND AGGLOMERATION INTERACTIONS IN SOLUTIONS

Ing. Abraham Kabutey

Doctoral Dissertation
2018

UNIVERZITA PARDUBICE
FAKULTA CHEMICKO-TECHNOLOGICKÁ

ENVIRONMENTÁLNÍ ASPEKTY VYBRANÝCH ELEKTROCHEMICKÝCH A AGLOMERAČNÍCH INTERAKCÍ V ROZTOCÍCH

Ing. Abraham Kabutey

Dizertační práce
2018

Prohlašuji:
Tuto práci jsem vypracoval samostatně. Veškeré literární prameny a informace, které jsem v práci využil, jsou uvedeny v seznamu použité literatury.
Byl jsem seznámen s tím, že se na moji práci vztahují práva a povinnosti vyplývající ze zákona č. 121/2000 Sb., autorský zákon, zejména se skutečností, že Univerzita Pardubice má právo na uzavření licenční smlouvy o užití této práce jako školního díla podle § 60 odst. 1 autorského zákona, a s tím, že pokud dojde k užití této práce mnou nebo bude poskytnuta licence o užití jinému subjektu, je Univerzita Pardubice oprávněna ode mne požadovat přiměřený příspěvek na úhradu nákladů, které na vytvoření díla vynaložila, a to podle okolností až do jejich skutečné výše.
Beru na vědomí, že v souladu s § 47b zákona č. 111/1998 Sb., o vysokých školách a o změně a doplnění dalších zákonů (zákon o vysokých školách), ve znění pozdějších předpisů, a směrnicí Univerzity Pardubice č. 9/2012, bude práce zveřejněna v Univerzitní knihovně a prostřednictvím Digitální knihovny Univerzity Pardubice.

V Pardubicích dne

Ing. Abraham Kabutey

ACKNOWLEDGEMENT

There is a time for everything and a season for every activity under the heavens. For no matter how many promises God has made, they are "Yes" in Christ. And so through him, the "Amen" is spoken by us to the glory of God (Ecclesiastes 3:1; 2 Corinthians 1:20).

First and foremost, I thank God the Father, the Son Jesus Christ, and the Holy Spirit – in one true God; for today and everything that I have achieved.

Special thanks and sincere appreciation go to my Supervisor, Assoc. Prof. Dr. Ing. Ladislav Novotný, Dr.Sc., Department of Environmental Protection, Faculty of Chemical Technology, University of Pardubice, for his immense contribution. In fact, this doctoral dissertation would not have been completed without his valuable assistance, support and guidance.

I would like to also thank prof. Ing. Petr Kalenda, CSc. (Dean of Faculty of Chemical Technology) and prof. Ing. Petr Mikulášek, CSc. (Head of Institute of Environmental and Chemical Engineering, Faculty of Chemical Technology), University of Pardubice; for the opportunity to complete my study programme and financial support.

Finally, I would like to thank my family and friends for their love, prayers, encouragement and financial support.

ANNOTATION

The first section of the work focused on further use, testing and new applications of the recently proposed new possibilities of preparation, arrangement and utilization of potentiometric interactions of amalgam electrodes, especially testing changes of potential responses of silver amalgam electrodes within the ion-exchange treatment of water as well as utilization of potentiometric signal of the zinc amalgam electrode for the detection of concentration changes of zinc sulphate. The second part of the work aimed attention at the special use or testing of the recently described (Novotny) relations for fitting or evaluating adsorption, electrosorption and agglomeration data. In view of this, the fitting kinetics of silver nanoparticles agglomeration in relation to time was described using appropriate statistical methods like the forward stepwise regression analysis.

KEYWORDS

water treatment, ion exchangers, potentiometry, amalgam electrodes, nanoparticles, agglomeration

TITUL

Environmentální aspekty vybraných elektrochemických a aglomeračních interakcí v roztocích

ANOTACE

První část práce byla zaměřena na využití, testování a nové aplikace nedávno navržených nových možností přípravy, uspořádání a využití potenciometrických interakcí amalgámových elektrod, zejména na testování změn potenciálové odezvy stříbrných amalgámových elektrod během iontoměničové úpravy vody a dále na využití potenciometrického signálu zinkové amalgámové elektrody pro detekci koncentračních změn roztoků síranu zinečnatého. Druhá část práce byla věnována speciálnímu užití nebo testování nedávno popsaných (Novotného) vztahů, například pro prokládání nebo vyhodnocování adsorpčních, elektrosorpčních a aglomeračních dat. Tímto způsobem bylo provedeno prokládání kinetiky časově závislé aglomerace nanočástic stříbra, přičemž byly použity statistické metody jako například tzv. postupná regresní analýza.

KLÍČOVÁ SLOVA

úprava vody, iontoměniče, potenciometrie, amalgámové elektrody, nanočástice, aglomerace

TABLE OF CONTENTS

LIST OF FIGURES

LIST OF TABLES

LIST OF ABBREVIATIONS AND SYMBOLS

AAS	-	Atomic Absorption Spectroscopy
AE	-	Amalgam Electrode
AFM	-	Atomic Force Microscopy
Ag/AgCl	-	Silver/Silver Chloride
Ag^+	-	Silver (I) ion
$AgNO_3$	-	Silver nitrate
AOX	-	Absorbable Organically bound Halogens
C	-	Carbon
$C_6H_{12}O_6$	-	Glucose
Ca	-	Calcium
$CaCl_2$	-	Calcium Chloride
CCDT	-	Controlled Convection Drop-Time Technique
Cd	-	Cadmium
Cl^-	-	Chloride ion
Cl	-	Chlorine
CSV	-	Cathodic Stripping Voltammetry
CuAE	-	Copper Amalgam Electrode
D	-	Nanoparticles or sub-micro-particles diameter
D_H	-	Hydrodynamic diameters
DLS	-	Dynamic Light Scattering
DNA	-	Deoxyribonucleic acid
EPA	-	Environmental Protection Agency
H^+	-	Hydrogen ion (proton)
H_2	-	Hydrogen gas
Hg	-	Mercury
$Hg_2(S_2O_3)$	-	Mercury (I) thiosulphate
Hg^{2+}	-	Mercury (II) (mercuric) ion
Hg_2^{2+}	-	Mercury (I) (mercuric) ion
Hg_2Cl_2	-	Mercury (I) Chloride or Mercurous Chloride
ICP-MS	-	Inductive Coupled Plasma-Mass Spectroscopy
ICP-OES	-	Inductive Coupled Plasma-Optical Emission Spectroscopy
ISE	-	Ion Selective Electrode

K^+	-	Potassium ion
KCl	-	Potassium Chloride
KNO_3	-	Potassium Nitrate
Mg	-	Magnesium
$MgSO_4$	-	Magnesium Sulphate
Na^+	-	Sodium ion
$Na_2S_2O_3$	-	Sodium thiosulphate
$NaHCO_3$	-	Sodium hydrogen carbonate/Sodium bicarbonate
NO_3^-	-	Nitrate ion
nm	-	Nanometres
μM	-	$\mu mol \cdot L^{-1}$
pH	-	Measure of hydrogen ion activity in aqueous solution
AgAE	-	Silver Amalgam Electrode
PT	-	Plastic Tip
SCE	-	Sodium Chloride Electrode
SE	-	Silver Electrode
SHS	-	Standard Hydrogen Electrode
SiO_2	-	Silicon dioxide
SO_4^{2-}	-	Sulphate ion
VA (V4)	-	Anion exchange column
VD (V1)	-	After decantation
VK (V3)	-	Cation exchange column
VKF (V2)	-	Coagulation and filtration
VZ (5)	-	Water Reservoir
Zn	-	Zinc
Zn^{2+}	-	Zinc ion
ZnAE	-	Zinc Amalgam Electrode
ZnE	-	Zinc Electrode
$ZnSO_4$	-	Zinc Sulphate
c	-	Concentration
c_i	-	Input concentration of samples/solution
c_{out}	-	Output concentration of samples/solution
c_{ox}	-	Concentration of oxidation form
c_{red}	-	Concentration of reduction form

γ	-	Surface tension of mercury
exp	-	Exponential function
i	-	Current density
A	-	Area
nAg	-	Silver nanoparticles
i_k, i_a	-	Partial cathodic and anodic current densities
v	-	Scan rate
Vi	-	Water samples
$\frac{d}{dt}$	-	Differential operator applied to a function
E_{cell}	-	Potential of the electrochemical cell
E_a	-	Anodic potential
E_c	-	Cathodic potential
E	-	Measured potential
E^0	-	Standard electrode potential
R	-	Gas constant
T	-	Absolute temperature
$^{\circ}C$	-	Celsius
n	-	Number of electrons involved in the electrode reaction
F	-	Faraday constant
ln	-	Natural logarithm
Q	-	Reaction quotient (a_{ox}/a_{red} denoting activities of ($_{ox}$) oxidation or ($_{red}$) reduction forms)
K, k, k_1, q	-	Constants
a	-	Activity
a_{H^+}	-	Activity of hydrogen ion
$a_{H^+_{rozt}}$	-	Hydrogen activity in solutions
$a_{H^+_{sklo}}$	-	Hydrogen activity in glass
$a_{Na^+_{rozt}}$	-	Sodium activity in solutions
$c_{Na^+_{sklo}}$	-	Sodium activity in glass
f	-	Correction coefficient for the non-Nernst slope
a_i ,$a_1$and a_j,a_2	-	Activities of the ionic analytes and interfering ions
z_i, z and z_j	-	Valence of the ionic analytes and the interfering ions

ISE	-	Ion Selective Electrodes
$k_{i,j}^{pot}, k_{12}^{pot}$	-	Selectivity coefficients for ion 1 (*i*) against ion 2 (*j*)
Ox, Red	-	Oxidized and reduced form of the substance
k_k, k_a	-	Cathodic and anodic rate constants
N_{ox}, N_{red}	-	Number of moles of electroactive material
c_{ox}, c_{red}	-	Concentrations of the oxidized and reduced forms at the surface of the electrode
k_k^0, k_a^0	-	Standard values of the rate constants of the measured potential
α	-	Charge transfer coefficient
$\Delta G_{red,0}$	-	Standard free enthalpy of reduction
$\Gamma (\Gamma_{max})$	-	Relative surface excess (its maximum value) i.e. the surface concentration
t, t_0	-	Time(s)
$t_i – t_1$, Δt_i, Δt_1	-	Time differences
D_0, D_1, D_{inf}	-	Diameters
y, Δy_i	-	Linearization terms/dependent variables
R	-	Correlation coefficient
R^2	-	Squared correlation coefficient
$\Delta D_i, \Delta D_{inf}$	-	Differences of diameters
D/D_m	-	Rate of diameters
V/V_m	-	Rate of volumes
θ	-	Relative surface coverage
μ	-	Chemical potential
$\sum_{i=0}^{n} C_i t^{i+1}$	-	Sum of polynomial terms
$c(t) = c_0$	-	Concentration at t = 0
N	-	Number of samples
b*	-	Standardized regression coefficients
b	-	Raw regression coefficeints
t-value	-	Measures the size difference relative to the variation in data
p-value	-	Significance level used for testing a statistical hypothesis
α	-	Significance level
F-value	-	Value of the F test used in combination with the p-value to measure significance

INTRODUCTION

Mutual interactions between different objects are part of the events occurring in the environment and living organisms. These interactions form the natural basis of the various detection, analytical or diagnostic methods and methods of preparation of substances or technological processes. Electrochemical methods or methods of preparation, study and application of systems using particle agglomerates are also part of these processes. Recently, nanochemistry has grown tremendously contributing to the understanding of the heterogeneous processes involving atomic and molecular structures or aggregates that may be desirable or undesirable from an environmental and health point of view.

In terms of electrochemistry[1-4] and its application in the environment and environmental protection, nanochemistry is a field being used widely. It encompasses processes that are part of the technological production and modification[4-8] of different substances, cleaning and separation processes, or control and diagnostic procedures. In addition, it is used in the chemical, biochemical and other reactions, the effect of electric voltage, electric current, electric charges or even electrochemical properties of the substances, relevant energy fields, etc. Electrochemistry significantly contributes[1-10] to electro-separation (electro-analytical, -deposition, -coagulation, -degradation) and other processes, purification processes of waters and aqueous solutions, etc., on the accompanying or separate applications of electro-analysis, -indication, -detection, -diagnostics, -signaling, etc. It is also used as a component or in combination with other methods such as filtration, nanofiltration, osmosis, chromatographic detection, optical and other techniques.

The objectives of the work, associated with environmental and health protection, comprised of two sections. The first section focused on further use, testing and new applications of the recently[10-14] proposed new possibilities[14-17,19-21,74] of preparation, arrangement and utilization of amalgam electrodes, their multicomponent potentiometric interactions (influenced by interfacial or limited amperometric processes). As a result of this, testing changes of potential responses of silver amalgam electrode (AgAE) within the ion-exchange treatment of water (after its technological pre-treatment) as well as utilization of potentiometric signal of the zinc amalgam electrode (ZnAE) for the detection of concentration changes of zinc sulphate by nanofiltration were investigated, using the potentiometric arrangements applicable under common operating conditions. The second part of the work aimed attention at the special use or testing of the recently described (Novotny) relations[4,9,10,22,23,73] for fitting or evaluating

adsorption, electrosorption and agglomeration data. In view of this, the fitting kinetics of silver nanoparticles (nAg) agglomeration with time (based on some similarities with fitting electrosorption data of sodium thiosulphate) was described using appropriate statistical methods like the stepwise regression analysis.

1. BRIEF INTRODUCTORY NOTES ON DIFFERENT TYPES OF ELECTRODE INTERACTIONS AND ARRANGEMENTS

1.1 Selected areas of electrochemistry

1.1.1 Electroanalytical techniques

Electroanalytical techniques or electrochemical methods[1-4] are mainly grouped into static and dynamic methods. In static methods, no current passes through the electrodes and the concentrations of species in the electrochemical cell remain unchanged or static. Potentiometry is one of the most important quantitative electrochemical methods under static conditions. The largest group of electrochemical techniques is the dynamic methods in which current flows and concentrations change as the result of a redox reaction (Figure 1). However, it is important to note that dynamic methods are subdivided into controlling the current or potential. Regardless of the kind of electrochemical method under consideration, there are only three experimental designs namely measuring the potential under static conditions of no current flow, measuring the potential while controlling the current and measuring the current while controlling the potential.

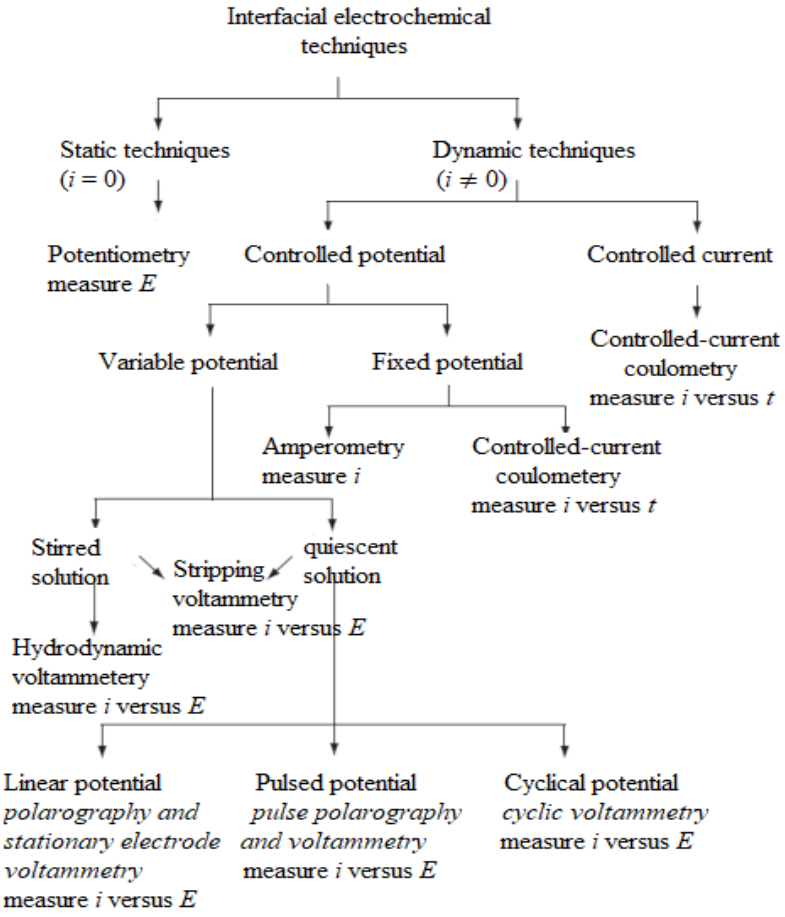

Figure 1 – Family tree of interfacial electrochemical techniques showing the experimental conditions and analytical signals (i = current; E = Potential; t = time)

1.1.2 Potentiometry

Potentiometry[2-4,25] is a useful quantitative method in which the potential of an electrochemical cell is measured under static conditions. The static conditions relate to the fact that no current or negligible current flows while measuring a solution's potential. The technique is relatively inexpensive and the electrodes (glass and reference electrodes) are reliable. The use of voltammetric methods of analysis offers several distinct advantages over potentiometric methods, notably the ease and rapidity with which samples can be prepared and analyzed, the ability to work outside the pH range of glass electrodes and to use non-protic media. The Nernst equation relates to an electrochemical cell's potential for the concentration of electroactive species in the cell. Actually, the potential of a potentiometric electrochemical cell is given by Eq. 1 as follows:

$$E_{cell} = E_a - E_c \qquad \text{Eq. 1}$$

where E_{cell} is the potential of the electrochemical cell and $E_a - E_c$ are oxidation potentials for the reactions occurring at the cathode and anode. These reductions potentials are a function of the concentrations of those species responsible for the electrode potentials as given by the Nernst equation (Eq. 2) as follows:

$$E = E^0 + \frac{RT}{nF} lnQ \qquad \text{Eq. 2}$$

where E^0 is the standard state reduction potential, R is the gas constant, T is the temperature in Kelvin, n is the number of electrons involved in the reduction reaction, F is the Faraday's constant and Q is the reaction quotient (a_{ox}/a_{red} denoting activities of oxidation or reduction forms). It is important to note that under laboratory conditions of temperature of 25°C or 298 K, the Nernst equation is written as shown in (Eq. 3) as follows:

$$E = E^0 + \frac{0.05916}{n} lnQ \qquad \text{Eq. 3}$$

1.1.3 Potentiometric measurements

To determine the potential of a solution in an electrochemical cell, a potentiometer, a working or indicator and a counter electrode are used in combination[2-4,25]. And since no significant current flows in potentiometry, the role of the counter electrode is reduced to that of a reference potential; thus, the counter electrode is usually called a reference electrode. Figure 2 is illustrated the set-up for potentiometric measurement of sample solutions.

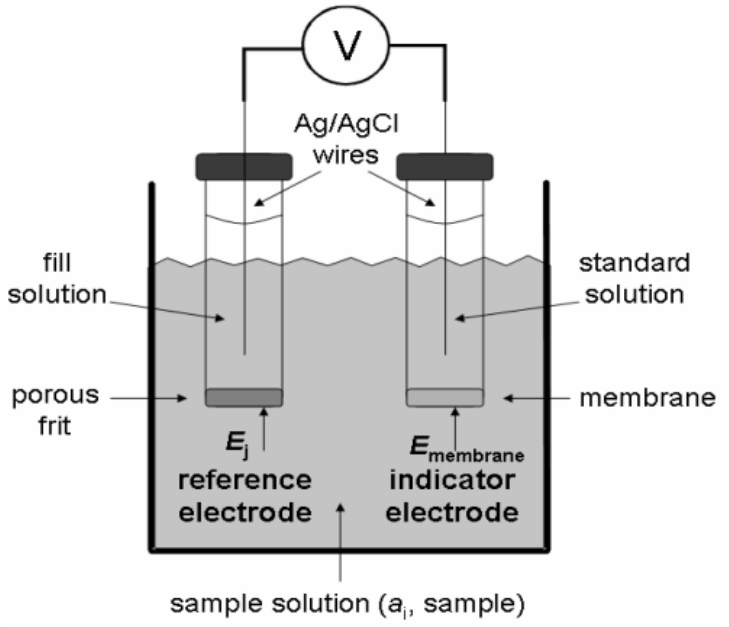

Figure 2 - Scheme of the potentiometric arrangement

1.1.3.1 Reference electrodes

Potentiometric electrochemical cells are designed such that one of the half-cells provides a known reference potential and the potential of the other half-cell indicates the analyte's concentration. The ideal reference electrode must provide a stable potential so that any change in the cell potential is attributed to the indicator electrode and also a change in the analyte's concentration. Usually, the reference electrode is separated from the analyte solution by a salt bridge of various forms. Standard Hydrogen Electrode, Saturated Calomel Electrode and Silver/Silver Chloride Electrode are the three most common reference electrodes.

1.1.3.1.1 Standard Hydrogen Electrode

For routine analytical work, the standard hydrogen electrode (SHE) is rarely used because it is difficult to prepare and inconvenient to use. However, it can be used to establish standard-state potentials in an electrochemical cell. Usually, it consists of a platinum electrode immersed in a solution in which the hydrogen ion activity is 1.00 and the H_2 gas is bubbled at a pressure of 1 atmosphere.

1.1.3.1.2 Saturated Calomel Electrode

This is a reference electrode which is based on the reduction of Hg_2Cl_2 to Hg in an aqueous solution saturated with KCl. The advantage of using this type of electrode is that the concentration of KCl, as well as the potential of the electrode, remains constant even if the

KCl solution partially evaporates. There are also some limitations associated with saturated calomel electrode which is that the solubility of KCl is sensitive to a change in temperatures and at higher temperatures the concentration of Cl^- increases and the electrode's potential decreases. This means that calomel electrodes cannot be used at temperatures exceeding 80°C.

1.1.3.2 Indicator electrodes

In a potentiometric electrochemical cell, the potential of the indicator electrode is proportional to the concentration of the analyte. Most of the indicator electrodes are grouped into metallic and ion-selective. Whiles the potential of a metallic electrode is determined by the position of a redox reaction at the electrode-solution interface that of the ion-selective electrode such as the glass pH electrode function by using a membrane that reacts selectively with a single ion. Electrodes of the First Kind, Electrodes of the Second Kind and Redox Electrodes are the common metallic used in potentiometry.

1.1.3.3 Glass pH Electrodes

These are ion-selective electrodes based on a glass membrane in which the potential develops from an ion-exchange reaction on the membrane's surface. Mathematically, the potential of the glass electrodes using Corning 015 over a pH between 0.5 and 9 is expressed in the form:

$$E_{cell} = K + 0.05916\ log[H^+] \quad \text{Eq. 4}$$

where K is a constant that includes the standard-state potential of species concentration. Above a pH of 9–10, the glass membrane could become very responsive to other cations such as Na^+ and K^+. Generally, glass membrane pH electrodes are often available in a combination form including both the indicator and reference electrodes and the use of a single electrode greatly simplifies the measurement of pH.

1.1.3 Measurement of pH

Potentiometric determination of pH using glass pH electrodes (Figure 3) is one of the frequent analytical measurements. The conventional definition of pH as presented in most Chemistry Textbooks is given as follows:

$$pH = -log[H^+] \quad \text{Eq. 5}$$

But, the pH of a solution is defined by the response of an electrode to the H^+ ion which is a measure of its activity (Eq. 6).

$$pH = -log(a_{H^+})$$ Eq. 6

For a glass membrane electrode, the cell potential, E_x for a solution of unknown pH is given as follows:

$$E_x = K - \frac{RT}{F}\ln\frac{1}{a_{H^+}} = K - \frac{2.303RT}{F}pH_X$$ Eq. 7

where *K* denotes the potential of the reference electrode, the asymmetry potential of the glass membrane and any liquid junction potentials in the electrochemical cell. Asymmetry potential is the membrane potential when opposite sides of the membrane are in contact with identical solutions yet a non-zero potential is observed. A liquid junction potential develops at the interface between any two ionic solutions that differ in composition and for which the mobility of the ions differs. A pH electrode must be calibrated using a standard buffer of known pH. The calibration or standardization of the pH electrode is done using two buffers: one near a pH of 7 and one that is more acidic or basic depending on the sample's expected pH. Using a standard buffer of known pH, then the cell potential for the standard, E_S is given as:

$$E_S = K - \frac{2.303RT}{F}pH_S$$ Eq. 8

Eqs. 7 and 8 are defined for a potentiometric electrochemical cell in which the pH electrode is the cathode whereby an increase in pH decreases the cell potential. However, it is relevant to mention here that most pH meters are designed with a pH electrode as the anode so that an increase in pH thus increases the cell potential. Therefore, the operational definition of pH is expressed as given in Eq. 9.

$$pH_X = pH_S - \frac{(E_x - E_S)F}{2.303RT}$$ Eq. 9

where pH_S is the pH of the standard and *F* is Faraday's constant (96487 C mol^{-1}).

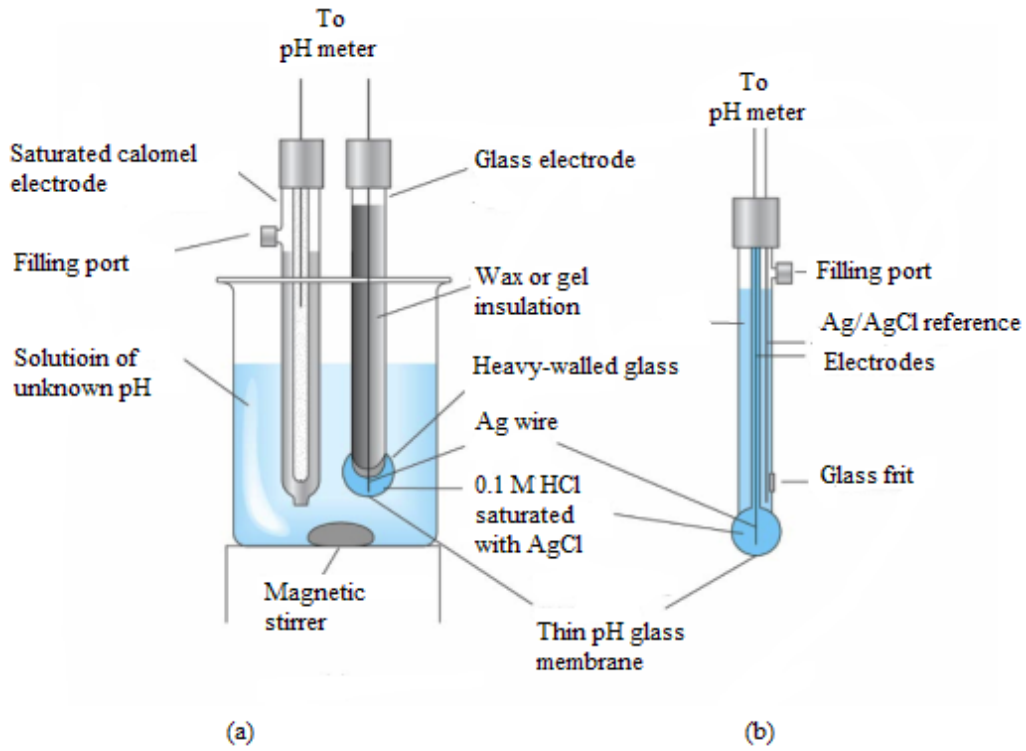

Figure 3 - A typical electrode arrangement for pH-measurements

(a) Glass electrode (indicator) and saturated calomel electrode (reference) immersed in a solution of unknown pH (b) Combination probe consisting of both an indicator glass electrode and a silver/silver chloride reference

1.1.4 Ion-selective electrodes (ISE)

Potentiometry with ISE[2-4,25] is one of the most important methods of modern analytical chemistry, based on the measurement of the equilibrium voltage of the cell, which contains the specific electrodes (its membrane potential is selectively determined by some types of ions) and the reference. The oldest ISE is a pH glass electrode that was described at the beginning of the twentieth century, although commonly used electrodes appeared around 1930 [3,25].

The function of the glass electrode is due to the exchange reactions occurring between the ions in the crystal lattice of the glass and the ions in the solution. Glass is a material that has a relatively regular silicate structure to which ions, especially hydrogen and alkali metals, are bound by electrostatic forces. Upon contact with the solution, a solvation layer or shell is formed on the surface of the glass, in which alkali metal ions and hydrogen ions are exchanged between the solution and glass, for example: $Na^+_{rozt} + H^+_{sklo} \leftrightarrow H^+_{rozt} + Na^+_{sklo}$, which leads to equilibrium characterized by the equilibrium constant K as follows:

$$K = \frac{a_{H^+_{rozt}} \cdot a_{Na^+_{sklo}}}{a_{Na^+_{rozt}} \cdot a_{H^+_{sklo}}} \qquad \text{Eq. 10}$$

Assuming that the ions activity on the glass surface is proportional to the concentrations and that the total number of ion exchange sites is constant, $c_0 = c_{H^+_{sklo}} + c_{Na^+_{sklo}} = \text{constant}$, applies to the equilibrium constant relationship as follows:

$$K = \frac{a_{H^+_{rozt}} \left(c_0 - c_{H^+_{sklo}}\right)}{a_{Na^+_{rozt}} \cdot c_{H^+_{sklo}}} \qquad \text{Eq. 11}$$

$$\frac{a_{H^+_{rozt}}}{a_{H^+_{sklo}}} = \frac{a_{H^+_{rozt}} + K \cdot a_{Na^+_{rozt}}}{c_0} \qquad \text{Eq. 12}$$

Taking into account that c_0 is a constant and that the composition of the internal solution of the glass electrode is constant, then the Nernst relationship after the last equation has been set is obtained as follows:

$$E = E_0 + \frac{RT}{F} ln\left(a_{H^+_{rozt}} + K \cdot a_{Na^+_{rozt}}\right) \qquad \text{Eq. 13}$$

where the constant E_0 contains the constant c_0.

This suggests that by measuring the potential difference on the glass membrane, the activity of hydrogen ions in the solution can be monitored and that sodium ions abrogate the determination if the product $K \cdot a_{Na^+_{rozt}}$ is not negligible in value $a_{Na^+_{rozt}}$ (soda glass electrode error). Thus, the more the glass electrodes are selective to the hydrogen ions, (allowing pH to be measured even in alkaline solutions), the lesser the equilibrium constant of the reaction. Soon after the successful introduction of the glass electrode into laboratory practice, attempts have been made to prepare electrodes selective for other ions. By the modification of the composition of the glass, in the 1950s, glass electrodes sensitive to alkali metal ions, ammonium ion and silver ions have been introduced. The use of materials other than glass then led to the construction of electrodes sensitive to a number of other ions.

Generally, any immiscible substance with measured solutions that have at least a low ionic conductivity can be used as ISE membranes and selectively interacts with the monitored component (ion) at the interface. This interaction may not only be based on ion exchange (as with a glass electrode) but also be in extraction equilibrium, selective adsorption or complex formation. The response theory of these electrodes has been further developed (in particular by [3,4,25], And it has been shown that the electrodes selectivity is determined in addition to the equilibrium constant of the interfacial interaction by the mobility of the

interacting ions in the interphase. Therefore, the general ion-selective electrode response equation is to some degree different from the last equation as follows:

$$E = E_0 + \frac{RT}{zF} ln(a_1 + k_{12}^{pot} \cdot a_2) \quad \text{Eq. 14}$$

where E_0 is a constant containing all constant members of the measured membrane potential, z is the number of charges that carry the determined ion 1 possessing the activity a_1, a_2 is the activity of the interfering ion 2 (for the same z), k_{12}^{pot} is the so-called selectivity coefficient for ion 1 against ion 2. The value of k_{12}^{pot} is determined by the combination of the equilibrium interaction constant which determines the value of the membrane potential and the ionic mobility member involved in the interaction. It is an important parameter characterizing the given electrode. If the k_{12}^{pot} value is smaller, the electrode is more selective to the ion 1. Figure 4 is the schematic representation of the basic types of ion-selective electrodes for potentiometric measurements.

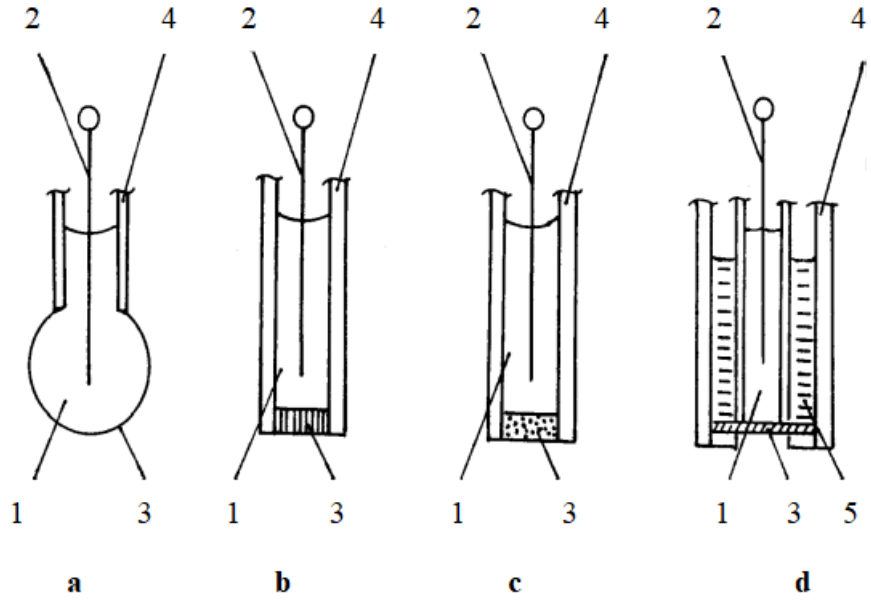

Figure 4 - Basic types of ion-selective electrodes

(a) glass (b) with a solid homogeneous membrane (c) a rigid heterogeneous membrane; (d) a liquid membrane (e) membrane coated with an enzyme

1 - Internal standard solution; 2 - internal reference electrode; 3 - membrane; 4 - electrode body; 5 - the electroactive material reservoir

For the potentials of the ion-selective electrodes, the formula of the Nikolski equation[3,4,25] generally applies as follows:

$$E = constant + f\frac{2{,}303RT}{z_iF} log\left(a_i + \sum_j k_{i,j}^{pot} a_j^{z_i/z_j}\right) \quad \text{Eq. 15}$$

where f is the correction for the non-Nernst progression, a_i and a_j are the activities of ion analyte and interfering ions, z_i and z_j are the valency of the ionic analyte and the interfering ions and $k_{i,j}^{pot}$ denotes the ISE selectivity constants.

1.2 Influence of amperometric reactions

With respect to the nature of the electrodes and the measurement systems used in electrochemical measurements, in addition to electrochemical interactions, and especially amidst the stabilization of the working electrode potential, the amperometric processes[1-4,26,69] could be applied (even to a small extent). For example, they can be described as the electrode reaction using the following kinetic relationships. For a simple electrode reaction, Eq. 16 can be written as follows:

$$Ox + n\,e^- \leftrightarrow Red \quad \text{Eq.16}$$

where *Ox*, *Red* – oxidized and reduced form of the substance, *n* – number of electrons exchanged. The rate of this reaction is controlled in both directions by cathodic velocity constants k_k and anodic k_a.

1.2.1 Kinetics of electrode reactions

$$-\frac{dN_{ox}}{dt} = \frac{dN_{red}}{dt} = k_k \cdot c_{ox} - k_a \cdot c_{red} \quad \text{Eq. 17}$$

where N_{ox} and N_{red} are the number of moles of electroactive material converted to the electrode per unit of time per unit area, k_k and k_a cathodic and anodic rate constants (cm·s^{-1}), c_{ox} and c_{red} are the concentrations of the oxidized and reduced form at the surface of the electrode, *c* (mol·cm^{-3}).The rate of electrode potential function is described as follows[3,69]:

$$k_k = exp\left(-\frac{\Delta\, G_{red,0}}{RT}\right) \quad \text{Eq. 18}$$

$$k_k = k_k^0 \cdot exp\left(-\frac{\propto nF}{RT}E\right) \quad \text{Eq. 19}$$

$$k_a = k_a^0 \cdot exp\left(\frac{(1-\propto)nF}{RT}E\right) \quad \text{Eq. 20}$$

where k_k^0, k_a^0 are the standard values of the speed constants for E = 0, and α is the charge transfer coefficient (transmission coefficient); 0 < α < 1 (usually ranging from 0.2 to 0.8); $\Delta G_{red,0}$ denotes a standard free enthalpy of reduction.

The electrode speed is therefore described as follows:

$$\upsilon = -\frac{\mathrm{dN_{ox}}}{\mathrm{dt}} = \frac{\mathrm{dN_{red}}}{\mathrm{dt}} = \mathrm{c_{ox}} \cdot \mathrm{k_k^0} \cdot \exp\left(-\frac{\propto \mathrm{nF}}{\mathrm{RT}}\mathrm{E}\right) - \mathrm{c_{red}} \cdot \mathrm{k_a^0} \cdot \exp\left(\frac{(1-\propto)\mathrm{nF}}{\mathrm{RT}}\mathrm{E}\right) \quad \text{Eq. 21}$$

The value of the flowing electric current is then obtained by multiplying the velocity of the electrode reaction by the surface area of the electrode *A* and the charge that is consumed to convert one mole of the electroactive substance, that is *nF*. For the current density (*A* = 1), Eq. 22 is obtained as follows.

$$i = nF\left[c_{ox} \cdot k_k^0 \cdot exp\left(-\frac{\propto nF}{RT}E\right) - c_{red} \cdot k_a^0 \cdot exp\left(\frac{(1-\propto)nF}{RT}E\right)\right] \quad \text{Eq. 22}$$

For the partial cathodic and anodic current densities, Eqs. 23 and 24 are written as follows:

$$i_k = nFc_{ox} \cdot k_k^0 \cdot exp\left(-\frac{\propto nF}{RT}E\right) \quad \text{Eq. 23}$$

$$i_a = -nFc_{red} \cdot k_a^0 \cdot exp\left(\frac{(1-\propto)nF}{RT}E\right) \quad \text{Eq. 24}$$

1.3 Specific adsorption-desorption interfacial interactions

In solving the problems or issues described in the dissertation, experience and some analogies from the field of specific adsorptive-desorption interfacial processes[2,4,9,10,36,75] were also applied. They were derived from the electro-capillary measurements of mercury surface tension dependencies γ on the input potential *E* at different concentrations of surfactants. From the measured dependencies γ versus log *c,* at the potential of pronounced adsorption, it is then possible to calculate the relative surface excess of the substance on the surface of the electrode. The relationship between γ and *c* at given *E* allowed to obtain (after differentiation γ versus log *c*) the course of the adsorption isotherm Γ versus *c* at given potential and substance.

1.4 Model agglomeration interactions and kinetics of growth of nanoparticles or submicro-particles

Currently, one of the objects of great interest in nanochemistry is aqueous solutions containing nanoparticles. Among its priorities is the monitoring of growth kinetics[22,23,27,18,10]. An example is the growth of nAg nanoscale particles with time. Also, the study of the

possibilities of interleaving and evaluation of these dependencies is also important. This work included a contribution of the breakdown of such dependencies, among other aspects, based on the previous experience, and possibly, the analogy of the research conditions (and in particular, the concept of my Supervisor) with adsorption-desorption and related interactions, combined with statistical data analysis[28,29].

2. EXPERIMENTAL

2.1 Assemblable arrangement for potentiometric measurements with amalgam electrodes and for interfacial or selected additional measurements

2.1.1 Measurements using silver and silver amalgam electrodes for ion exchange water treatment

Prior to the measurement, the entire potentiometric arrangement was tested using a glass ion-selective pH electrode combined with a reference chloride electrode immersed in pH-buffered standard solutions (Electrochemical detectors, s.r.o., Turnov, Czech Republic). Potentiometric measurements were carried out in a circuit made of a specific silver or silver amalgam electrode, reference Ag/AgCl (3 M KCl) with a salt bridge of 0.1 M KNO_3 (Electrochemical detectors, s.r.o., Turnov, Czech Republic) and BM 551 voltmeter (Laboratory devices, Prague, Czech Republic) with the potentiometric module attached, as shown in the studies of[8,18]. The electrodes were inserted into a rack and a computer receptacle Eco-Tribo Polarograph (Eco-Trend Plus s.r.o., Prague, Czech Republic) in a report according to the authors[30-32]. The specific silver electrode (SE) was in the form of a disk of approximately 0.6 mm diameter, which was created by grinding silver wire in a plastic wrap. It was polished with an aluminium emulsion of 0.3 μm (Electrochemical Detectors, s.r.o., Turnov, Czech Republic). Solid silver amalgam electrode (AgAE) in a plastic tip from micropipettes, "Plastic tip"[15,33] (similar to the former "plastic tip" of mercury[34]) or PT-AgE was prepared[15,16,33,34] after filling the silver powder with a particle size of 2 μm by amalgamation and then inserting the tip for about 8 hours into dry mercury.

The electrode preparation was terminated by a slight alignment of the mouth followed by brushing or cleaning. For the gradual purification, water from the natural water tank after decantation (VD) containing about 0,1 $mg \cdot L^{-1}$ C10-C40, 41 $mg \cdot L^{-1}$ Ca, 14 $mg \cdot L^{-1}$ Mg, 5 $\mu g \cdot L^{-1}$ Cu, 1 $\mu g \cdot L^{-1}$ Cd, 39 $mg \cdot L^{-1}$ Cl, 7 $mg \cdot L^{-1}$ NO_3, 57 $mg \cdot L^{-1}$ SO_4^{2-}, 12 $mg \cdot L^{-1}$ SiO_2, 75 $\mu g \cdot L^{-1}$ AOX, pH ~7,5 was used. The (VD) was conditioned by coagulation and filtration (VKF) after the cation exchange column (VK) and the anion exchange column (VA), then collected and stored in the water reservoir (VZ). Lewatit S 100 (Lanxess, Cologne, Germany) served as a cation, with a mean particle size of about 640 μm. The annex column contained a slightly basic Lewatit MonoPlus MP 64 (Lanxess, Cologne, Germany) with a mean particle size of about 600 μm, mixed in a 1:1 ratio with a strongly basic anion of Lewatit MonoPlus M 600 (Lanxess, Cologne, Germany) with a mean particle size of about 610 μm. Stock solutions

of 0.1 M and 1 M $AgNO_3$ (Merck, Germany) and other solutions were prepared using demineralized water with a conductivity of < 0.1 $\mu S \cdot cm^{-1}$. Prior to the measurement, the solution was bubbled with a nitrogen purge for 5 minutes and the nitrogen was fed over the solution during the measurement. The measurements were carried out at 293 K.

2.1.2 Measurements using the zinc amalgam electrode for the detection of concentration changes of zinc sulphate by nanofiltration

The potentiometric experimental arrangement included a cell and a stand of the Eco-Tribo Polarograph (Eco-Trend Plus, Prague) and accessories, an industrial digital multimeter IP67 (EXTECH Instruments, USA) connected via a special input/output interface [17,18] to the Zinc and Zinc Amalgam Electrodes (ZnE or ZnAE) and the reference mercury sulphate electrode. All the three electrodes, an electromagnetic stir bar, and a gas-inlet were inserted into the solution in a closed glass cell. The solutions were prepared from demineralized water (< 0.1 $\mu S \cdot cm^{-1}$, from the Milli-Q Plus water-purification system, Millipore, Bedford, USA) and reagent-grade chemicals. The linear least-square regression in Origin Pro 7.5 (OriginLab Corporation, USA) was used for fitting calibration curves and the relevant results (slope and intercept) were reported with a confidence interval of 95 % probability.

The nanofiltration experiments were carried out using small aqueous samples from 25 to 170 $mg \cdot L^{-1}$ Zinc Sulphate ($ZnSO_4$) and a tubular nanofiltration arrangement of a cross-flow separation unit which has been described in detail elsewhere[5,6,35]. A commercially available type of membrane made of poly-amid film, AFC 40, PCI Membrane Systems (Poland), was used. Effective membrane area was 240 cm^2 (two tubes, each with a length of 30 cm and an internal diameter of 1.25 cm, pH ranged from 1.5 to 9.5 and maximum temperature of 333 K).

2.2 Experimental conditions under which the treated data on agglomeration processes were collected

2.2.1 Assessment of the agglomeration kinetics of waste nanoparticles based on its partial similarities with the electrosorption processes

The adsorption data of sodium thiosulfate at the constant potential E = -0.1 V versus SCE (Sodium Chloride Electrode) in a concentration range of its surface access Γ between $0.4 \cdot 10^{-6}$ and $2 \cdot 10^{-6}$ $mol \cdot m^{-2}$ were obtained by the improved controlled convection drip-time technique

CCDT[10,36] using a glass spindle capillary with drop time of about 70 s. The solution was stirred during the drop-growth to ensure the attainment of adsorption equilibrium; as a result, the stirrer was stopped at about 10 s before the fall of the drop. The reproducibility of the CCDT method was better than ±0.3 $mN \cdot m^{-1}$.

The electrocapillarity measurements were calibrated assuming that the electrocapillary maximum in the base electrolyte was γ = 426.7 $mN \cdot m^{-1}$ at 293.2 K. Repeatability of Γ versus *c* concentration of sodium thiosulfate was better than ± 10 %. The experimental arrangement included PC-controlled voltammetric analyzer PC-ETP (Eco-Trend Plus Co., Czech Republic[30-32,56]), a laboratory-made electrocapillary arrangement and a digital counter for the drop-time measurements. The stock solution was 1 mM of nAg, prepared by a modified Tollens process[27] based on the chemical reduction of silver nitrate ($AgNO_3$) by glucose ($C_6H_{12}O_6$). The studied solution of nAg[27] of a concentration 10 $\mu mol \cdot L^{-1}$ was prepared using dilution of the stock solution by liquid Medium 203 and its concentration was verified by the optical emission spectroscopy (OES) with inductively coupled plasma (ICP-OES). The medium 203 was the aqueous solution containing 2 mM $CaCl_2$, 0.5 mM $MgSO_4$, 0.77 mM $NaHCO_3$ and 0.075 mM KCl. Its pH value was 6.8. The hydrodynamic diameters (D_H) were measured[27] by dynamic light scattering (DLS) with ZetaPALS Potential Analyzer (Brookhaven Instruments Corp., USA). The experimental set-up of the OES with ICP-OES[27] was done using the instrument IntegraXL2 (GBC, Dandenong, Australia). The pH was measured by the portable laboratory arrangement. The solutions used were prepared from bidistilled water and reagent grade chemicals (Sigma-Aldrich). Thiosulfate anions were added in the form of their sodium salt $Na_2S_2O_3$. The aqueous solutions were stored at laboratory temperature. The working standard solutions were prepared daily by dilution of the stock solutions.

2.3 Statistical data analysis of experimental data

The experimental data were analyzed and graphically represented using the Statistica software (version 13), OriginPro software (version 7.5) and Microsoft Excel 2010 respectively.

3. RESULTS AND DISCUSSION

3.1 Utilization of changes in the Nerstian potentiometric behaviour of silver amalgam electrodes AgAE during ion exchange water treatment

3.1.1 Background of the study

The most significant advantages of potentiometry in the field of water and waste management, for example, when monitoring the pH or metal content, are its relative simplicity, availability and operational applicability[2,3,8]. The new knowledge of its use is therefore of great interest, especially if it can be applied sooner or later under normal (operational) conditions. Water purification methods and control procedures are many. As to the common technological conditions, conductometry is the most preferable technique used for pure water quality control[1-3,7,8]. Generally, in principle, when monitoring the water treatment process, the control system, in particular, develops a flow chart in a sequence of individual cleaning steps when passing the sample from one purification step to the sample from the following step. If the character of such a diagram is sufficiently pronounced and repeatable, then the control system requires further research attention. Therefore, the water purification processes used, in particular, may be associated with relatively pure water accompanied by the release of relatively trace amounts of substances for which a single control method – otherwise widely used – is less sensitive. Then, the use of two control methods (systems) operating on mutually independent principles is recommended in such cases. Such a situation may occur, for example, water purification using organic ion exchangers. Column traces, which can be released particularly through a more demanding long-lasting cleaning regime, can be low-polar substances with low or inadequate detection conductivity sensitivity. For this purpose, it was recently proposed[14,15,19] to test the behaviour of modified new types of solid amalgam electrodes that have been introduced successfully in voltammetry[10-13,33,37-39] and also rarely tested in potentiometry[14,19].

3.1.2 Results and discussion

All potentiometric measurements were performed by adding 1 ml of 0.1 M $AgNO_3$ stock solution to 10 ml of the collected water sample so that the $AgNO_3$ content of the sample was 0.007 $mol \cdot l^{-1}$. Samples were sequenced, starting with decantated water (VD), water after coagulation and filtering (VKF), water after cation (VK), using anion (VA) and water from the reservoir (VZ). As the samples varied considerably from each other, the anions, cations and organic substances contained in them varied to the Ag^+ ions hence reduced the activity of these ions. In the case of the AgAE, both Hg_2^{2+} and Hg^{2+} ions were active concurrently to

Ag^{+}. Hg^{2+} was present near the surface of the electrode. Therefore, in the transition from one sample to another, greater changes in the mixed potentials *E* in the case of AgAE were observed. As a result of this, the sensitivity and repeatability of AgAE were better than that of AgE. The results[14] are documented in the following figures. Figure 5 shows the three repeated measurements of potential *E* of samples in the order V1, V2, V3, V4 and V5 for the corresponding VD, VKF, VK, VA and VZ using AgE. The diagrams of potential *E* versus *Vi* showed poorly repeatable waveforms that did not have characteristic courses in the sequence from V1 to V5.

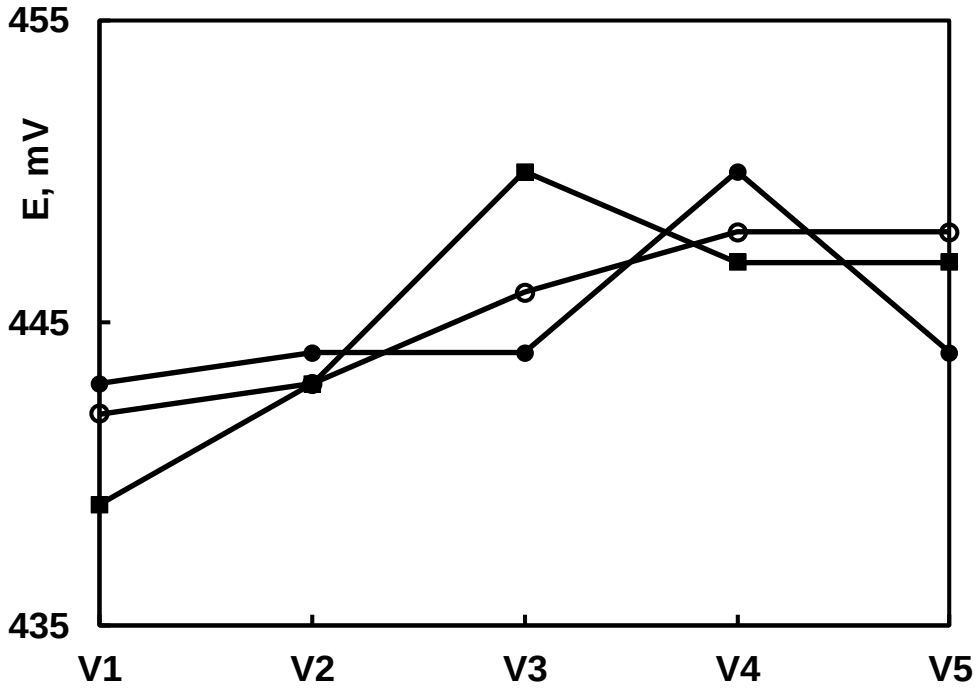

Figure 5 - *E* versus *Vi* diagrams of three repeated measurements on the silver electrode (AgE)

However, for AgAE as shown in Figure 6, the course of the potential *E* versus *Vi* was significantly different. The diagrams obtained had satisfactory repeatability and the character of their course was quite reproducible.

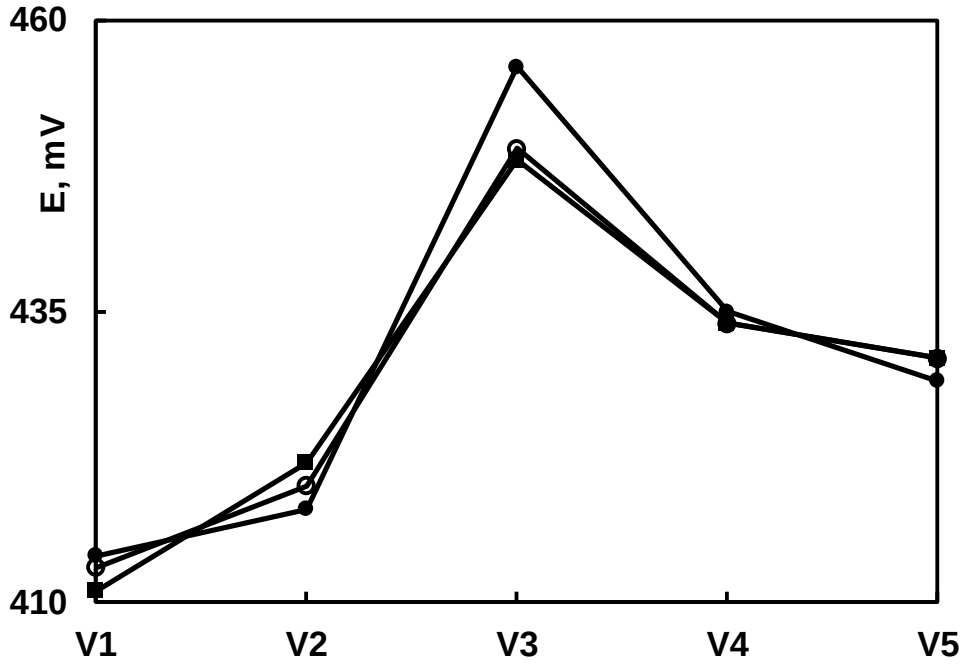

Figure 6 - *E* versus *Vi* diagrams of three repeated measurements on the silver amalgam electrode AgAE

One reason for the AgE behaviour can be attributed to the fact that Ag^+ ions exhibit significant interactional activity in the solution not only against many anions but also with organic components. Surface layers of chemical products of cations and anions could even act as a filter against most of the interfering organic components present in V1 and V2, however, their influence often causes other components into the monitored solutions to which the SE may also be sensitive. The oxidative attack of the strongly acidic cation system according to the scheme in Figure 7, for example, is accompanied by hydrolysis and molecular segments of exchanges are released[40].

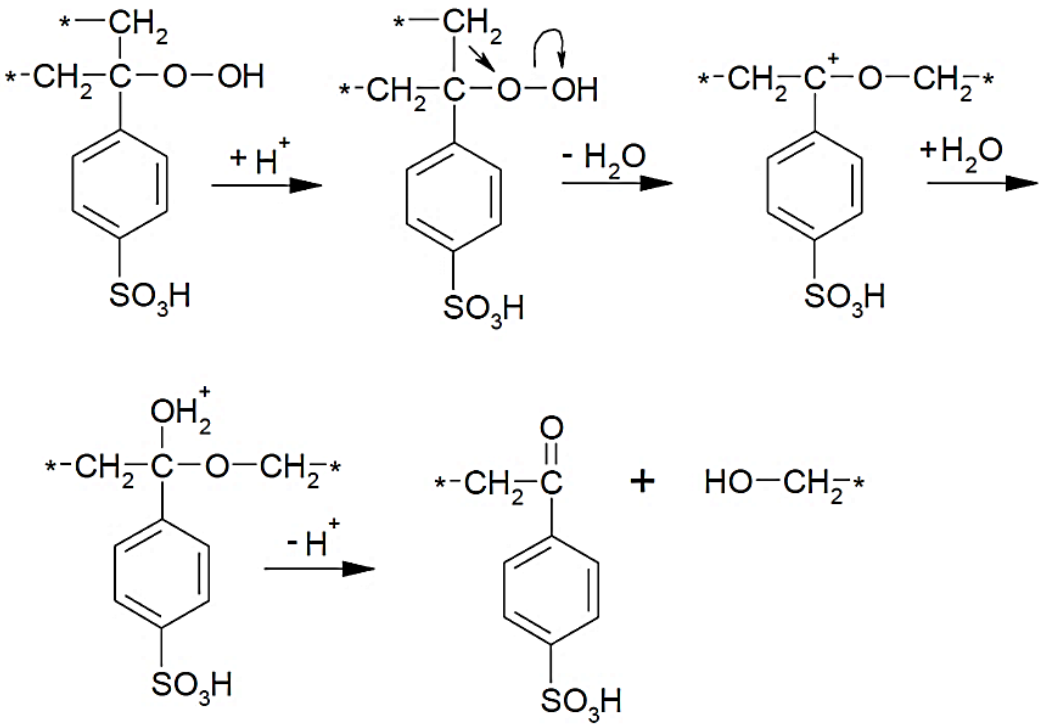

Figure 7 - Oxidation attack of the strongly acidic cation exchanger

Other events that are applied to the anion are dealkylation of its functional groups[41] by the temperature according to the scheme in Figure 8.

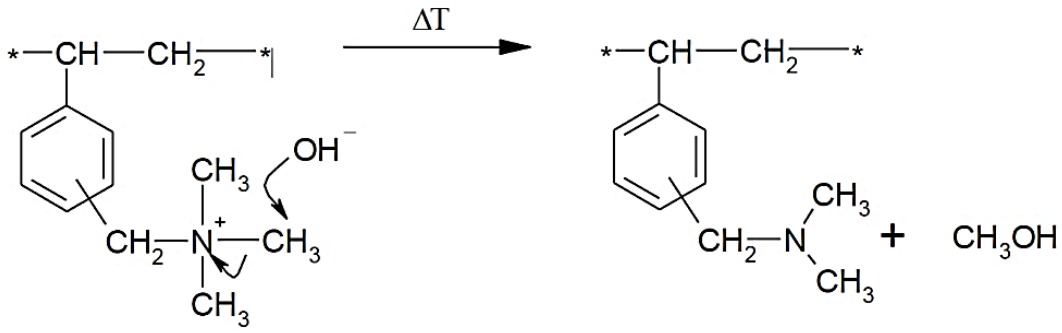

Figure 8 - Dealkylation of the anion exchangers

Similarly, traces of organics may be released in the presence of humic acids in their interactions[42] with the strongly basic anion according to the scheme in Figure 9.

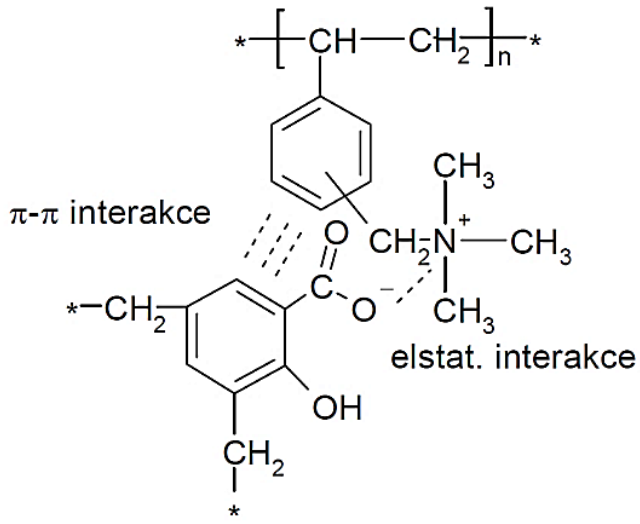

Figure 9 - Interaction of humic acid with a strongly basic anion exchanger

These interactions with organic solvents can also be applied to AgAE. However, as the results of the measurements showed, the extent of the manifestations of the disturbing events by this electrode was considerably limited compared to AgE. In addition to the differences in material composition, great differences in surface quality could have contributed to this, which is significantly smoother (compared to polished AgE) and is more isotropic than AgE surface. Schematically, the potential changes *E* (cited in[14]) by AgE are based on Eqs. 25 and 26 as follows:

$$E_{Ag} = E^0_{Ag} + \frac{RT}{F} lna_{Ag^+} \qquad \text{Eq. 25}$$

$$E_{Ag/AgY} = E^0_{Ag/AgY} - \frac{RT}{F} lna_{Y^-} \qquad \text{Eq. 26}$$

where *Y* denotes the solution component integrating with Ag^+; *R*, *T* and *F* are universal gas constant, absolute temperature and Faraday constant. Similarly, Eqs. 27, 28 and 29 can be written based on the mixed potential *E* of the AgAE electrode.

$$E_{Ag(Hg)} = E^0_{Ag(Hg)} + \frac{RT}{F} lna_{Ag^+} \qquad \text{Eq. 27}$$

$$E_{Hg} = E^0_{Hg} + \frac{RT}{2F} lna_{Hg_2^{2+}}, \qquad \text{Eq. 28}$$

$$E_{Hg/Hg_2Y_2} = E^0_{Hg/Hg_2Y_2} - \frac{RT}{F} lna_{Y^-} \qquad \text{Eq. 29}$$

Furthermore, the surface of AgAE did not require renewal or restoration earlier than after the first and second week, unlike the AgE, which was mechanically or practically restored before each series of measurements. However, for the renewal of the AgAE surface, usually, it was enough to wipe the face of the electrode slightly. The results have shown that continuing research in the direction discussed earlier may need further improvements.

3.2 Utilization of the potentiometric signal of the zinc amalgam electrode ZnAE for the detection of concentration changes of dissolved ZnSO4 by nanofiltration

3.2.1 Background of the study

The study of nanofiltration of aqueous solutions has made much progress during the past 20 years[35]. One of the most attractive results is its success in possible separation of ionic heavy metals or other molecular pollutants, which can be applied, for example, in the treatment of drinking, waste or industrial waters and effluents[5,6,35,43]. One of the well-known metallic pollutants[44] is zinc present in the form of its divalent ions. Zn is an essential element necessary for living organisms. It is important, for example, for a proper functioning of the immune system, enzymes and DNA synthesis or gene expression. On the other hand, its uptake by human above a certain level causes some acute and chronic illness, fever, gastroenteritis, anaemia, renal failure, allergies, and internal organ damage[45]. The limit for zinc in waste-water according to the National Secondary drinking Water regulation of the EPA[46] is 2.61 $mg \cdot L^{-1}$, which is in good agreement with that of 1.5 to 3 $mg \cdot L^{-1}$ valid in the Czech Republic[47]. Zinc concentration is rising in the environment. It is released by electrotechnical industry, electroplating, mining, metallurgical, and pharmaceutical and paint production, coal-power stations as well as from other industrial production and use, for example, catalysts.

Recent studies[5] have outlined some relevant technological applicability of nanofiltration using a pressure-driven membrane[48,49,6] for separation of zinc[50-52] (or its salts) provided that the proper arrangements and working parameters (like the type of the thin-film composite membrane, cross-flow velocity, pressure, temperature, flow-rate, etc.) can be verified experimentally. It simply means that many experiments must be accompanied by several analyses focused on the determination of the input/output ratio of the analyte concentrations.

For these purposes (regardless of the required independent analytical background); the rapid, relatively simple, disposable and low-cost techniques and applicability (proximity); are desirable for reducing the corresponding effort, time and cost associated with its application. Recently[14,19,53], such methods and arrangements for the purposes described were suggested based on potentiometry with a modified new generation of the detection metal amalgam electrodes or sensors. For zinc, in well-equipped analytical laboratories, the available methods for its determination include inductive coupled plasma-optical emission spectroscopy (ICP-OES), atomic absorption spectrometry (AAS), ICP-mass spectrometry (ICP-MS)[54,55],

potentiometry, and voltammetry[3]. As indicated, potentiometry could principally meet the above-mentioned demands on the condition that the proper detection electrode is found. However, at present, zinc ion selective electrode is not commercially available. On the other hand, the last two decades have shown much progress in the application of voltammetry by using a new generation of solid (or modified) amalgam electrodes[11-13,37,38]. And some recent communications or notes[14,19,53] concerning the advanced special (or modified) amalgam electrodes (AE) (including AgAE, CuAE, ZnAE etc.) have outlined their new possibilities in the field of potentiometry, as well. Nevertheless, as for ZnAE, there is basic or relevant experimental data regarding its application in this respect. Thus, the work aimed at presenting basic testing of a potentiometric sensitivity of the zinc solid amalgam electrode (ZnAE) (partly in comparison with a zinc electrode, ZnE) with respect to concentration changes of $ZnSO_4$ in aqueous solutions, among others under the experimental conditions similar to those applied by using the nanofiltration technologies.

3.2.2 Results and discussion

The zinc electrode (ZnE) was prepared from a zinc wire of 1 mm diameter by either sealing into a conically tapered glass capillary or by its tight fit in an inert plastic tip[15,34] of a micropipette. Cutting and polishing of the orifice of this electrode resulted in a smooth zinc disk electrode. The zinc amalgam electrode (ZnAE) of diameter 1 mm was prepared using ZnE by applying an amalgamation of the zinc disc through its direct contact with liquid mercury under its overpressure about 30 millibars for 15 hours. After resting period of about 10 hours, the tip of the ZnAE was polished (for example, by a clean glass plate) or in case of a plastic tip arrangement; a fine cutting-off its amalgam orifice, eventually, the ZnAE was ready to use. The above-mentioned inert plastic tip versions of ZnE or ZnAE were given preference to the glass or the other versions[15,34] with plastic-tip electrodes. The active surface of the orifice in the form of a disk can be repeatedly renewed by cutting the plastic tip with a razor blade. Of course, ZnAE-electrodes may also be renewed by polishing their orifice using, for example, a glass or polyethylene plate or a 0.3 mm suspension of alumina. The behaviours of both electrodes and proper functioning of the whole experimental arrangement, as well as the procedures used, were verified by the potential E versus time (t) measurements at different concentrations c of $ZnSO_4$ or by the E versus log c dependences.

For the first step, ZnE was inserted into $1 \cdot 10^{-5}$ mol·L^{-1} of $ZnSO_4$. As it was expected, the obtained E-t dependence exhibited its strong non-monotonous course reaching a non-stable

quasi-steady state after about 400 s. It was probably due to the activation of a complex of surface processes like a zinc oxidation, its interaction with other components present in the solution, precipitation of Zn^{2+}, etc. As shown in Figure 10, the potential *E* did not reach its constant time-independent value even within a period of time of more than 3000 s.

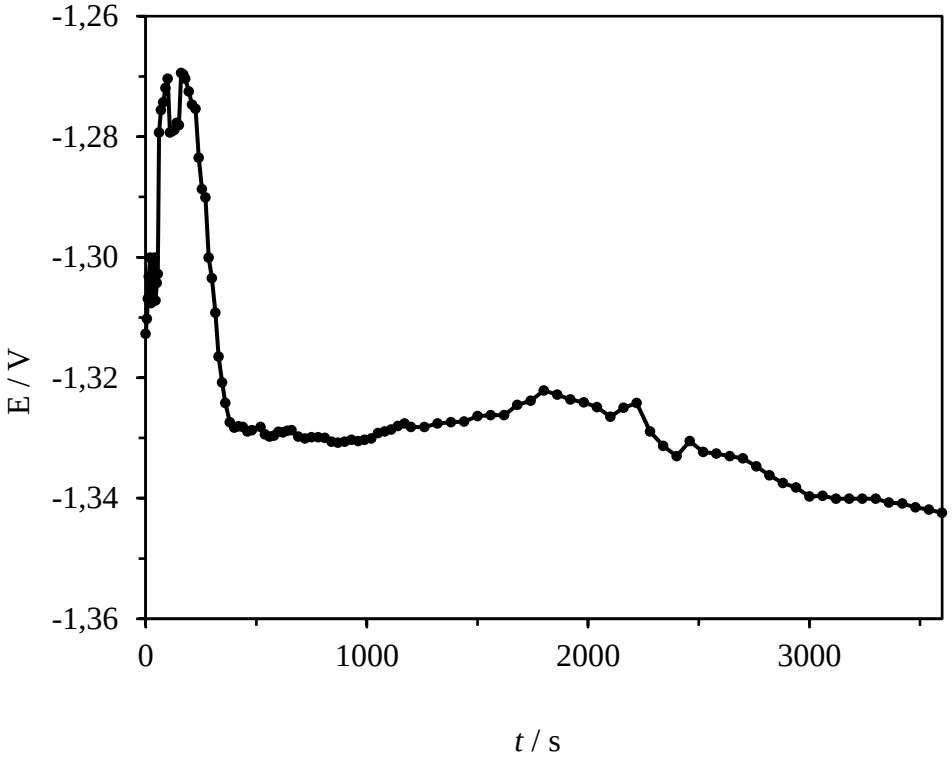

Figure 10 - Potential *E-t* dependence on ZnE after its first insertion into $1 \cdot 10^{-5}$ mol·L^1 of $ZnSO_4$

Further insertion of ZnE into the solution provided rather monotonous *E-t* dependences of the type as shown in Figure 11. The most sudden changes of the potential *E* occurred within the first 10 minutes. Nevertheless, no equilibrium values of *E* were reached, even at higher concentrations of $ZnSO_4$. A potential role of dissolved air oxygen was tested, as well. Prior to the measurements, a reasonable absence of atmospheric oxygen was reached by bubbling nitrogen through the solution for 5 minutes. It was partly surprising that a profile of the obtained *E-t* dependences corresponding to the measurements under the air atmosphere was much better than that after bubbling out of oxygen by nitrogen. It indicated that further measurements can be carried out in the presence of the dissolved air.

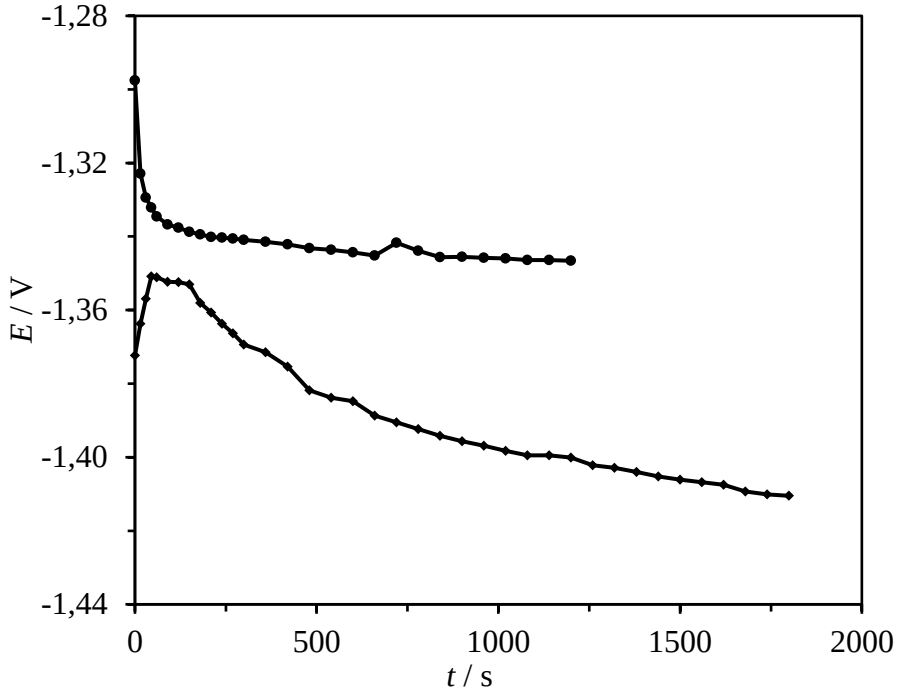

Figure 11 - Profiles of *E-t* dependences obtained under the air (●) atmosphere or after bubbling out of oxygen by nitrogen (♦) for 5 minutes prior to the measurements

It is worth mentioning that owing to a reasonable repeatability of the measurements, ZnE was polished prior to each set of experiments. A certain loss of the electrode material, ZnE during its experimental use was probably due to its slow parallel background chemical reactions and its dissolution. For the ZnAE, the analogous potentiometric *E-t* measurements produced approximately hyperbolic dependences. Some few examples are illustrated in Figure 12 comprising the upper *E-t* curve obtained with ZnAE after the first insertion into $1 \cdot 10^{-5}$ mol·L^{-1} $ZnSO_4$ and the lower set of consecutive six repeated measurements with ZnAE after inserting into the said solution. As shown in Figure 12, in comparison with ZnE, the system with ZnAE reached the quasi-steady state more rapidly and its stability was much better. However, as expected, certain irreproducibility of *E-t* dependences were observed.

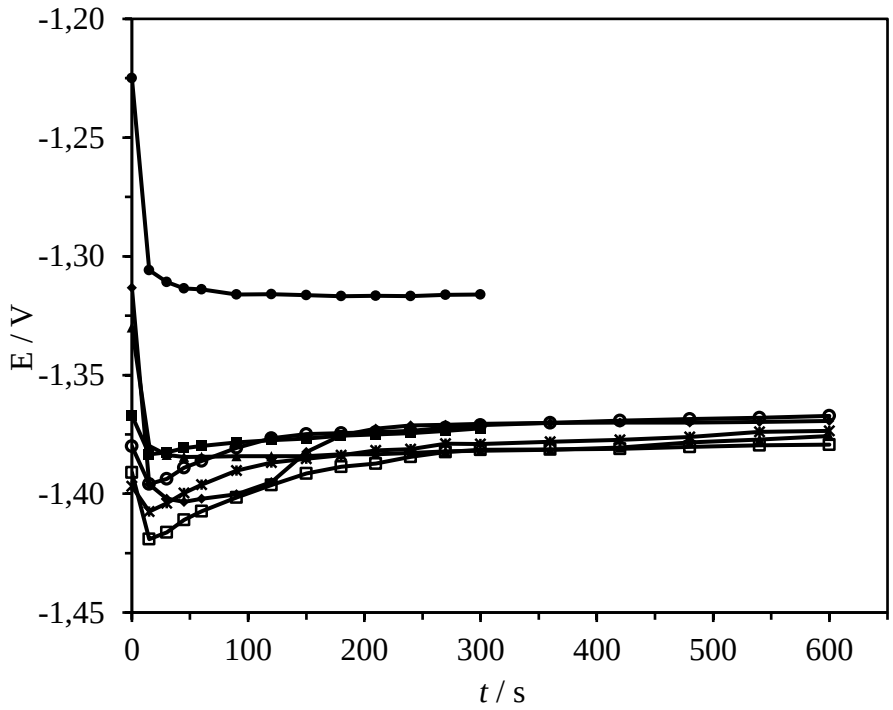

Figure 12 - Potentiometric *E-t* measurements with ZnAE in $1 \cdot 10^{-5}$ mol·L^{-1} of $ZnSO_4$. The upper curve – the electrode after the first insertion into the solution; the lower 6 curves show the next 6 repeated measurements

The consecutive *E-t* plots as shown in Figure 13 at different concentrations of $ZnSO_4$ from $1 \cdot 10^{-4}$ to $1 \cdot 10^{-1}$ mol·L^{-1} confirmed the above-mentioned advantages of ZnAE compared to ZnE. It implies that after the ZnAE was inserted into the solutions, the measured potentials *E* reached their quasi-constant values in 250 to 300 s, which can be utilized analytically. Therefore, further measurements of *E* with ZnAE in solutions containing various concentrations of $ZnSO_4$ were performed in 300 s after the electrode was inserted into the solution. In this way, the calibration *E-log c* dependence (see Table 1 and Figure 14) in a concentration range from $5 \cdot 10^{-5}$ to $1 \cdot 10^{-2}$ mol·L^{-1} of $ZnSO_4$ was obtained. A linear relationship between potential *E* and *log c* exhibited an analytically utilizable slope $\delta E/\delta \log c$ = -35.9 mV. The reason for the decrease of the *E* versus *log c* dependence is probably connected with a complex of present interactions and reactions including the formation of insoluble salts, hydroxides, oxides, or other products on the electrode. The obtained *E-log c* dependences shifted a little of the potential while maintaining their slope and the linear relationship between potential and the logarithm of concentration. The finding was confirmed by further analysis of the data as summarized in Table 2.

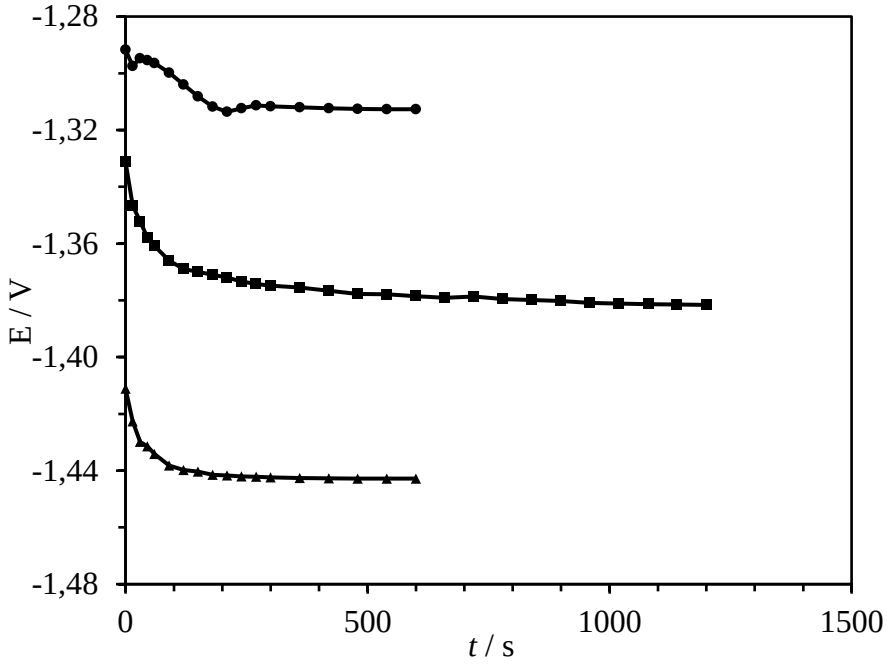

Figure 13 - The *E-t* plot on ZnAE corresponding to concentrations $1 \cdot 10^{-4}$ mol·L^{-1}(●), $1 \cdot 10^{-3}$ mol L^{-1}(■); $1 \cdot 10^{-1}$mol·L^{-1}(▲) $ZnSO_4$

Table 1 - Potentiometry of ZnAE in $ZnSO_4$; calibration of *E-log c* data

c (mol·L^{-1})	*log c*	*E* (V)
$5 \cdot 10^{-5}$	-4.3010	-1.3245
$1 \cdot 10^{-4}$	-4.0000	-1.3309
$2 \cdot 10^{-4}$	-3.6990	-1.3438
$5 \cdot 10^{-4}$	-3.3010	-1.3555
$2 \cdot 10^{-3}$	-2.6990	-1.3769
$5 \cdot 10^{-3}$	-2.3010	-1.3932
$1 \cdot 10^{-2}$	-2.0000	-1.4071

$$E = -(0.0359 \pm 0.0011) \cdot log\ c - (1.4761 \pm 0.0037)$$

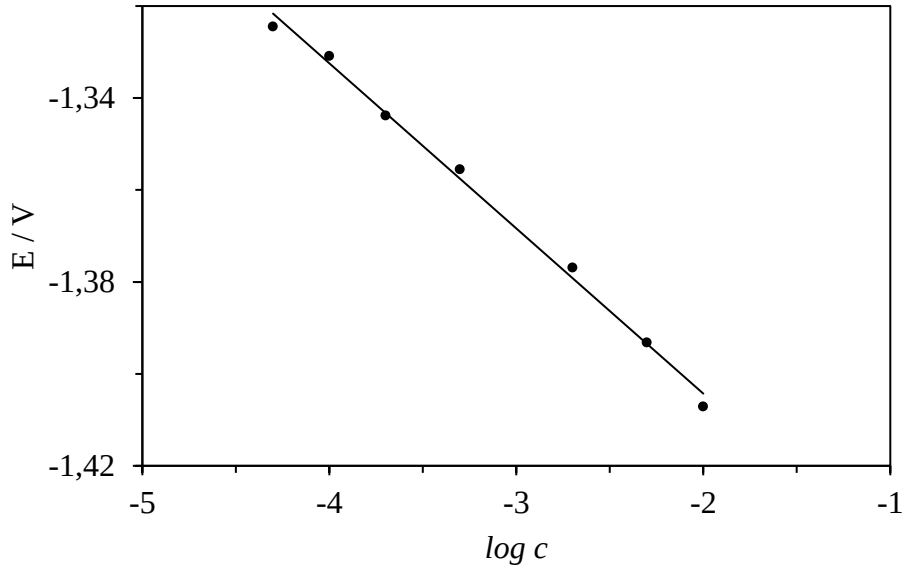

Figure 14 - Calibration of *E-log c* dependence in $ZnSO_4$ using ZnAE

Table 2 - Repeated potentiometric calibration measurements of ZnAE in $ZnSO_4$

c (mol·L^{-1})	*log c*	*E* (V)
$1 \cdot 10^{-4}$	-4.0000	-1.3436
$2 \cdot 10^{-4}$	-3.6990	-1.3491
$5 \cdot 10^{-4}$	-3.3010	-1.3570
$1 \cdot 10^{-3}$	-3.0000	-1.3757
$2 \cdot 10^{-3}$	-2.6990	-1.3750
$5 \cdot 10^{-3}$	-2.3010	-1.3927
$1 \cdot 10^{-2}$	-2.0000	-1.4053
$2 \cdot 10^{-2}$	-1.6990	-1.4195
$5 \cdot 10^{-2}$	-1.3010	-1.4385
$E = -(0.0351 \pm 0.0021) \cdot log\ c - (1.4775 \pm 0.0037)$		

Further potentiometric measurements utilizing the above-mentioned constant slope value of the *E-log c* calibration curve were employed to estimate the efficiency in nanofiltration applied on five model samples containing input zinc concentrations c_i (mg·L^{-1}): 26; 51; 101; 151 and 167 respectively. According to ICP-OES, the corresponding output concentrations c_{out} (mg·L^{-1}) were 0.7; 0.7; 1.3; 1.8 and 1.6 respectively. On the basis of the known input

concentration *ci*, the slope of *E-log c* and the measured potential differences ΔE_i corresponding to every couple of "input-output" of all the samples potentiometrically estimated, the corresponding output concentrations c_{out} were < 2 $mg \cdot L^{-1}$. For all the measurements, calibration or other analyses with the ZnAE were performed without any treatment, maintenance or renewal of its surface during the measurements.

3.3 Characterization of the kinetics of silver particles agglomeration

3.3.1 Background of the study

In recent years, silver nanoparticles or sub-microparticles (or colloidal agglomerates) have gained significant applications in the textile and food industry, pharmaceutical products and household appliances[57]. The colloidal nanosilver solution based on a silver nanomaterial has the potential for practical applications in the anti-bacterial treatment. However, its potential toxicity, content in water and the ratio between the content of silver in colloidal agglomerates in its soluble ionic form Ag^+ has raised an immediate attention of researchers. In fact, thanks to the antibacterial effects, colloidal solutions of nanosilver[58] as disinfectants have been used for centuries to combat infectious diseases, such as traumatic, diabetic or chronic infected wounds[59]. The Woodrow Wilson database contained 259 commercially available products with silver nanoparticles in 2010. The increase in their production[60] resulted in an increased risk of silver toxicity on the environment and potential impacts on human health. Generally, electrochemical composites made of silver powder have proven to be good electrode material[11,12,61-65], usable like mercury[66-69] for the study or analysis of a series of bioactive species.

In the literature, the study of silver nanoparticles or sub-microparticles toxicity has received little attention[70] and results of terrestrial studies as well as laboratory tests of ecotoxicity are unclear[27,71], because the toxicity of silver colloidal agglomerates is obviously influenced by a wide range of factors, such as particle size, ionic composition of the solution, pH, presence of other components of the solution, etc. For instance, the reaction of minor aquatic organisms for the presence of Ag indicates a considerable influence of particle size on the harmful effects of silver colloidal agglomerates. Considering the various factors mentioned above, the size of silver nanoparticles or sub-microparticles and the evaluation of kinetics of the particles growth depending especially on silver concentration and time are of primary importance. Fitting the time-dependence of the silver nanoparticles or sub-microparticles diameter *D* was carried out in the range of 0 to 250 minutes. The aim of the study was to investigate the

concentration and time dependent changes of diameter D using the spectroscopic analysis combined with the atomic force microscopy and dynamic light scattering[23,27].

Preliminary results of monitoring the effects of silver nanoparticles or sub-microparticles on carp embryos indicated that the major effect was observed in solutions of silver concentration > 10 μmol·L^{-1} (abbreviated also μM). It was observed that the strong toxic effects of silver nanoparticles on the embryos occurred owing to the presence of the bigger silver colloidal particles (usually $D \sim 400$ nm or more). Moreover, from the toxicological viewpoint kinetics of particles growth seemed to be significant, as well. For this reason the analysis of tthe ime-dependent growth of silver nanoparticles or sub-microparticles (D versus t) concerning solutions of 25 μM and 50 μM of silver was performed. For the sake of completeness, the changes of $D - t$ for 5 μM and 10 μM of silver nanoparticles were measured, too. The use of silver concentrations (25 μM and 50 μM) caused a primary nucleation of silver nanoparticles. The formation of primary the nucleus was demonstrated using atomic force techniques after application and stabilization of samples on a highly orientated pyrolytic graphite, and subsequent vacuum evaporation of the solvent. The results of atomic force microscopy (AFM) measurements are given in Figure 15, indicating the overall picture of atomic force microscopy and signal profile of the initial size of silver nanoparticles. In comparison with the displayed scale, a relatively sharply defined particle distribution with a diameter of about 50 nm was observed. It was in good agreement with the published studies, for instance, the study on transmission electron spectroscopy[72].

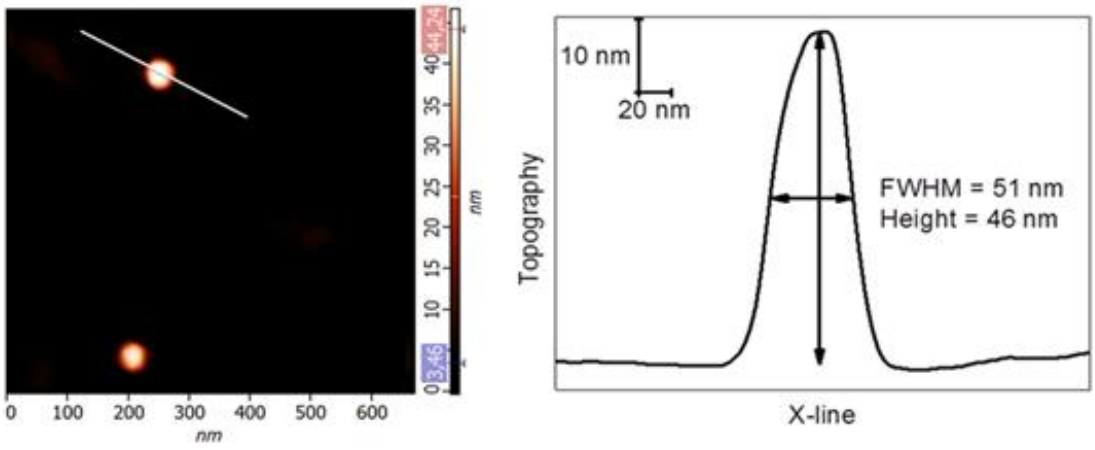

Figure 15 - Atomic force micrograph and signal profile of the initial size of the silver nanoparticles

The dynamic light scattering and its dependency on the diameter *D* of the present particles on time *t* were measured. As shown in Figure 16[22,23,27], significant changes in *D* occurred within the time span of more than 200 minutes approaching their limit values D_{inf} of hundreds of nanometres (nm). As a result of the rapid formation of the primary nucleus at a time t_0 (close to 0 seconds) dependencies in Figure 16 at the beginning did not pass through the point at $D = 0$. The most significant changes to the size *D* on time subsequently occurred in the range between 0 and 100 minutes.

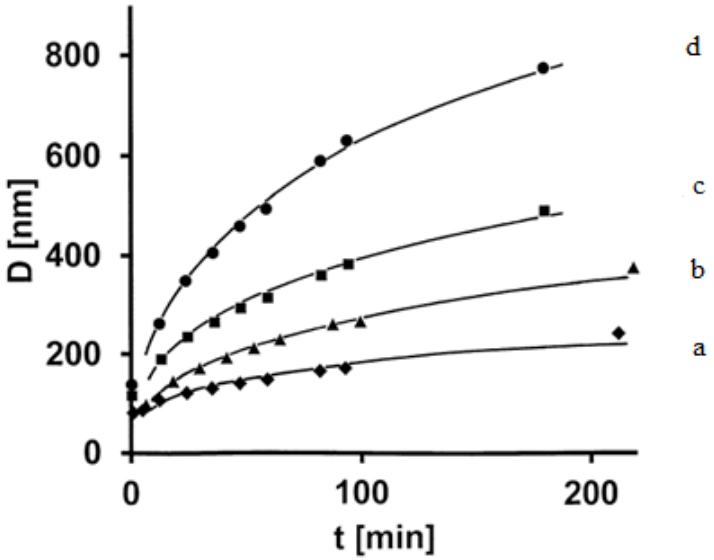

Figure 16 - Kinetics of the growth of silver nanoparticles (diameter *D* versus time *t*) for concentrations of (a) 5 μM (b) 10 μM (c) 25 μM (d) 50 μM

3.3.2 Results and discussion

In this respect, the behaviour of the systems resembled that of the adsorption type of a quantity of surface active species[10] which (under appropriate conditions) provided adsorption isotherms (i.e. dependencies of surface concentration of the substance Γ on its volume concentration *c*) not starting from the beginning of coordinates. In view of this, the analysis of kinetic growth and fitting of the appropriate curves were performed, separately for silver concentrations 25 μM and 50 μM. This was based on the assumption that the changes in *D* with time often correspond approximately to the model (Eq. 30)[27].

$$ln[(D_{inf} - D)/(D_{inf} - D_0)] = -k\,t \qquad \text{Eq. 30}$$

The measured data for 25 μM Ag, the magnitude $y = ln[(D_{inf} - D)/(D_{inf} - D_0)]$ versus t for gradually selected values of D_0 at ($t_0 \to 0$) from 20 nm to 100 nm and $D_{inf} = 510$ nm (estimated from Figure 16) were linearized (Table 3). The optimum linearization

$y = kt + q$, at correlation coefficient R, using OriginPro 7.5 (OriginLab Corporation, USA) was reached at $D_0 = 50$ nm and $D_{inf} = 510$ nm, respectively.

Table 3 - Linearization parameters k, q, R of $y = kt + q$ following Eq. 30; 25 μM Ag; $D_{inf} = 510$ nm; q – intercept

D_0 (nm)	k (min^{-1})	q	R
20	–0.0159±0.0010	–0.0765±0.0754	0.9824
30	–0.0159±0.0010	–0.0601±0.0749	0.9825
40	–0.0159±0.0010	–0.0434±0.0745	0.9826
50	–0.0158±0.0010	–0.0264±0.0742	0.9828
60	–0.0158±0.0010	–0.0090±0.0741	0.9826
70	–0.0157±0.0010	–0.0089±0.0741	0.9825
80	–0.0157±0.0010	–0.0271±0.0742	0.9823
90	–0.0156±0.0010	–0.0457±0.0745	0.9821
100	–0.0156±0.0010	–0.0648±0.0750	0.9818

The extrapolated value of the diameter D_0 corresponded to the above mentioned diameter of the initial nucleus D_0 obtained using atomic force microscopy. Following Eq. 30 for $D_0 = 50$ nm the value of k was -0.0158 ± 0.0010 [min^{-1}] and the intercept q was -0.0264 ± 0.0742. The evaluated uncertainty in values of the mentioned coefficients were apparently associated with the application of other factors (inter-particle interactions, the combination of the type of transport processes, etc.) which influenced the kinetics of the particles growth. Hence, the obtained slopes for k using Eq. 30 represented in fact their average values. For different nature of the nucleation processes close to $t \to 0$ and in opposite to the steady state processes at higher t, the linearization of experimental data was carried out starting from the first experimental value D_1 at t_1 (see the first experimental point in Figure 16). The aim was to obtain parameters k_1, q, R under the steady growth of silver nanoparticles. The model Eq. 31 was utilized.

$$ln[(\Delta D_{inf} - \Delta D_i)/(\Delta D_{inf} - \Delta D_1)] = k_1(t_i - t_1) = k_1 \Delta t_i \quad \text{Eq. 31}$$

where $\Delta D_i = D_i - D_1$, $\Delta t_i = t_i - t_1$, $\Delta D_{inf} = D_{inf} - D_1$. From the experimental data, the values $\Delta y_i = ln[(\Delta D_{inf} - \Delta D_i)/(\Delta D_{inf} - \Delta D_1)]$ vs. $\Delta t_i = t_i - t_1$ were consecutively plotted. Dependencies Δy_i vs. Δt_i were then linearized at different estimated values ΔD_{inf} in the

range of 450 nm to 600 nm. The resulting linearization parameters are summarized in Table 4. They indicated that the optimum linearization was achieved at $\Delta D_{inf} = 480$ nm.

Table 4 - Linearization parameters k_1, q, R of Δy_i vs. Δt_i following Eq. 31 and Figure 16; 25 μM Ag

ΔD_{inf} (nm)	k_1 ($\min^{-1}$)	q	R
450	–0.0096±0.0002	–0.0361±0.0173	0.9958
480	–0.0081±0.0002	–0.0571±0.0145	0.9959
500	–0.0074±0.0002	–0.0649±0.0155	0.9943
550	–0.0061±0.0002	–0.0739±0.0181	0.9887
600	–0.0052±0.0002	–0.0760±0.0193	0.9826

At this optimal value ΔD_{inf} a segmented linearization of Δy_i vs. Δt_i was then applied[73]. It consisted of gradual linearization of segments of Δy_i vs. Δt_i (see Eq. 31 and the points in Figure 16), or more exactly of the following consecutive sets of always five successive points: 1st set $[(0; 0); (\Delta t_1; \Delta y_1); (\Delta t_2; \Delta y_2); (\Delta t_3; \Delta y_3); (\Delta t_4; \Delta y_4)]$; 2nd set $[(\Delta t_1; \Delta y_1); (\Delta t_2; \Delta y_2); (\Delta t_3; \Delta y_3); (\Delta t_4; \Delta y_4); (\Delta t_5; \Delta y_5)]$; 3rd set $[(\Delta t_2; \Delta y_2); (\Delta t_3; \Delta y_3); (\Delta t_4; \Delta y_4); (\Delta t_5; \Delta y_5); (\Delta t_6; \Delta y_6)]$; 4th set $[(\Delta t_3; \Delta y_3); (\Delta t_4; \Delta y_4); (\Delta t_5; \Delta y_5); (\Delta t_6; \Delta y_6); (\Delta t_7; \Delta y_7)]$; 5th set $[(\Delta t_4; \Delta y_4); (\Delta t_5; \Delta y_5); (\Delta t_6; \Delta y_6); (\Delta t_7; \Delta y_7); (\Delta t_8; \Delta y_8)]$. The results of the segmented linearization are shown in Table 5.

Table 5 - Segmented linearization of five sets of $\Delta y_i \; vs. \; \Delta t_i$ data (see points in Figure 16 and Eq. 31), i.e., following consecutive sets of five successive points $(\Delta t_i; y_i)$: 1st set, $i = 1, 2, 3, 4, 5$; 2nd set, $i = 2, 3, 4, 5, 6$; 3rd set, $i = 3, 4, 5, 6, 7$; 4th set, $i = 4, 5, 6, 7, 8$; 5th set, $i = 5, 6, 7, 8, 9$; $\Delta D_{inf} = 480$ nm

Number of sets	$k_1(\min^{-1})$	q	R
1.	–0.0092±0.0007	–0.0258±0.0203	0.9886
2.	–0.0075±0.0004	–0.0799±0.0158	0.9942
3.	–0.0068±0.0001	–0.1101±0.0063	0.9994
4.	–0.0070±0.0001	–0.1049±0.0098	0.9991
5.	–0.0072±0.0001	–0.0899±0.0088	0.9997

This implies that the time constants by (variable Δt) for individual segments were not quite constant in fact since they were more or less changing during the progress of agglomeration (and therefore also with t). It can be assumed that one of the reasons of the variations of k_1 (see Eq. 31) in the case of the different mentioned segments of the given dependence is the fact that the behaviour of the system does not meet exactly the conditions valid for kinetic equations of the first order. The latter equations are rather useful for approximation in the given case. This explanation is consistent with that of the adsorption/agglomeration processes[10,73] at interfaces where strong mutual interactions of particles, reorientation, etc., occurred. For these reasons, the equations (Eq.32) and (Eq.33), originally suggested[10,73] for evaluation of adsorption data could alternatively be applied for fitting or describing of agglomeration processes, as well.

$$f_1(Y)\ exp\ f(Y) = k\,X \qquad \text{Eq.32}$$

$$-ln(1-Y) = K(t)c \qquad \text{Eq.33}$$

where variable $Y = D/D_{inf}$, $X = t$ or $(t-t_1)$, $K = K(t)$, $c = c_0 = \text{constant}$ or $c = c(t)$. Although both concentrations (25 μM Ag and 50 μM Ag) showed similar types of dependences, their parameters were different. Their linearization $ln\left[(D_{inf}-D)/(D_{inf}-D_0)\right]$ versus t according to Eq.30 for selected values of D_0 varying between 20 nm and 100 nm resulted to the estimation of the optimum D_0 between 30 and 50 nm (Table 6).

Table 6 - Linearization parameters k, q, R of $y = kt + q$ following Eq. 30; 50 μM Ag; $D_{inf} = 800$ nm; q – intercept

D_0 (nm)	k (min^{-1})	q	R
20	–0.0176±0.0008	–0.0383±0.0617	0.9901
30	–0.0176±0.0008	–0.0280±0.0615	0.9902
40	–0.0176±0.0008	–0.0176±0.0614	0.9902
50	–0.0175±0.0008	–0.0071±0.0613	0.9902
60	–0.0175±0.0008	–0.0036±0.0613	0.9901
70	–0.0175±0.0008	–0.0144±0.0614	0.9901
80	–0.0175±0.0008	–0.0254±0.0615	0.9900
90	–0.0174±0.0008	–0.0365±0.0617	0.9899
100	–0.0174±0.0008	–0.0478±0.0620	0.9910

For $D_0 = 50$ nm and $D_{inf} = 800$ nm (estimated from Figure 16), the analogous linearization produced the average time constant $k = -0.0175 \pm 0.0008$ [min^{-1} . By plotting the analogous dependencies of $y_i = ln[(\Delta D_{inf} - \Delta D_i)/(\Delta D_{inf} - \Delta D_1)]$ versus $\Delta t_i = t_i - t_1$ for 50 μM Ag and their linearization according to Eq.31 for selected values D_{inf} between 700 and 900 nm produced the data summarized in Table 7. The maximum value of the correlation coefficient R corresponded to the value $\Delta D_{inf} = 700$ nm.

Table 7 - Linearization parameters k_1, q, R of $\Delta y_i \; vs. \; \Delta t_i$ following Eq. 31 and Figure 16; 50 μM Ag

ΔD_{inf} (nm)	k_1(min^{-1})	q	R
700	–0.0131±0.0002	–0.0079±0.0189	0.9986
750	–0.0104±0.0002	–0.0608±0.0177	0.9981
800	–0.0087±0.0003	–0.0823±0.0251	0.9946
850	–0.0076±0.0004	–0.0919±0.0287	0.9907
900	–0.0067±0.0004	–0.0959±0.0302	0.9870

The results of the segmented linearization (similar to Table 7) of Δy_i vs. Δt_i for 50 μM Ag and for $\Delta D_{inf} = 700$ nm are shown in Table 8. In this case the time constant k_1 by variable Δt (in Eq. 31) was to some extent time-dependent, as well.

Table 8 - Segmented linearization of five sets of $\Delta y_i \; vs. \; \Delta t_i$ data (see points in Figure 16 and Eq. 31), i.e., following consecutive sets of five successive points $(\Delta t_i; y_i)$: 1st set, $i = 1, 2, 3, 4, 5$; 2nd set, $i = 2, 3, 4, 5, 6$; 3rd set, $i = 3, 4, 5, 6, 7$; 4th set, $i = 4, 5, 6, 7, 8$; 5th set, $i = 5, 6, 7, 8, 9$; $\Delta D_{inf} = 700$ nm

Number of sets	k_1 (min^{-1})	q	R
1.	–0.0130±0.0007	–0.0252±0.0203	0.9941
2.	–0.0112±0.0006	–0.0817±0.0220	0.9948
3.	–0.0115±0.0005	–0.0782±0.0284	0.9956
4.	–0.0126±0.0006	–0.0209±0.0422	0.9949
5.	–0.0136±0.0003	–0.0563±0.0270	0.9992

Following Eq. 30 the fitting kinetics of silver nanoparticles agglomeration with time was further evaluated using forward stepwise regression analysis[28,29]. The results are shown in Tables 9 to 12 and Figures 17 to 20 respectively.

Table 9 - Regression summary of the dependent variable *y*

N=180	b*	Standard Error of b*	b	Standard Error of b	t-value	p-value α = 0.05
Intercept	-	-	0.013691	0.043637	0.3138	0.754076
t (min)	-0.984674	0.012267	-0.016629	0.000207	-80.2686	0.000000
D_0 (nm)	0.047443	0.012267	0.001610	0.000416	3.8675	0.000155
c_D_{inf} (μM)	-0.041004	0.012267	-0.002875	0.000860	-3.3426	0.001014

N=Number of samples; t = time; D_0 = diameters; c_D_{inf} = concentration at maximum diameters; b* = standardized regression coefficients; b = raw regression coefficeints; t-value = measures the size difference relative to the variation in data; p-value = significance level used for testing a statistical hypothesis; α = significance level

Table 10 - Summary statistics of the dependent variable *y*

Statistic	Value
Multiple R	0.986668451
Multiple R^2	0.973514633
Adjusted R^2	0.973063177
F	2156.39291
p	0.000000
Standard Error	0.144252687

R = Correlation coefficient, R^2 = Coefficient of determination, F-value = value of the F test used in combination with the p-value to measure significance

Table 11 - Regression summary of the dependent variable D_H

N=180	b*	Standard Error of b*	b	Standard Error of b	t-value	p-value α = 0.05
Intercept	-	-	-35.3427	19.15861	-1.84475	0.066746
t (min)	0.824815	0.030784	2.9726	0.11094	26.79324	0.000000
c_D_{inf} (μM)	0.389794	0.030784	5.8325	0.46063	12.66205	0.000000

D_H = hydrodynamic diameter (nm)

Table 12 - Summary statistics of the dependent variable D_H

Statistic	Value
Multiple R	0.912282909
Multiple R^2	0.832260106
Adjusted R^2	0.83036474
F	439.102575
p	0.000000
Standard Error	77.2499755

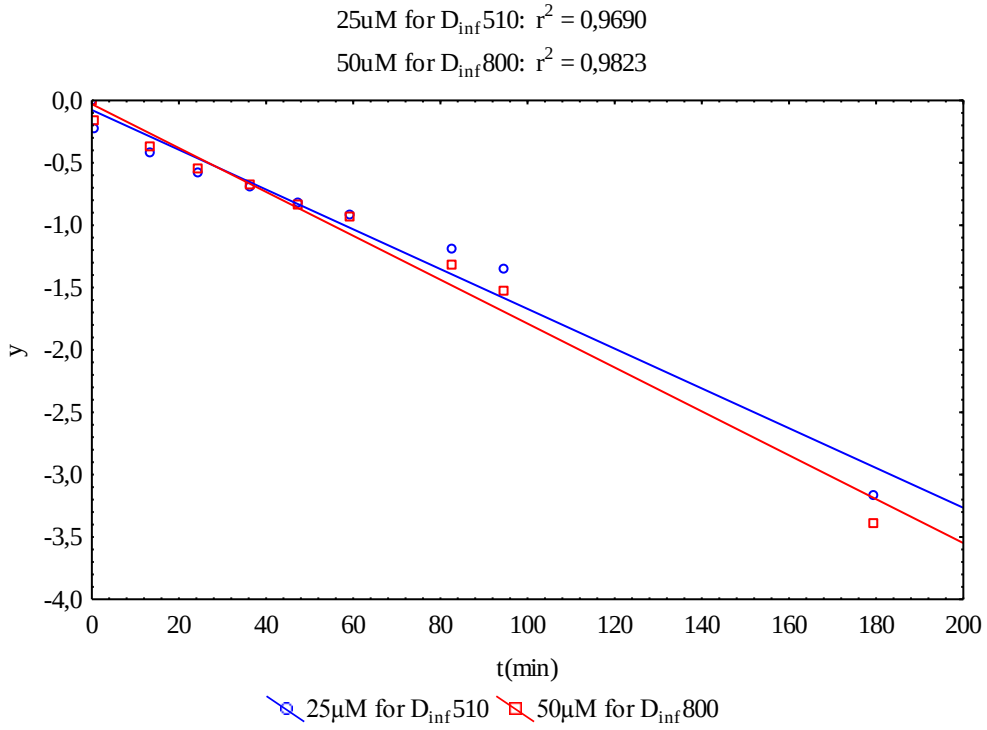

Figure 17 - 2D scatterplots of y versus *t* at D_0 20 (nm) in relation to different concentrations *c* of 25 µm of D_{inf} 510 and 50 µm of D_{inf} 800

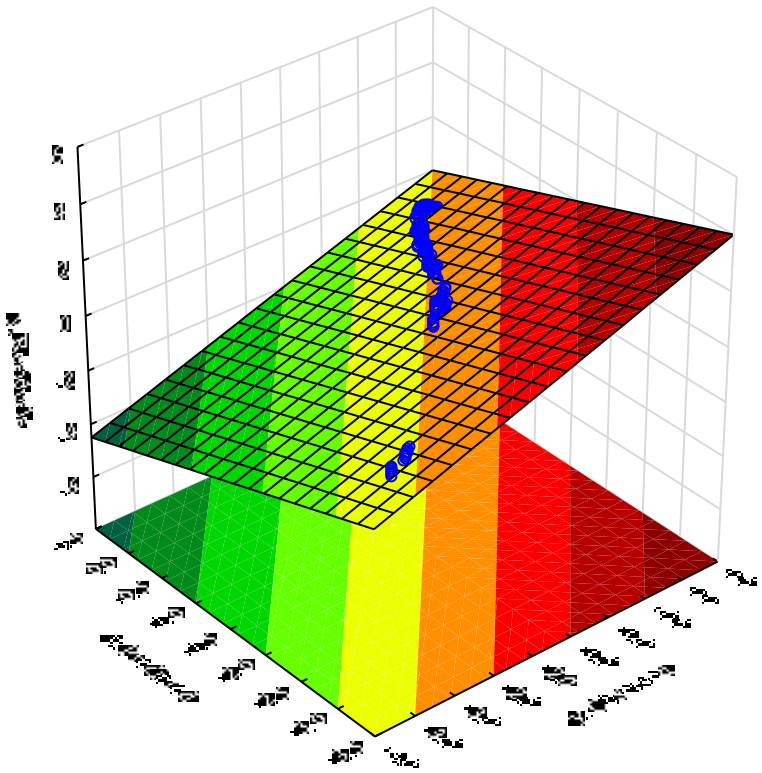

Figure 18 – Dependent variable y observed versus predicted versus residuals

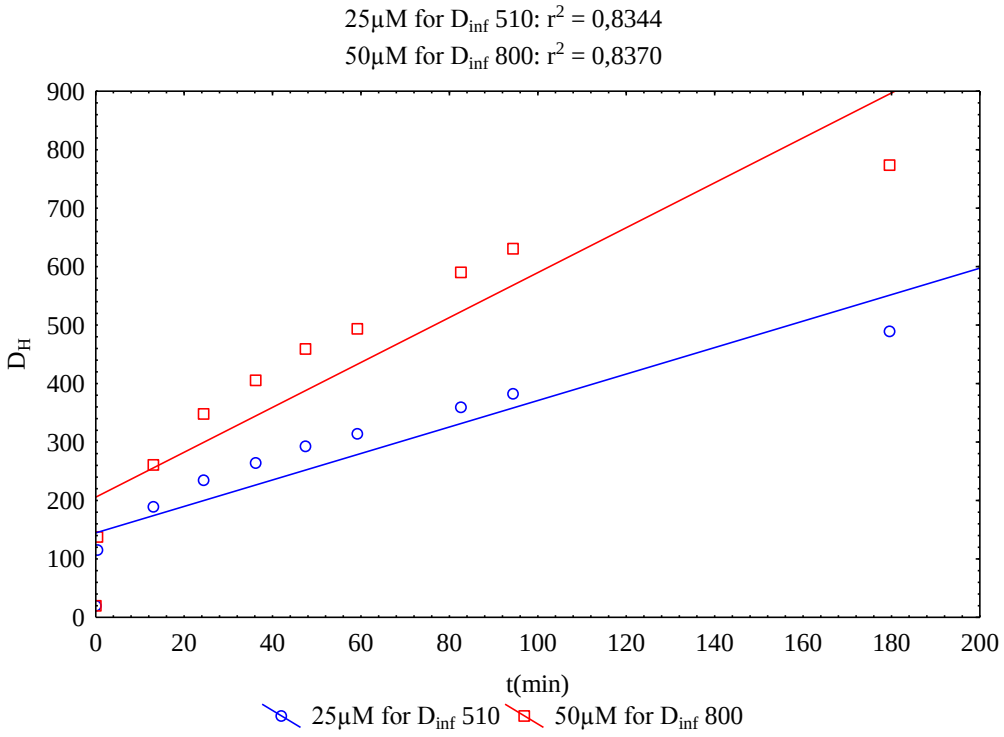

Figure 19 - 2D scatterplots of D_H versus t at D_0 20 (nm) in relation to different concentrations c of 25 µm of D_{inf} 510 and 50 µm of D_{inf} 800

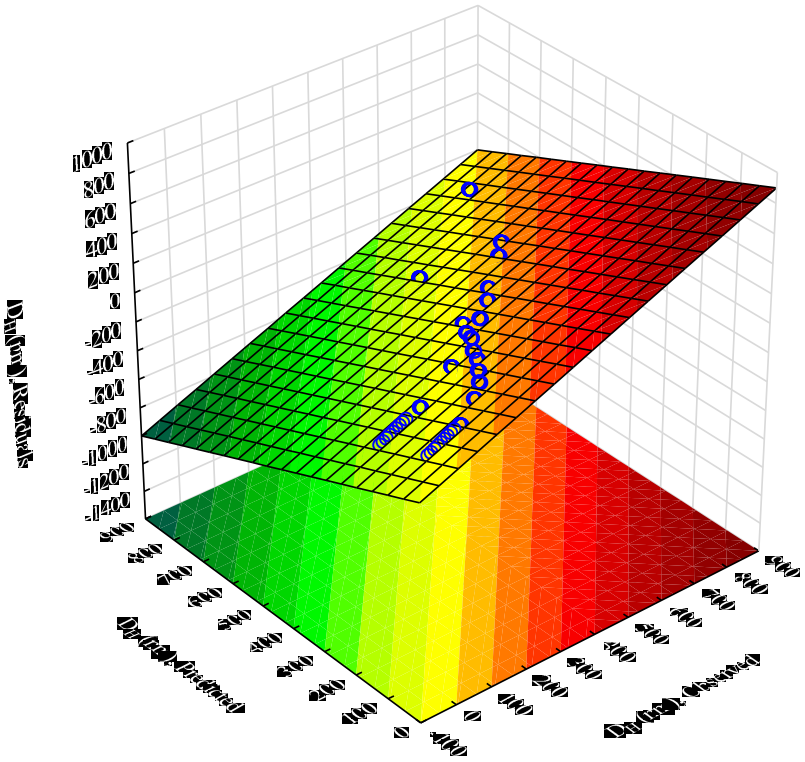

Figure 20 - Dependent variable D_H (nm) observed versus predicted versus residuals

The significance of each regression model coefficients obtained for the dependent variables y and D_H (Tables 9 and 11) was evaluated by the coefficient of determination (R^2), F-value and p-value at the probability level ($\alpha = 0.05$) respectively (Tables 10 and 12). A larger F-value and a smaller p-value explain a more significant effect on the corresponding dependent or response variables. The regression equation obtained for the dependent variable y is given in Eq. 34 as follows:

$$y = 0.013691 - 0.016629 \cdot t + 0.001610 \cdot D_0 - 0.002875 \cdot c \qquad \text{Eq. 34}$$

On the other hand, the regression equation obtained for the dependent variable D_H (nm) is given in Eq. 35 as follows:

$$D_H = -35.3427 + 2.9726 \cdot t + 5.8325 \cdot c \qquad \text{Eq. 35}$$

It is important to mention that for the dependent variable y, all the independent variables examined were statistically significant ($p < 0.05$) (Tables 9 and 10). The independent variable

D_0 was not statistically significant ($p > 0.05$) for describing or predicting the dependent variable D_H (nm), hence it was excluded in the model (Eq. 35).

Figures 17 to 20 show the graphical descriptions of the dependent variables y and D_H for D_0 20 nm for concentrations c at 25 µM for D_{inf} 510 nm and 50 µM for D_{inf} 800 nm. The results were similar to the various diameters at D_0 30, 40, 50, 60, 70, 80, 90 and 100 nm respectively for both concentrations (see Appendix 7.1).

The experimental data (Appendix 7.1) were subjected to further comparative regression analyses, and the results including their graphical representations are given in the Appendix (7.1.1 to 7.1.3) and (7.1.4) respectively. Based on the results, the interaction effects of the independent variables (t and D_0) as well as (D_0 and c_D_{inf}) on the responses (y and D_H) were also not statistically significant in comparison with the interaction effects of (t and c_D_{inf}) which had a significant effect on the above-mentioned responses (see Appendix 7.1.1 to 7.1.3). In addition, the profiles for the predicted values and their desirability based on (Mean and Optimum) set factors of the dependent and independent variables are presented in Appendix (7.1.4 - Figures 42 to 45). The optimum desirability values between 0.564 and 1 were obtained for predicting the responses of y and D_H at different combinations of the independent variables t, D_0 and c. Generally, the desirability values range from 0 to 1; where 0, means undesirable and 1 means very desirable.

The graphical representations of the data by using matrix plots of correlations, histograms, normal probability plots, 2D plots, 3D surface plots and response surface plots (Appendix 7.1.4 - Figures 29 to 45) show the good fit or lack of fit relationship between the dependent (y and D_H) and independent variables (t, D_0 and c).

3.4 Testing possible application of special versions of Novotny generalized isotherms for fitting time-dependent changes of agglomeration of nanoparticles

3.4.1 Background of the study

One of the most interesting results of the nanoparticle research is its success in the accumulation of findings from various disciplines and their rapid application in practice. Recent observations (although in the meantime based on limited data) revealed that agglomeration kinetics, which is closely connected with their respective toxicity, comprises

some useful similarities to the electrosorption of species like sodium thiosulfate. In the past, the study of interactions of thiosulfate ions on charged surfaces was usually associated with their voltammetric determination on the surface of polarized electrodes. Collection of more data and findings on the electrosorption accumulation of the thiosulfate on the electrode could be utilized, for example, in "cathodic stripping voltammetry" (CSV) for its determination. This effect takes place in the potentiostatically initiated electrosorption of thiosulfate and the formation of products of $Hg_2S_2O_3$ at a surface of a mercury electrode[75]. On the other hand, the application of a cathodic potential scan resulted in a reduction of Hg_2^{2+} to Hg. Therefore, CSV-signal of thiosulfate is useful for its analytical determination. Direct indicative of electrocapillary measurements[10,36] proved an adsorption of thiosulfate at potentials more positive than −0.35 V versus (SCE).

More accurate measurements and theoretical considerations[14,76,77] led to the model's relationships which captured much better the complex of present interactions between the particle and the charged interface as well as particle-particle interactions, including the formation of agglomerates of nano dimensions. One of the most up-to-date researches is the study of the formation and behaviour of nano-particles, for example, nanosilver particles[27]. Significant toxic effects of the size of silver nanoparticles have been proved recently. It comprises research on their growth kinetics, dependence on time, concentration and experimental conditions. An essential part of this study is to search for sensitive and effective ways of data fitting and evaluation. In practice, for the growth of the observed agglomerates, the model kinetics of the first order is applied. Such a simple model which is used in a wide-ranging of monitored transformable variables provides only average values of the kinetic parameters. For instance, it does not distinguish the initial formation of the initial aggregates from their next steady growth, hence the application of the present particle-particle and other interactions. Therefore, the study on the adsorption/electro-sorption processes and more or less closer analogies between adsorption and aggregation improved the possibilities of fitting and evaluating (nano) particle agglomeration.

3.4.2 Results and discussion

On the basis of the previously published findings associated with the study of the conditions of determining thiosulfate ions by using adsorptive voltammetry techniques, it can be assumed that for a polarized mercury electrode at potentials around −0.1 V against the

saturated calomel electrode (SCE), specific interactions between the thiosulfate and the electrode surface[10,36] occurred producing $Hg_2(S_2O_3)$. The extent of this effect would have grown fairly well with potentials *E* more positive than –0.1 V versus (SCE). The results indicated the presence of strong particle-particle interactions in the adsorbed $Hg_2(S_2O_3)$-layer. At a constant potential of –0.1 V therefore, using the above-mentioned electrocapillary CCDT technique, a dependence of interfacial tension γ versus the logarithm of the concentration *log c* of the thiosulfate ions was obtained.

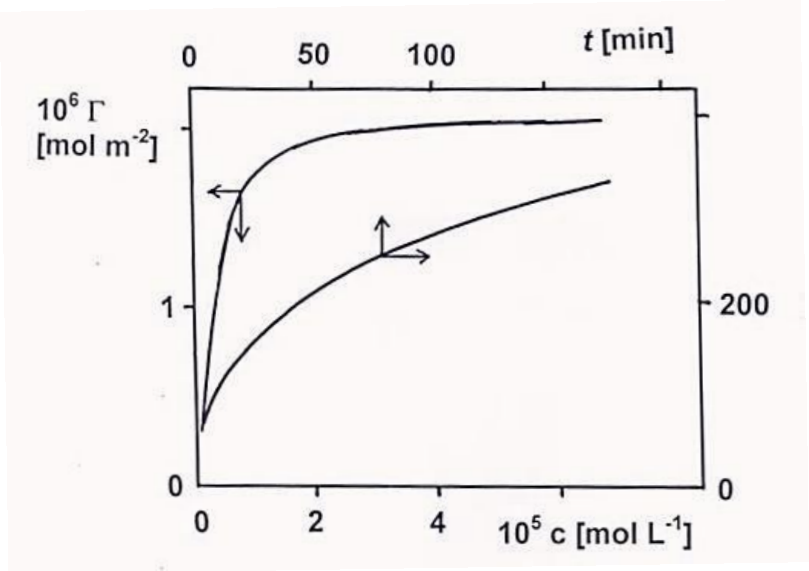

Figure 21 - Adsorption isotherm Γ versus concentration *c* of the thiosulfate; time-dependent changes of diameter *D* of nAg

From the Gibbs-Lippmann equation (Eq. 36)[10,36], the corresponding adsorption isotherm Γ of the thiosulfate, i.e. the dependence of its surface concentration Γ on the volume concentrations *c* (Figure 21) was calculated as follows:

$$d\gamma = -qdE - \Gamma d\mu, \; and \;\; \Gamma = -(d\gamma/d\mu)_E \qquad \text{Eq. 36}$$

where γ, *q*, *E*, Γ and μ denote the interfacial tension, surface charge density, potential, surface concentration (excess) of the adsorbate and the chemical potential, respectively. Under increasing *c*, the Γ versus *c* dependence approached its maximum (limit) value Γ_{max}. Eq.36 can be used to determine the dependence of the relative surface coverage $\theta = \Gamma/\Gamma_{max}$ versus *c*. Using the recent findings, it can be[9,10,76] expressed (or fitted) mathematically, for example, by the model relationship (Eq. 37) as follows:

$$\frac{\theta}{1-\theta} exp\left(-\sum_{1=0}^{n} A_i \theta^i\right) = \beta \, c \qquad \text{Eq. 37}$$

where A_i, i and β denote the coefficients, order of the polynomial term and interaction (adsorption) coefficient. Eq. 37, therefore, represents a special case of its more general form (Eq. 38)[9,10,76] as follows:

$$f_1(Y)exp[f_2(Y)] = kx \; or \; f(X,Y) \qquad \text{Eq. 38}$$

which generally include the functions of (relative) magnitudes defined as the independent (X) and dependent (Y) variables in the following way (Eq.39):

$$X = \frac{x-x_0}{x_m-x_0} \; or \; (x-x_0) \; or \; \frac{x}{x_m}; \; Y = \frac{y-y_0}{y_m-y_0} \; or \; \frac{y}{y_m} \qquad \text{Eq. 39}$$

where x, y, X, Y denote the general or relative magnitudes and x_0, y_0, x_m, y_m are the parameters. The logarithmic and modified equation (Eq. 37)[9,10,76] resulted in Eq. 40 as follows:

$$Z = ln\frac{\theta}{(1-\theta)c} = \sum_{i=0}^{n} A_i\theta^i = A_0 + A_1\theta + A_2\theta^2 + \cdots \qquad \text{Eq. 40}$$

In the case of the thiosulfate, the expressions Z versus θ at various estimated Γ_{max} values are plotted in Figure 22.

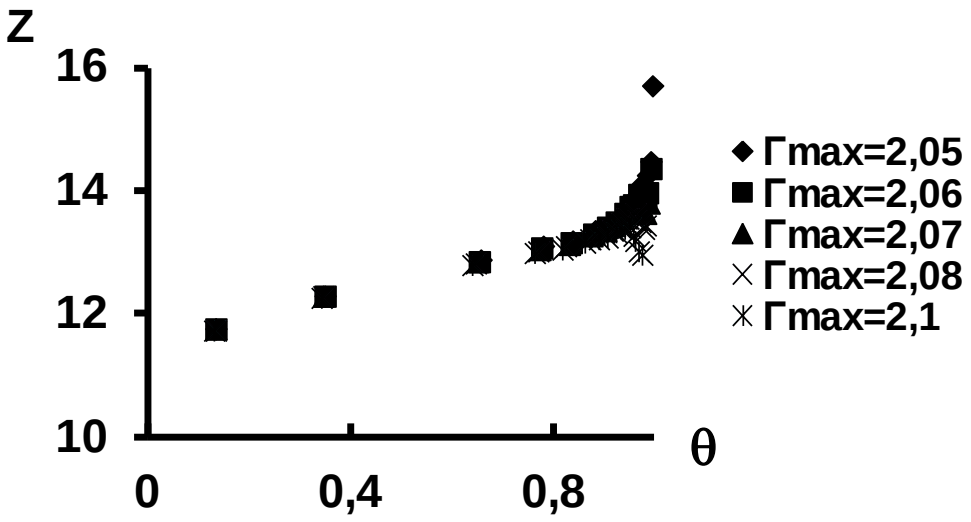

Figure 22 - Dependence of Z versus θ according to equation (Eq.40); adsorption of the sodium thiosulfate at various $\Gamma_{max} \cdot 10^{-6}$ mol.m^{-2}

The optimum fitting of Z versus θ at various Γ_{max} using the quadratic polynomial and based on the maximum correlation coefficient R provided the optimum at $\Gamma_{max} = 2.07 \cdot 10^{-6}$ mol·m^{-2}. The resulting dependence is illustrated in Figure 23.

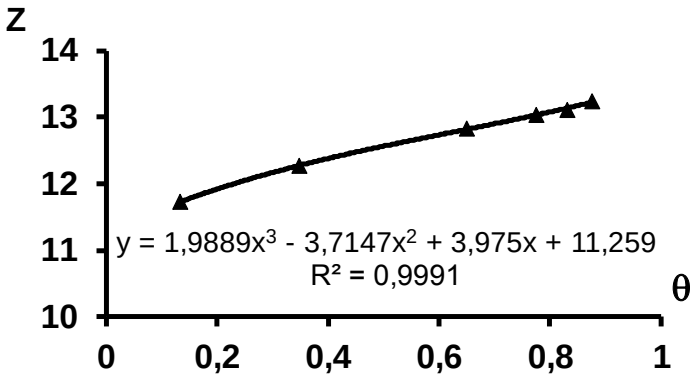

Figure 23 - Dependence of Z versus θ according to equation (Eq.40); adsorption of the sodium thiosulfate at $\Gamma_{max} = 2.07 \cdot 10^{-6}$ mol.m^{-2}

Based on the need for other alternative versions of the general relations, (Eq. 38) could be applied as well. Therefore, this assessment of adsorption data corresponds well to the assumption that due to relatively slow adsorption processes of the analyte at the interface, its concentrations c as well as θ discussed earlier are time-dependent. Taking into account a simple model, the increase in θ with time, i.e. the kinetics, can be expressed as follows:

$$\frac{d\theta}{dt} = K(1-\theta)c \qquad \text{Eq. 41}$$

$$\frac{d\theta}{(1-\theta)} = -dln(1-\theta) = K\,c\,dt \qquad \text{Eq. 42}$$

$$\frac{(1-\theta)}{(1-\theta)_0} = exp(-K't)\ or\ 1-\theta = exp(-K't), K' = K\,c \qquad \text{Eq. 43}$$

$$\frac{(1-\theta)}{(1-\theta)_0} = exp\left(-K\sum_{i=0}^{n} C_i t^{i+1}\right), at\ c = c(t) = c_0 + \sum_{i=1}^{n} c_i t^i, C_0 = c_0 = c_{t=0} \qquad \text{Eq. 44}$$

Assuming a similar model of aggregation of nanoparticles, where the growth of the relative size of the dominant particles D/D_m, their relative volumes V/V_m, etc., at the given conditions can reach their limiting values hence equation (Eqs. 37 to 41) can also be used for fitting and describing the growth of micro-or nano-aggregates. For electrosorption of the thiosulfate, it can be assumed that the initial aggregation step of adsorption of the substance is followed by the increase in θ with an increasing concentration c or with time t. Near $c = 0$ or $t = 0$, the fitting of the obtained dependencies θ versus c or t (especially at small and medium values of

c or *t*) can thus reveal whether or not and to what extent the above-mentioned initial agglomeration processes occurred and how further adsorption process can continue.

Regarding the adsorption of the thiosulfate for both types of processes; the initial agglomeration and the ongoing (steady) adsorption can be affected by applying electric potential *E*. Depending on its value, the extent of initial agglomeration can be significant or negligible, more or less characterized by parameters of θ versus *c* or *t* dependences. Analogously, the description of the agglomeration process of nanoparticles can also comprise the formation of the initial aggregates and subsequent growth of nano- or micro-particles (undergoing a transport mechanism). For silver nanoparticles, it was schematically illustrated by the hydrodynamic diameters *D* versus *t* dependence (see Figures 16 above). Its fitting, based on Eqs. 37 to 40 or 43 and 44 can be applied, as well as, producing the size of the initial diameter D_0 and the parameters of *D=D(t)*. As shown in Figures 24 and 25, Eqs. 45 and 46 can be used to estimate the value of D_0~50 nm corresponding to the best linearity of *Z* versus *Y* in the range of *Y* from 0.1 to 0.4, and to provide optimum fitting of *Y* versus *t* (Figure 26).

$$Z = ln\frac{Y}{(1-Y)t} = \sum_{i=0}^{n} A_i Y^i \, , n = 2 \qquad \text{Eq. 45}$$

$$Y = \frac{\Delta D}{\Delta D_m};\ \Delta D = D - D_0;\ \Delta D_m = D_m - D_0; x = t\ or\ \Delta t \qquad \text{Eq. 46}$$

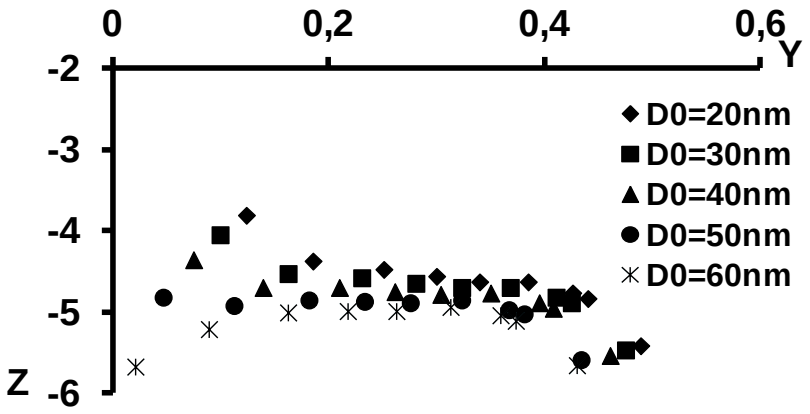

Figure 24 - Z versus *Y* plot at D_m = 400 nm and various values of D_0 (see Eq. 45)

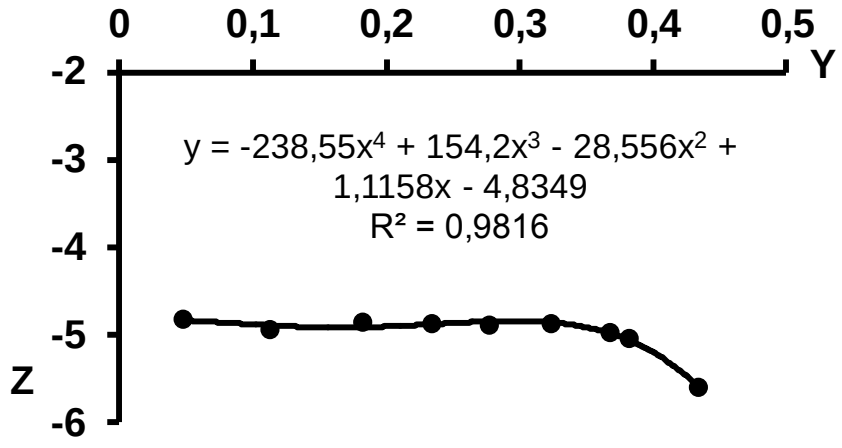

Figure 25 - Fitting *Z* versus *Y* following Eq. 45 at D_0=50 nm and D_m=400 nm

Based on the data for 10 μM Ag and for the above-estimated D_0 = 50 nm and D_m = 400 nm (see Figure 16) the dependencies $y = ln[(D_m–D)/(D_m–D_0)]$ versus $x = t$ could also be linearized as clearly as described in Eq. 47[27].

$$ln\frac{(D_m-D)}{(D_m-D_0)} = -kt \qquad \text{Eq. 47}$$

This linearization $y=k_1x+q$ in Excel provided the values of the parameters *k*, *q* and the correlation coefficient R^2 as shown in Figure 26.

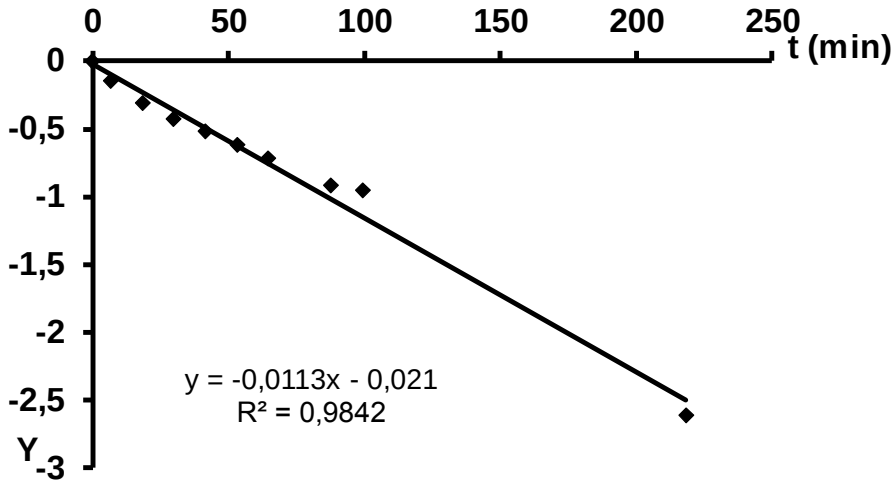

Figure 26 - Linearization $y=k_1x+q$ following Eq. 47; 10 μM Ag; D_0=50 nm; D_m=400 nm

Further, the linearization of the experimental data was repeated excluding the value of D_0 and starting with the first experimental value obtained for D_1 at t_1. The parameter values k_1, q, R^2 evaluated from Eq.48 under steady growth conditions of nAg (excluding D_0) are plotted in Figure 27. For these purposes, Eq. 46 was utilized.

$$ln\frac{(\Delta D_m-\Delta D_i)}{(\Delta D_m-\Delta D_1)} = k_1(t_i - t_1) = k_1\Delta t \qquad \text{Eq. 48}$$

where $\Delta D_i=D_i-D_1$, $\Delta t=t_i-t_1$, $\Delta D_m=D_m-D_1$ are the differences in diameters, time and rate of diameters. From the experimental data, $y_i = ln[(\Delta D_m-\Delta D_i)/(\Delta D_m-\Delta D_1)]$ versus $x_i = t_i-t_1$ was subsequently determined. Dependencies of y_i versus x_i were linearly described at progressively different selected values ΔD_m, in the range of 320 nm to 400 nm. The results indicated that the best linearization was achieved at ΔD_m=360 nm. At this optimum value ΔD_m, a segmented linearization was then applied[14] on y_i versus x_i. The linearization dependencies (y_i versus x_i) were always selected from a group sets of five points: 1st set (x_i;y_i), i from 0 to 4; 2nd set (x_i; y_i), i from 1 to 5; 3rd set (x_i; y_i), i from 2 to 6; 4th set (x_i; y_i), i from 3 to 7; 5th set (x_i; y_i), i from 4 to 8. Results of the segmented linearization are shown in Figure 28.

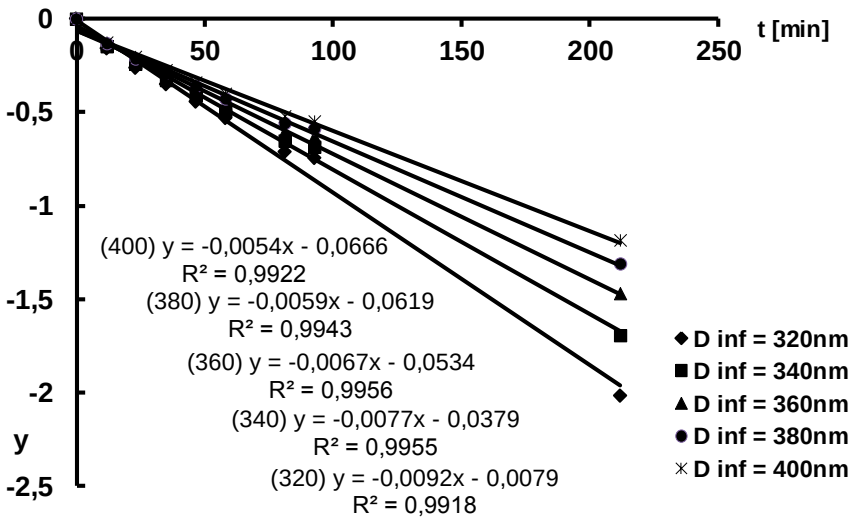

Figure 27 - Linearization of the sets of (x_i; y_i) data following Eq. 48; 10 μM Ag; ΔD_m between 320 nm and 400 nm

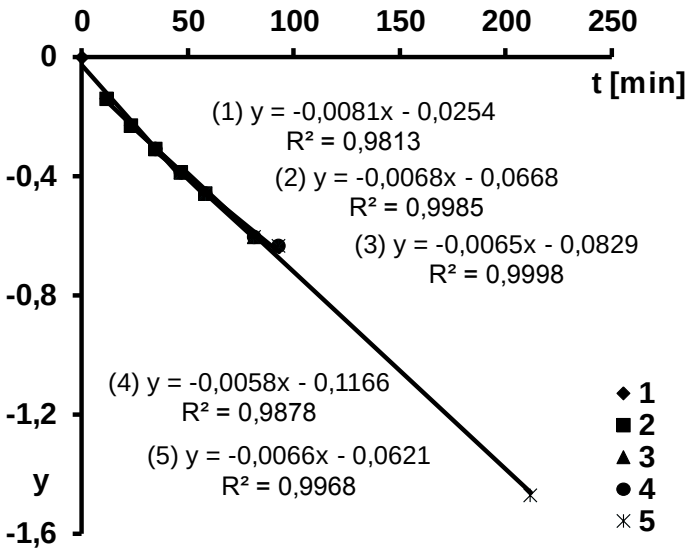

Figure 28 - Linearization of the sets of (x_i; y_i) data following Eq. 48; 10 μM Ag; ΔD_m= 360 nm

This implies that the time constants (by variable x) for the individual segments were not quite constant and were to some extent changing within the progress of agglomeration (also with t). This information was consistent with the assumption on the similarities between aggregation and adsorption processes discussed earlier.

4. CONCLUSIONS

4.1 Utilization of the potential response of the silver amalgam electrodes (AgAE) for assessing the process of ion exchange water treatment and pre-treatment

The study described the results of the changes in the Nernstian potentiometric behaviour of the silver electrode (AgE) and solid silver amalgam electrode (AgAE) for ion exchange water treatment including their pre-treatment. After the addition of $AgNO_3$ to the monitored sequence of water samples *Vi*, the diagrams of the *E* versus *Vi* for AgE and AgAE were measured and plotted. Unlike the AgE, AgAE provided acceptable reproducibility of results, useful for further research and practice, for example, in the field of water treatment monitoring.

4.2 Utilization of the potential signal of the silver amalgam electrodes (AgAE) for estimating changes in the concentration of an aqueous $ZnSO_4$ solution by nanofiltration

Basic potentiometric testing of sensitivity and behaviour of the advanced zinc amalgam electrode (ZnAE) in aqueous solutions of $ZnSO_4$ was reported. The calibrations of mixed potential *E* versus *log c* dependences were obtained. The reproducible linear concentration ranged from $2 \cdot 10^{-5}$ to $5 \cdot 10^{-2}$ mol·L^{-1}. The zinc amalgam electrode (ZnAE) allowed sufficiently sensitive detection of concentration changes of $ZnSO_4$ (from 60 mg·L^{-1} to 2 mg·L^{-1}) corresponding to the use of nanofiltration. Such potentiometric detection carried out in model solutions before and after the nanofiltration steps provided data that were in a reasonable agreement with the analysis of Zn using ICP-OES.

4.3 Characterization of the kinetics of silver particles agglomeration

The study on the analysis of the kinetics of particles growth of electrically charged silver nanoparticles or sub-microparticles of toxic concentrations between 25 and 50 μmol·L was investigated. The analysis and fitting time-dependences of the diameters *D* of the silver colloidal agglomerates employing atomic force microscopy and optical analytical techniques showed significant findings on the behaviour of the silver nanoparticles or sub-microparticles concerning their growth kinetics, maximum diameters D_{inf} and the initial nanoparticles diameters D_0.

4.4 Verification of the possible application of special variants of Novotny generalized isotherm for fitting time changes of the agglomeration of nanoscale particles

The assessment of the agglomeration kinetics of waste nanoparticles based on its partial similarities to the electrosorption processes was discussed. In the case of the agglomeration of silver nanoparticles and the electrosorption of the sodium thiosulfate on the mercury polarized electrode at –0.1 V versus (SCE), specified useful similarities between both types of the processes were presented and applied. Alternative possibilities of fitting and evaluating some kinetic average parameters of aggregation utilizing the recently proposed relationships and isotherms were described.

4.5 Determined regression equations for the dependent variables y and D_H

Regression equations were described for the responses y and D_H in relation to *t*, D_0 and *c* respectively. The models were statistically significant ($p < 0.05$) or (F-value > p-value) with high values of the coefficient of determination (R^2) between 91 and 99 %. It is recommended that replications of the experimental data would be necessary to confirm the present findings established herein.

5. LITERATURE

1. COMNINELLIS, C., CHEN, G. *Electrochemistry for the Environment.* Springer, New York: 2010, 563 p. ISBN 978-0-387-36922-8.
2. KORYTA, J., DVOŘÁK, J. *Principles of Electrochemistry*. J. WILEY & SONS, New York: 1987.
3. SCHOLZ, F. *Electroanalytical Methods*, Springer-Verlag, Berlin: 2002.
4. NOVOTNÝ, L. *Obecná a aplikovaná elektrochemie pro životní prostředí*. Výukové materiály. ÚEnviChI, FCHT, Univerzita Pardubice: 2017.
5. GHERASIM, C. V., HANCKOVÁ, K., PALARČÍK, J., MIKULÁŠEK, P. *J. Membr. Sci.* 2015, 490, 9(15), 46-56. ISSN: 0376-7388.
6. GHERASIM, C. V., MIKULÁŠEK, P. *Desalination* 2014, 343, 67-74. ISSN: 0011-9164.
7. HÜBNER, P. *Úprava vody v energetice.* Praha: Vydavatelství VŠCHT, 2010. ISBN 978-80-7080-746-0.
8. PITTER, P. *Hydrochemie*. 3. dopl. vyd. Praha: Vydavatelství VŠCHT, 1999. 568 s. ISBN 80-03-00525-62.
9. NOVOTNÝ, L. Proceedings: (ŠTULÍK, K., KALVODA, R. Editors). *Electrochemistry for Environmental protection*. UNESCO-ROSTE, Venice: 1996, p. 49-87.
10. NOVOTNÝ, L. Prague, 1998. 695 s. Dr.Sc. Thesis. Acad. Sci. of the Czech Republic.
11. NOVOTNÝ, L., YOSYPCHUK, B. *Chem. Listy* 2000, 94(12), 1118-1120.
12. YOSYPCHUK, B., NOVOTNÝ, L. *Rev. Anal. Chem.* 2002 32, 141-151.
13. ŠELEŠOVSKÁ, R. Pardubice, 2015. Habilitation thesis. Univerzita Pardubice.
14. NOVOTNÝ, L. Úřad průmyslového vlastnictví Praha, UV 2014-30527, 2014.
15. NOVOTNÝ, L. Úřad průmyslového vlastnictví Praha, UV 2007-19501, 2007.
16. NOVOTNÝ, L. Úřad průmyslového vlastnictví Praha, PV 2001-1, 2001.
17. NOVOTNÝ, L. Úřad průmyslového vlastnictví Praha, PVZ 2017-41111, 2018.
18. NOVOTNÝ, L. *ChemZi* 2017, 13(1), p. 204.
19. NOVOTNÝ, L., PETRÁŇKOVÁ, R. *Anal Lett*. 2016, 49(1), 161-168. ISSN: 0003-2719.
20. NOVOTNÝ, L., KABUTEY, A., PETRÁŇKOVÁ, R., LANGÁŠEK, P. Změny nernstovského potenciometrického chování stříbrné a stříbrné amalgámové elektrody během iontoměničových úprav vody. *WASTE FORUM* 2018, 2, 209-213, accepted. ISSN: 1804-0195.
21. NOVOTNÝ, L., KOČANOVÁ, V., KABUTEY, A., KARÁSKOVÁ, A., DUŠEK, L., PETRÁŇKOVÁ, R., MIKULÁŠEK, P. Potentiometric signal of the zinc amalgam

electrode for the detection of concentration changes of zinc sulphate due to its nanofiltration, *WASTE FORUM* 2018, 2, 117-123, 2018, accepted. ISSN: 1804-0.

22. NOVOTNÝ, L., KABUTEY, A., HRDÁ, K. Tentative assessment of the agglomeration kinetics of waste nanoparticles based on its partial similarity to the electrosorption processes. *WASTE FORUM* 2018, 2, 124-131, accepted. ISSN: 1804-0195.
23. NOVOTNÝ, L., OPRŠAL, J., PETRÁŇKOVÁ, R., KABUTEY, A., POUZAR, M., LANGÁŠEK, P. *Anal. Lett.* 2016, 49(1), 152-160. Attainable: https://doi.org/10.1080/00032719.2015.1045587.
24. OPRŠAL, J., POUZAR, M., KNOTEK, P., PETRÁŇKOVÁ, R., NOVOTNÝ, L. Proceedings (FOJTA, M., NAVRÁTIL, T., PIVOŇKOVÁ, H. Editors). *Book of Abstracts of 47th Heyrovsky Discussion.*, 2014, p. 33, ISBN 978-80-87351-29-1.
25. VYTŘAS, K. *Kapitoly ze současné potenciometrie.* 2. dopl. vyd. Praha: ALIT, 1997. 72 s.
26. WANG J. *Analytical Electrochemistry*. VCH Publ., New York: 1994. 193 p. ISBN 1-56081-575-2.
27. OPRŠAL, J., KNOTEK, P., POUZAR, M., PALARČÍK, J., NOVOTNÝ, L. *Chem. Listy* 2013, 107, 386-392. ISSN 0009-2770.
28. KABUTEY, A. *Statistical Analysis of Multivariate Data – Exercises*. Pardubice, 2016. 130 pages. University of Pardubice, Faculty of Chemical Technology, Institute of Environmental and Chemical Engineering. Guarantor: prof. RNDr. Milan Meloun, Dr.Sc.
29. Statsoft, 2013. Inc. Tulsa, OK74104, USA
30. NOVOTNÝ, L. US Patent 5,173,101, 1992.
31. NOVOTNÝ, L. US Patent 5,294,324, 1994.
32. NOVOTNÝ, L. *Chem. Listy* 2001, 95, 147.
33. NOVOTNÝ, L. *XXIX. Moderní elektrochemické metody*, Jetřichovice, 25.5.-29.5.2009, Sborník přednášek (BAREK, J., NAVRÁTIL, T., Editors.), s. 82.
34. NOVOTNÝ, L. *Electroanalysis* 2000, 12, 1240.
35. FRARÈS, N. B., TAHA, S., DORANGE, G. *Desalination* 2005, 185, 245.
36. KRISTA, J., KOPANICA, M., NOVOTNY, L. *Anal. Chim. Acta* 1999, 386, 221.
37. BAREK, J., FISCHER, J., NAVRÁTIL, T., PECKOVÁ, K., YOSYPCHUK, B., ZIMA, J. *Electroanalysis* 2007, 19, 2003.
38. YOSYPCHUK, B., BAREK, J. *Crit. Rev. Anal. Chem*. 2009, 39, 189.
39. DANHEL, A., YOSYPCHUK, B., VYSKOČIL, V., ZIMA, J., BAREK, J. *J. Electroanal. Chem*. 2011, 656, 218.

40. STAHLBUSH, J. R., STROM, R. M. *React. Polym*. 1990, 13, 233.
41. DE DARDEL, F., ARDEN, T. V. *Ion Exchangers*, Wiley-VCH verlag GmbH & Co. KGaA, 2008.
42. JELÍNEK, L. a kol. *Desalinační a separační metody v úpravě vody*. 1. vyd., VŠCHT, Praha 2009.
43. SCHÄFER, A. I., FANE, A. G., WAITE, T. D. *Nanofiltration – Principles and Applications*. Elsevier Ltd., Oxford, UK p 147, 2005.
44. SHAHEEN, S. M., EISSA, F. I., GHANEMB, K. M., GAMAL EL-DINC, H. M., AL ANANYB, F. S. *J. Environ Manage* 2013, 128, 514.
45. VILA, M., SANCHEZ-SALCEDO, S., CICUENDEZ, M., IZQUIERDO-BARBA, I., VALLET-REGI, M. *J. Hazard Mater* 2011, 192, 71.
46. Agency for Toxic Substances and Disease Registry (ATSDR), Regulations and Advisories - Regulations and Guidelines Applicable to Zinc and Zinc Compounds, 2003, http://www.atsdr.cdc.gov/toxprofiles/tp60-c8.pdf.
47. Government Order of the Czech Republic No. 61 of January 29th, 2003. On the indicators and values of permissible pollution of surface water and wastewater, mandatory elements of the permits for discharge of wastewater into surface water and into sewerage systems, and on sensitive areas.
48. CHOO, K. H., KWON, D. J., LEE, K. W., CHOI, S. *J. Environ Sci. Technol*. 2002, 36, 1330.
49. BOURANENE, S., FIEVET, P., SZYMCZYK, A., EL-HADISAMER, M., VODONNE, A. *J. Membr. Sci*. 2008, 325, 150.
50. GONZÁLEZ-MUÑOZ, M. J., RODRÍGUEZ, M. A., LUQUE, S., ÁLVAREZ, J. R. *Desalination* 2006, 200, 742.
51. BELKHOUCHE, N. E., DIDI, M. A., TAHA, S., FARÈS, N. B. *Desalination* 2009, 239, 58.
52. BORBÉLY, G., NAGY, E. *Desalination* 2009, 240, 218.
53. NOVOTNÝ, L., KOČANOVÁ, V., LANGÁŠEK, P., PETRÁŇKOVÁ, R. *XXXV. Modern Electrochemical Methods*, Jetřichovice, 18-22 May 2015, Proceedings (BEST Servis Ústí nad Labem, eds.), p. 108.
54. MONTASER, A., GOLIGHTLY, D. W. *Inductively coupled plasmas in analytical atomic spectrometry*, 3rd edition, VCH Publisher, Inc, New York 1992.
55. WELZ, B., SPERLING, M. *Atomic absorption spectrometry*, 3rd edition, Verlag Chemie, Weinheim:1999.

56. NOVOTNÝ, L. *Fresenius J. Anal. Chem*. 1998, 342, 184.
57. WIJNHOVEN, S. W. P., PEIJNENBURG, J. G. M., HERBERTS, C. A., HAGENS, W. I., OOMEN, A. G., HEUGENS, E. H. W., ROSZEK, B. *Nanotoxicology* 2009, 3: 109-138. doi:10.1080/17435390902725914.
58. LEE, S. M., SONG, K. C., LEE, B. S. *Korean Journal of Chemical Engineering* 2010, 27: 688-692. doi:10.1007/s11814-010-0067-0.
59. NOWACK, B., KRUG, H. F., HEIGHT, M. *Environmental Science & Technology* 2011, 45: 1177–1183. doi:10.1021/es200435m.
60. RIBEIRO, F., GALLEGO-URREA, J. A., JURKSCHAT, K., CROSSLEY, A., HASSELLOV, M., TAYLOR, C., SOARES, A. M. V. M., LOUREIRO, S. *Science of the Total Environment* 2014, 466-467: 232-241. doi:10.1016/j.scitotenv.2013.06.101.
61. BANDŽUCHOVA, L., ŠELEŠOVSKA, R., NAVRATIL, T., CHYLKOVA, J. *Electroanalysis* 2013, 25: 213-222. doi:10.1002/elan.201200365.
62. FADRNA, R., CAHOVA-KUCHARIKOVA, K., HAVRAN, L., YOSYPCHUK, B., FOJTA, M. *Electroanalysis* 2005, 17: 452-59. doi:10.1002/elan.200403181.
63. NAVRATIL, T., BAREK, J. *Critical Reviews in Analytical Chemistry* 2009, 39:131-147. doi:10.1080/10408340903011796.
64. SELESOVSKA, R., BANDZUCHOVA, L., NAVRATIL, T., CHYLKOVA, J. *Electrochimica Acta* 2012, 60: 375-383. doi:10.1016/j.electacta.2011.11.071.
65. YOSYPCHUK, B., BAREK, J. *Critical Reviews in Analytical Chemistry* 2009, 39:189–203. doi:10.1002/chin.200944275.
66. POLASKOVA, P., NOVOTNY, L., OSTATNA, V., PALECEK, E. *Electroanalysis* 2009, 21: 625-630. doi:10.1002/elan.200804459.
67. VESELA, H., SUCMAN, E. *Acta Veterinaria Brno* 2013a, 82: 203–208. doi:10.2754/avb201382020203.
68. VESELA, H., SUCMAN, E. *Czech Journal of Food Science* 2013b, 31:401-06.
69. HEYROVSKÝ, J., KŮTA, J. *Principles of polarography*, Publishing House of the Czech Acad. Sci, Prague 1965.
70. OBERDORSTER, E. *Environmental Health Perspectives* 2004, 112: 1058. doi:10.1289/ehp.7021.
71. ROMER, I., WHITE, T. A., BAALOUSHA, M., CHIPMAN, J. K., VIANT, M. R., LEAD, J. R. *Journal of Chromatography A.* 2011, 1218: 4226-4233. doi:10.1016/j.chroma.2011.03.034.

72. GUZMAN, M. G., DILLE, J., GODET, S. *International Journal of Chemical and Biomolecular Engineering*. 2009, 2:104-111.
73. NOVOTNY, L. *Book of Abstracts of the 15th International Conference on Electroanalysis*, (2014a), Malmo, Sweden, June 11-15, 2014, 189.
74. NOVOTNY, L. *Chem. Listy*. 2014b, 108: 777.
75. CIGLENECKI, I., COSOVIC, B. *Electroanalysis* 1997, *9*, 775.
76. NOVOTNÝ, L. *69. Zjazd chemikov, Vysoké Tatry 11-15 September 2017*, (ChemZi 13/1, Slovenská chemická spoločnosť, ed.), str. 203, 2017.
77. NOVOTNÝ, L. *XXXVI. Modern Electrochemical Methods,* Jetřichovice, 23-27 May 2016, Proceedings (BEST Servis Ústí n. L, ed.), p. 152.

6. PUBLICATION ACTIVITIES

6.1 Papers

1. NOVOTNÝ, L., OPRŠAL, J., PETRÁŇKOVÁ, R., KABUTEY, A., POUZAR, M., LANGÁŠEK, P. *Anal. Lett.* 2016, 49(1), 152-160. Attainable: https://doi.org/10.1080/00032719.2015.1045587.
2. NOVOTNÝ, L., KABUTEY, A., PETRÁŇKOVÁ, R., LANGÁŠEK, P. Změny nernstovského potenciometrického chování stříbrné a stříbrné amalgámové elektrody během iontoměničových úprav vody. *WASTE FORUM* 2018, 2, 209-213, accepted. ISSN: 1804-0195.
3. NOVOTNÝ, L., KABUTEY, A., HRDÁ, K. Tentative assessment of the agglomeration kinetics of waste nanoparticles based on its partial similarity to the electrosorption processes. *WASTE FORUM* 2018, 2, 124-131, accepted. ISSN: 1804-0195.
4. NOVOTNÝ, L., KOČANOVÁ, V., KABUTEY, A., KARÁSKOVÁ, A., DUŠEK, L., PETRÁŇKOVÁ, R., MIKULÁŠEK, P. Potentiometric signal of the zinc amalgam electrode for the detection of concentration changes of zinc sulphate due to its nanofiltration, *WASTE FORUM* 2018, 2, 117-123, 2018, accepted. ISSN: 1804-0.

6.2 Oral presentations

5. KABUTEY, A., NOVOTNÝ, L., PETRÁŇKOVÁ, R. Application of potentiometric analytical technique for heavy metals determination. *E.I.D.S. Summer Workshop*, Aveiro, Portugal, 26.4.-2.5.2015.
6. KABUTEY, A., NOVOTNÝ, L., PETRÁŇKOVÁ, R., KOČANOVÁ, V., WALLACE, E. *Proc. of the 3rd Int. Conf. Chem. Technol.* 1st ed. Prague (KALENDA, P., LUBOJACKÝ, J. Editors). Czech Society of Industrial Chemistry, 2015, Annex. ISBN: 978-80-86238-79-1.

6.3 Proceedings of conferences, posters

7. NOVOTNÝ, L., DUŠEK, L., VYSTRČILOVÁ, B., PETRÁŇKOVÁ, R., KABUTEY, A. *Chem. Listy* 2012, 106, 601, ISSN 1213-7103.
8. NOVOTNÝ, L., PETRÁŇKOVÁ, R., KABUTEY, A. *ChemZi* 2013, 9(1), 231. ISSN 1336-7242.
9. NOVOTNÝ, L., PETRÁŇKOVÁ, R., OPRŠAL, J., KABUTEY, A., POUZAR, M. *13th Workshop of physical chemists and electrochemists: sborník příspěvků 29.-30.5.2013*. Brno: Masarykova univerzita, 2013, p. 156-157. ISBN 978-80-7375-757-1.

10. NOVOTNÝ, L., LANGÁŠEK, P., PETRÁŇKOVÁ, R., KABUTEY, A. *Chem. Listy* 2014, 108(8), 795. ISSN 0009-2770.
11. NOVOTNÝ, L., PETRÁŇKOVÁ, R., OPRŠAL, J., KABUTEY, A., POUZAR, M. *Proc. of the 15th Int. Conf.* Malmö, 2014 (ESEAC, eds.), p. 199.
12. NOVOTNÝ, L., PETRÁŇKOVÁ, R., KABUTEY, A. *Sborník přednášek XXXIV. Moderní Elektrochemické Metody*. 2014 (BEST Servis Ústí n. L., ed.), s. 118-120. ISBN 978-80-905221-2-1.
13. NOVOTNÝ, L., LANGÁŠEK, P., PETRÁŇKOVÁ, R., KOČANOVÁ, V., KABUTEY, A., DUŠEK, L. *ChemZi* 2015, 11(1), 170. ISSN 1336-7242.
14. KABUTEY, A, NOVOTNÝ, L., KOČANOVÁ, V., PETRÁŇKOVÁ, R., LANGÁŠEK, P., WALLACE, E., DUŠEK, L. *ChemZi* 2015, 11(1), 170. ISSN 1336-7242.
15. NOVOTNÝ, L., KOČANOVÁ, V., DUŠEK, L., KABUTEY, A., PETRÁŇKOVÁ, R., KARÁSKOVÁ, A. *Sborník přednášek XXXVI. Moderní Elektrochemické Metody*. 2016, p. 155-157, ISBN 978-80-905221-4-5.
16. NOVOTNÝ, L., KOČANOVÁ, V., KABUTEY, A., DUŠEK, L. *Sborník příspěvků 68. sjezd chemiků*. Praha, 2016, p. 191, 1P-14. ISSN 2336-7202.
17. NOVOTNÝ, L., KOČANOVÁ, V., DUŠEK, L., KABUTEY, A., MIKULÁŠEK, P., PETRÁŇKOVÁ, R., KARÁSKOVÁ, A. *ChemZi* 2017, 13(1), p. 203.
18. NOVOTNÝ, L., KARÁSKOVÁ, A., KABUTEY, A., PETRÁŇKOVÁ, R. *Sborník přednášek XXXVIII. Moderní Elektrochemické Metody*. 2018 (BEST Servis Ústí n. L. ed.), p. 183-186, ISBN 978-80-905221-6-9.
19. NOVOTNÝ, L., KOČANOVÁ, V., KABUTEY, A., KARÁSKOVÁ, A., DUŠEK, L., PETRÁŇKOVÁ, R., MIKULÁŠEK, P. *Proc. of the 17th Int. Conf.* Rhodes, 2018 (ESEAC, eds.), p. 159.
20. NOVOTNÝ, L., KABUTEY, A., KARÁSKOVÁ, A., KOČANOVÁ, V., MIKULÁŠEK, P. *Proc. of the 17th Int. Conf.* Rhodes, 2018 (ESEAC, eds.), p. 224.

6.4 Seminar/Symposium

21. Eastern Analytical Symposium, 18.11. – 20.11.2013, New Jersey, USA.
22. Scientific Writing and Academic Conference, University of Pardubice, 24.11.–25.11.2014, Pardubice, Czech Republic.

7. APPENDIX

7.1 Statistical data processing

Table 13 – Content of silver in a solution containing nAg of 25 μmol·L^{-1}

D_{inf} = 510	D_0=20	D_0=20	D_0=30	D_0=30	D_0=40	D_0=40
t [min]	D_H [nm]	y	D_H [nm]	y	D_H [nm]	y
0	20	0	30	0	40	0
0.42	115.41	-0.22	115.41	-0.20	115.41	-0.17
13.07	189.04	-0.42	189.04	-0.40	189.04	-0.38
24.43	234.55	-0.58	234.55	-0.56	234.55	-0.53
36.13	264.05	-0.69	264.05	-0.67	264.05	-0.65
47.44	292.92	-0.81	292.92	-0.79	292.92	-0.77
59.19	314.07	-0.92	314.07	-0.90	314.07	-0.87
82.57	359.78	-1.18	359.78	-1.16	359.78	-1.14
94.41	382.40	-1.35	382.40	-1.32	382.40	-1.30
179.54	489.35	-3.17	489.35	-3.15	489.35	-3.13

D_0 = Diameters, D_{inf}, 500 = Maximum/optimum diameters, t (time), y = Linearization term, D_H = Hydrodynamic diameter, nAg = Silver nanoparticles

Table 14 – Content of silver in a solution containing nAg of 25 μmol·L^{-1}

D_{inf} = 510	D_0=50	D_0=50	D_0=60	D_0=60	D_0=70	D_0=70
t [min]	D_H [nm]	y	D_H [nm]	y	D_H [nm]	y
0	50	0	60	0	70	0
0.42	115.41	-0.15	115.41	-0.13	115.41	-0.11
13.07	189.04	-0.36	189.04	-0.34	189.04	-0.32
24.43	234.55	-0.51	234.55	-0.49	234.55	-0.47
36.13	264.05	-0.63	264.05	-0.60	264.05	-0.58
47.44	292.92	-0.75	292.92	-0.73	292.92	-0.71
59.19	314.07	-0.85	314.07	-0.83	314.07	-0.81
82.57	359.78	-1.12	359.78	-1.10	359.78	-1.07
94.41	382.40	-1.28	382.40	-1.26	382.40	-1.24
179.54	489.35	-3.10	489.35	-3.08	489.35	-3.06

Table 15 – Content of silver in a solution containing nAg of 25 μmol·L^{-1}

D_{inf} = 510	D_0=80	D_0=80	D_0=90	D_0=90	D_0=100	D_0=100
t [min]	D_H [nm]	y	D_H [nm]	y	D_H [nm]	y
0	80	0	90	0	100	0
0.42	115.41	-0.09	115.41	-0.06	115.41	-0.04
13.07	189.04	-0.29	189.04	-0.27	189.04	-0.24
24.43	234.55	-0.45	234.55	-0.42	234.55	-0.40
36.13	264.05	-0.56	264.05	-0.54	264.05	-0.51
47.44	292.92	-0.68	292.92	-0.66	292.92	-0.64
59.19	314.07	-0.79	314.07	-0.76	314.07	-0.74
82.57	359.78	-1.05	359.78	-1.03	359.78	-1.00
94.41	382.40	-1.21	382.40	-1.19	382.40	-1.17
179.54	489.35	-3.04	489.35	-3.01	489.35	-2.99

Table 16 – Content of silver in a solution containing nAg of 50 μmol·L^{-1}

D_{inf} = 510	D_0=20	D_0=20	D_0=30	D_0=30	D_0=40	D_0=40
t [min]	D_H [nm]	y	D_H [nm]	y	D_H [nm]	y
0	20	0	30	0	40	0
0.42	137.99	-0.16	137.99	-0.15	137.99	-0.14
13.07	260.99	-0.37	260.99	-0.36	260.99	-0.34
24.43	348.16	-0.55	348.16	-0.53	348.16	-0.52
36.13	405.29	-0.68	405.29	-0.67	405.29	-0.66
47.44	459.08	-0.83	459.08	-0.81	459.08	-0.80
59.19	493.94	-0.94	493.94	-0.92	493.94	-0.91
82.57	590.05	-1.31	590.05	-1.30	590.05	-1.29
94.41	630.67	-1.53	630.67	-1.51	630.67	-1.50
179.54	773.53	-3.38	773.53	-3.37	773.53	-3.36

Table 17 – Content of silver in a solution containing nAg 50 μmol·L^{-1}

D_{inf} = 510	D_0=50	D_0=50	D_0=60	D_0=60	D_0=70	D_0=70
t [min]	D_H [nm]	y	D_H [nm]	y	D_H [nm]	y
0	50	0	60	0	70	0
0.42	137.99	-0.12	137.99	-0.11	137.99	-0.10
13.07	260.99	-0.33	260.99	-0.32	260.99	-0.30
24.43	348.16	-0.51	348.16	-0.49	348.16	-0.48
36.13	405.29	-0.64	405.29	-0.63	405.29	-0.61
47.44	459.08	-0.79	459.08	-0.78	459.08	-0.76
59.19	493.94	-0.90	493.94	-0.88	493.94	-0.87
82.57	590.05	-1.27	590.05	-1.26	590.05	-1.25
94.41	630.67	-1.49	630.67	-1.47	630.67	-1.46
179.54	773.53	-3.34	773.53	-3.33	773.53	-3.32

Table 18 – Content of silver in a solution containing nAg 50 μmol·L^{-1}

D_{inf} = 510	D_0=80	D_0=80	D_0=90	D_0=90	D_0=100	D_0=100
t [min]	D_H [nm]	y	D_H [nm]	y	D_H [nm]	y
0	80	0	90	0	100	0
0.42	137.99	-0.08	137.99	-0.07	137.99	-0.06
13.07	260.99	-0.29	260.99	-0.28	260.99	-0.26
24.43	348.16	-0.47	348.16	-0.45	348.16	-0.44
36.13	405.29	-0.60	405.29	-0.59	405.29	-0.57
47.44	459.08	-0.75	459.08	-0.73	459.08	-0.72
59.19	493.94	-0.86	493.94	-0.84	493.94	-0.83
82.57	590.05	-1.23	590.05	-1.22	590.05	-1.20
94.41	630.67	-1.45	630.67	-1.43	630.67	-1.42
179.54	773.53	-3.30	773.53	-3.29	773.53	-3.28

7.1.1 Standard regression analysis

Table 19 - Mean and Standard Deviations of variables

Variables	Means	Standard Deviation	Number
t (min)	53.72000	52.04322	180
D_0 (nm)	60.00000	25.89191	180
c_D_{inf} (μM)	37.50000	12.53487	180
y	-0.89083	0.87892	180

Table 20 – Correlations of variables

Variables	t (min)	D_0 (nm)	c_D_{inf} (μM)	y
t (min)	1.000000	0.000000	0.000000	-0.984674
D_0 (nm)	0.000000	1.000000	-0.000000	0.047443
c_D_{inf} (μM)	0.000000	-0.000000	1.000000	-0.041004
y	-0.984674	0.047443	-0.041004	1.000000

Table 21 - Regression summary of the dependent variable *y*

N=180	b*	Standard Error of b*	b	Standard Error of b	t-value	p-value ($\alpha = 0.05$)
Intercept	-	-	0.013691	0.043637	0.3138	0.754076
t (min)	-0.984674	0.012267	-0.016629	0.000207	-80.2686	0.000000
D_0 (nm)	0.047443	0.012267	0.001610	0.000416	3.8675	0.000155
c_D_{inf} (μM)	-0.041004	0.012267	-0.002875	0.000860	-3.3426	0.001014

N=Number of samples; t = time; D_0 = diameters; c_D_{inf} = concentration of diameters; b* = standardized regression coefficients; b = raw regression coefficeints; t-value = measures the size difference relative to the variation in data; p-value = significance level used for testing a statistical hypothesis; α = significance level

Table 22 - Summary statistics of the dependent variable *y*

Statistic	Value
Multiple R	0.986668451
Multiple R^2	0.973514633
Adjusted R^2	0.973063177
F	2156.39291
p	0.000000
Standard Error	0.144252687

R = Correlation coefficient, R^2 = Coefficient of determination, F-value = value of the F test used in combination with the p-value to measure significance

Table 23 - Mean and Standard Deviations of variables

Variables	Means	Standard Deviation	Number
t (min)	53.7200	52.0432	180
D_0 (nm)	60.0000	25.8919	180
c_D_{inf} (μM)	37.5000	12.5349	180
D_H (nm)	343.0635	187.5600	180

Table 24 - Correlations of variables

Variables	t (min)	D_0 (nm)	c_D_{inf} (μM)	D_H (nm)
t (min)	1.000000	0.000000	0.000000	0.824815
D_0 (nm)	0.000000	1.000000	-0.000000	0.013805
c_D_{inf} (μM)	0.000000	-0.000000	1.000000	0.389794
D_H (nm)	0.824815	0.013805	0.389794	1.000000

Table 25 - Regression summary of the dependent variable D_H (nm)

N=180	b*	Standard Error of b*	b	Standard Error of b	t-value	p-value (α = 0.05)
Intercept	-	-	-41.3427	23.42131	-1.76518	0.079268
t (min)	0.824815	0.030854	2.9726	0.11120	26.73263	0.000000
D_0 (nm)	0.013805	0.030854	0.1000	0.22351	0.44741	0.655127
c_D_{inf} (μM)	0.389794	0.030854	5.8325	0.46167	12.63341	0.000000

Table 26 - Summary statistics of the dependent variable D_H (nm)

Statistic	Value
Multiple R	0.912387348
Multiple R^2	0.832450673
Adjusted R^2	0.829594719
F	291.478975
p	0.000000
Standard Error	77.4251065

7.1.2 Polynomial regression analysis

Table 27 - Statistical values of the polynomial regression analysis of the dependent variable y

Effect	*Regression equation y	Standard Error	t-value	p-value ($\alpha = 0.05$)
Intercept	-0.113971	0.041142	-2.7702	0.006211
t (min)	-0.010294	0.000363	-28.3229	0.000000
t $(min)^2$	-0.000037	0.000002	-18.4871	0.000000
D_0 (unit)	0.001427	0.001311	1.0886	0.277847
D_0 $(unit)^2$	0.000002	0.000011	0.1422	0.887053
c_Dinf (µM)	-0.002875	0.000502	-5.7222	0.000000
c_Dinf $(\mu M)^2$	0.000000	-	-	-

* Polynomial function of second degree

Table 28 - Statistical values of the polynomial regression analysis of the dependent variable D_H (nm)

Effect	*Regression equation D_H (nm)	Standard Error	t-value	p-value ($\alpha = 0.05$)
Intercept	-104.094	26.37639	-3.9465	0.000115
t (min)	5.981	0.23301	25.6695	0.000000
t $(min)^2$	-0.018	0.00129	-13.6936	0.000000
D_0 (unit)	0.100	0.84057	0.1190	0.905438
D_0 $(unit)^2$	0.000	0.00688	0.0000	1.000000
c_Dinf (µM)	5.833	0.32213	18.1062	0.000000
c_Dinf $(\mu M)^2$	0.000	-	-	-

* Polynomial function of second degree

Table 29 - Statistical values of the whole model polynomial regression analysis

Dependent variables	F-value	p-value	R^2
y	3860.142	< 0.05	0.991
D_H (nm)	396.733	< 0.05	0.919

7.1.3 Response surface regression analysis

Table 30 - Statistical values of the response surface regression analysis for y

Effect	Regression equation y	Standard Error	t-value	p-value ($\alpha = 0.05$)
Intercept	-0.311584	0.054526	-5.7145	0.000000
t (min)	-0.007933	0.000492	-16.1360	0.000000
t $(min)^2$	-0.000037	0.000002	-22.0212	0.000000
D_0 (unit)	0.002416	0.001277	1.8913	0.060281
D_0^2 (unit)	0.000002	0.000009	0.1694	0.865656
c_Dinf (µM)	0.002701	0.001153	2.3429	0.020287
c_Dinf ^{2} (µM)	0.000000	-	-	-
t (min· D_0 (unit)	0.000004	0.000004	0.9070	0.365670
t (min)·c_Dinf (µM)	-0.000069	0.000008	-8.4469	0.000000
D_0 (unit)·c_Dinf (µM)	-0.000031	0.000016	-1.9265	0.055705

Table 31 - Statistical values of the response surface regression analysis for D_H (nm)

Effect	Regression equation D_H (nm)	Standard Error	t-value	p-value ($\alpha = 0.05$)
Intercept	16.62776	26.67022	0.6235	0.533814
t (min)	3.73399	0.24049	15.5267	0.000000
t $(min)^2$	-0.01772	0.00083	-21.3794	0.000000
D_0 (unit)	0.20714	0.62478	0.3315	0.740637
D_0^2 (unit)	-0.00000	0.00441	-0.0000	1.000000
c_Dinf (µM)	2.44184	0.56397	4.3298	0.000025
c_Dinf ^{2} (µM)	0.00000	-	-	-
t (min· D_0 (unit)	-0.00199	0.00192	-1.0363	0.301537
t (min)·c_Dinf (µM)	0.06312	0.00398	15.8765	0.000000
D_0 (unit)·c_Dinf (µM)	0.00000	0.00799	0.0000	1.000000

Table 32 - Statistical values of the whole model response surface regression analysis

Dependent variables	F-value	p-value	R^2
y	3432.640	< 0.05	0.994
D_H (nm)	636.056	< 0.05	0.967

7.1.4 Graphical representations

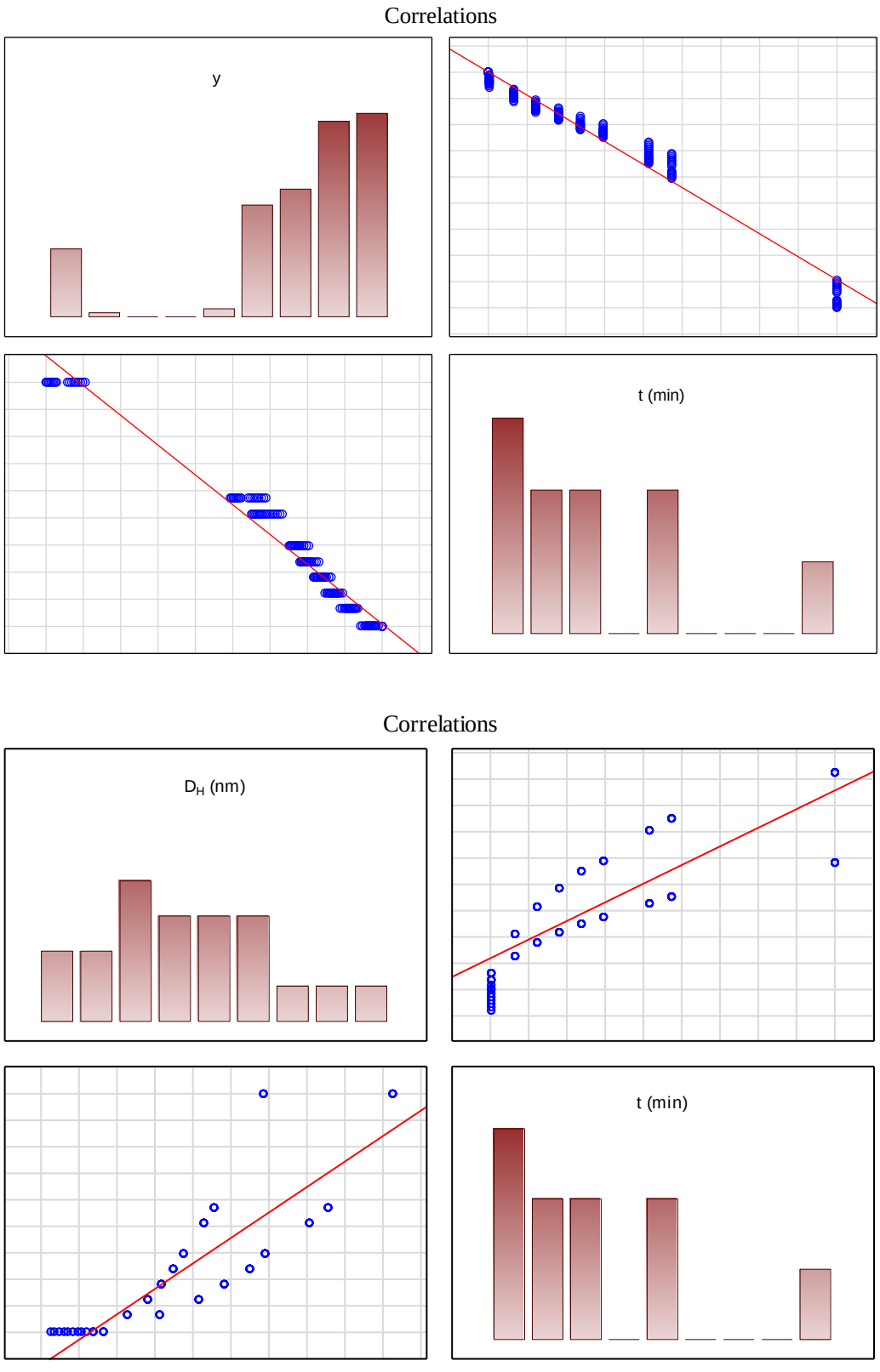

Figure 29 - Matrix plots of correlations between dependent variables y and D_H and independent variable (time, t min)

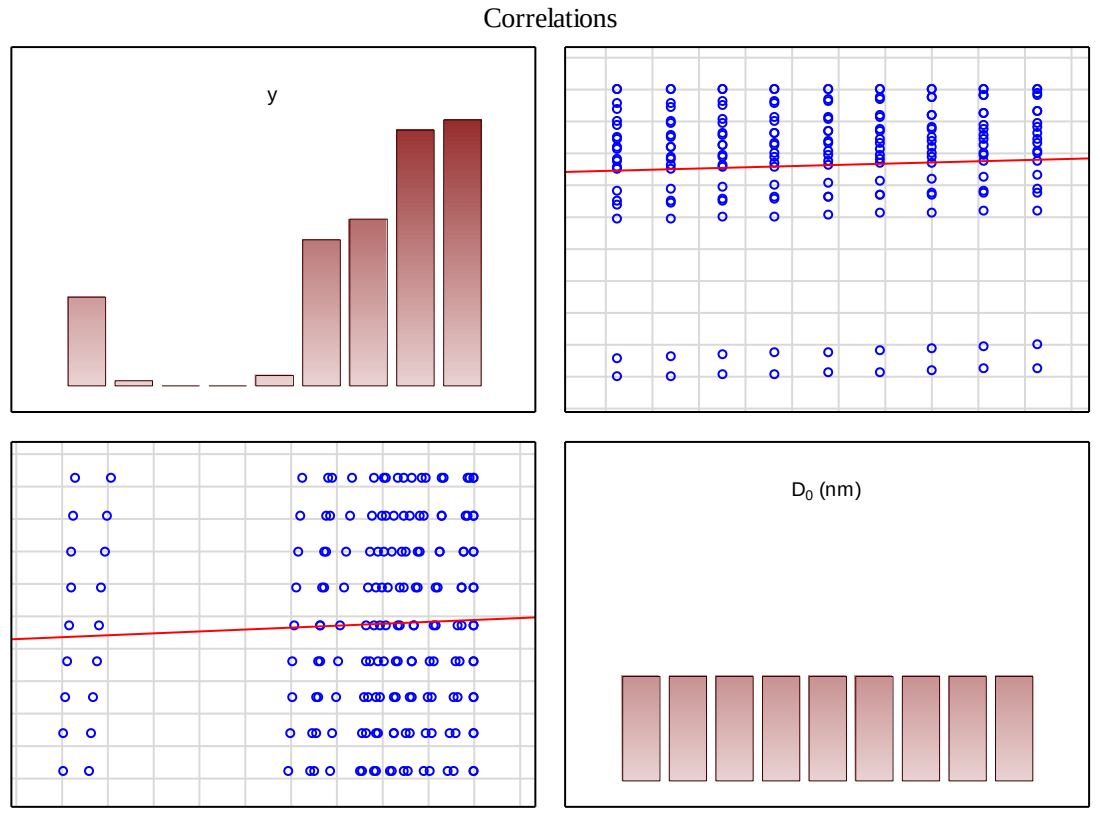

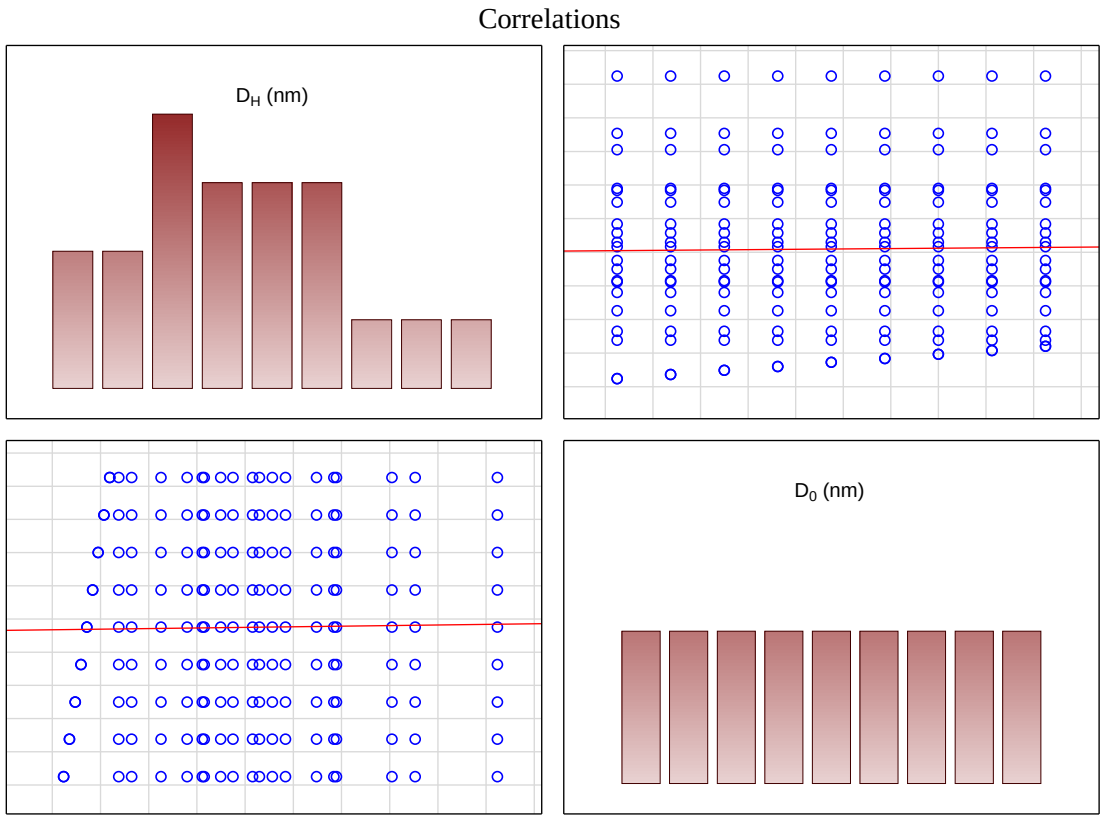

Figure 30 - Matrix plots of correlations between dependent variables y and D_H and independent variable (D_0, nm)

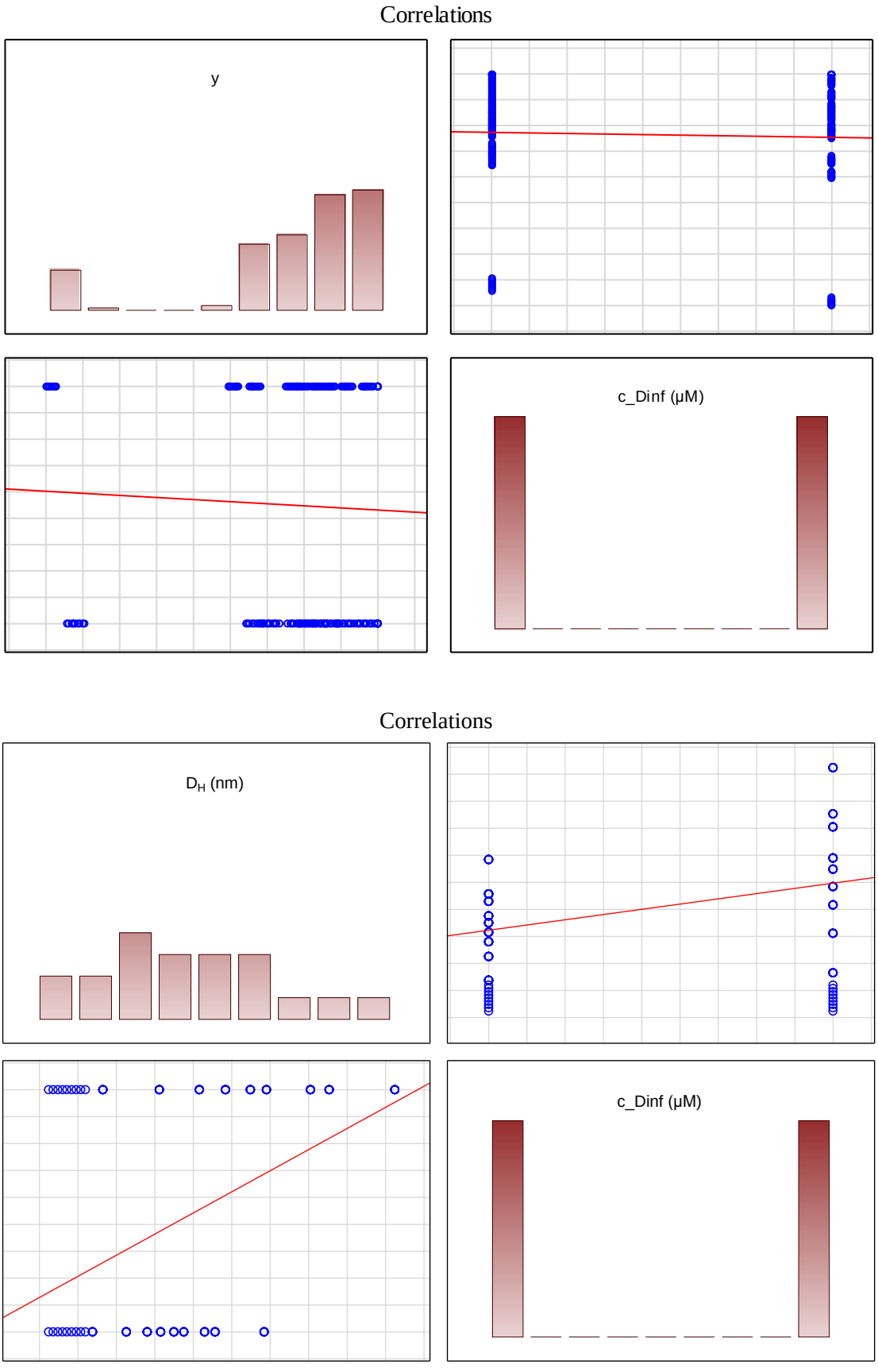

Figure 31 - Matrix plots of correlations between dependent variables y and D_H and independent variable (c_D_{inf} (µM)

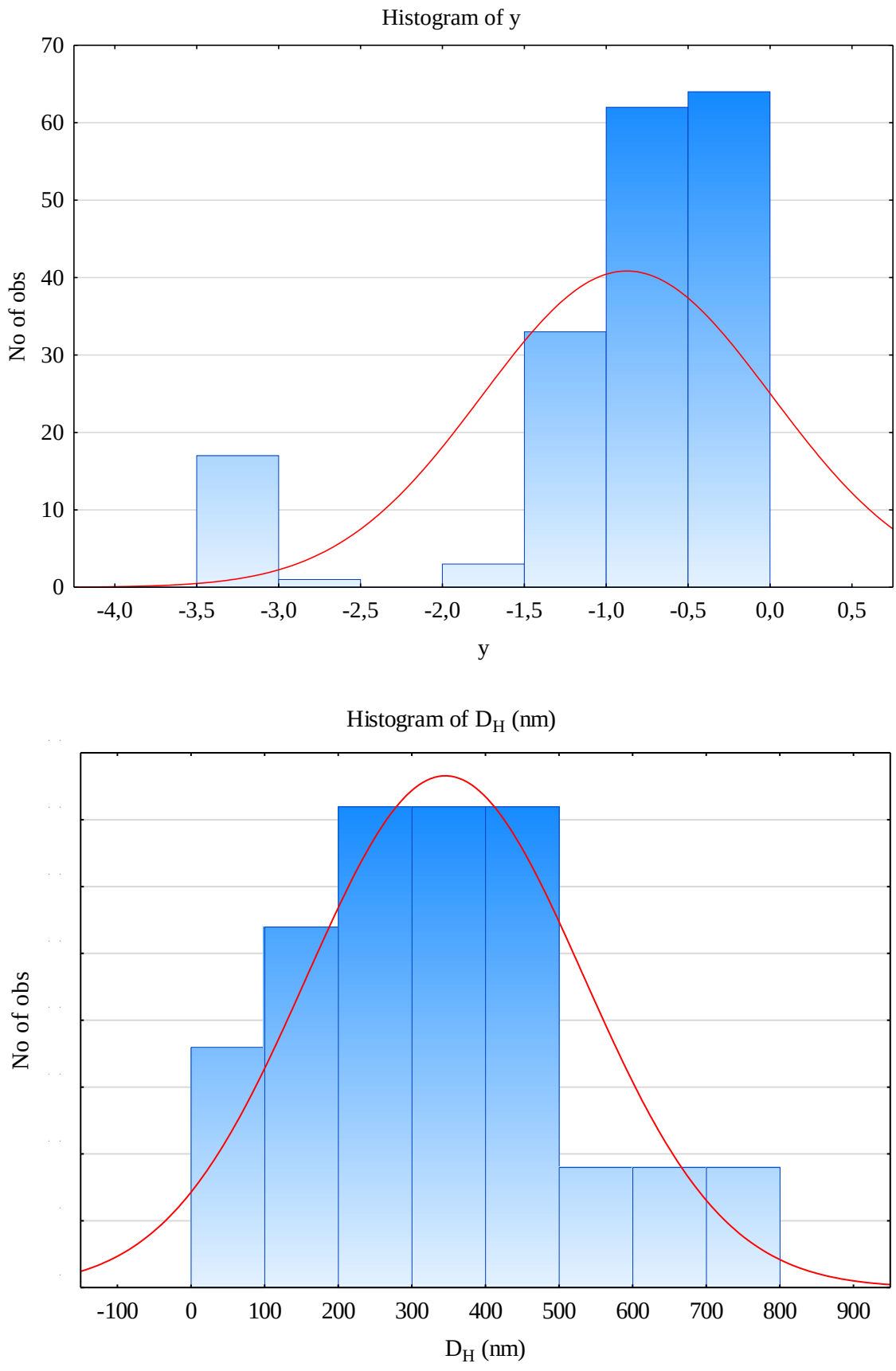

Figure 32 - 2D Histograms of the dependent variables y and D_H

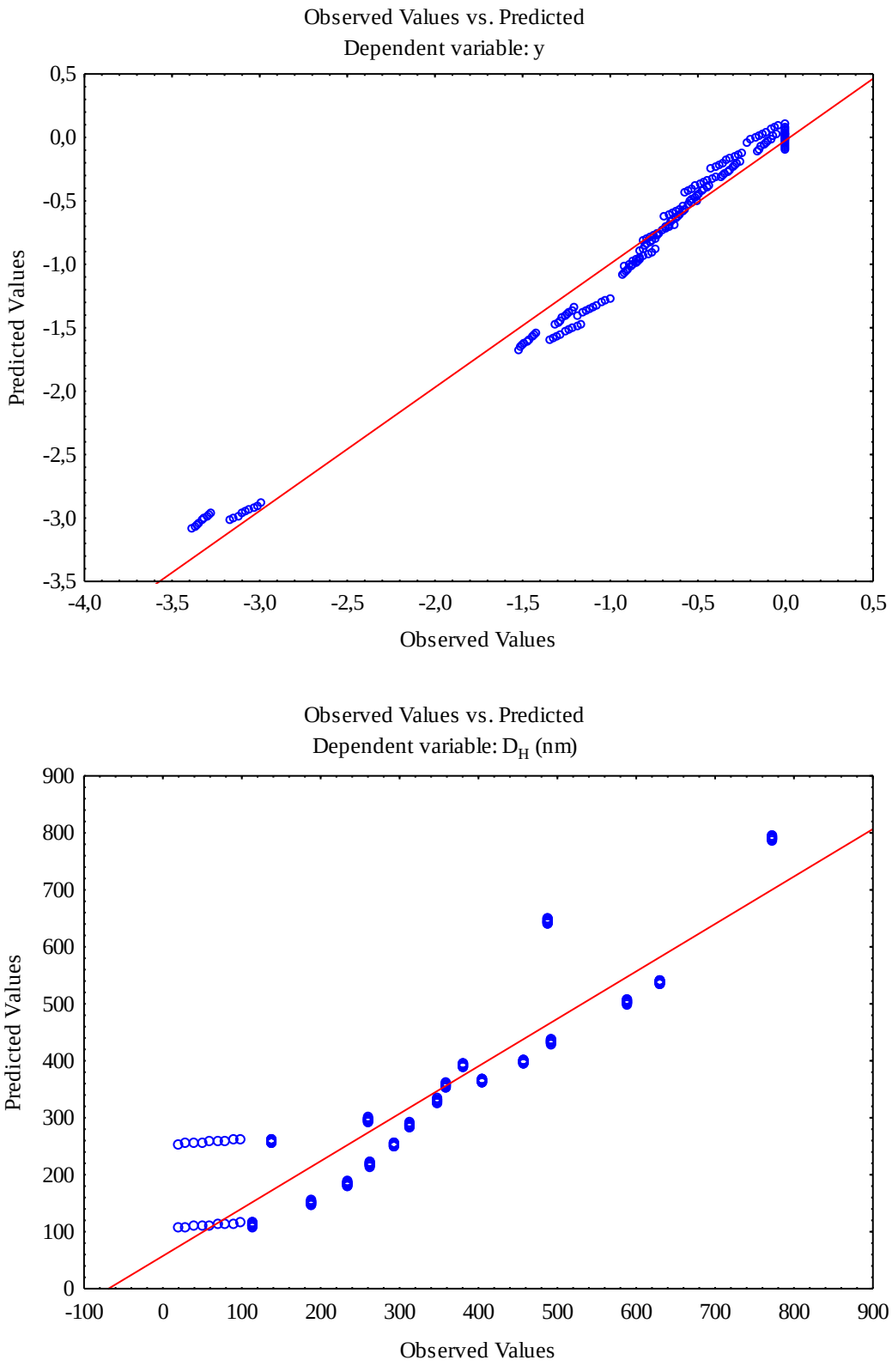

Figure 33 - Relationship between the predicted and observed for y and D_H

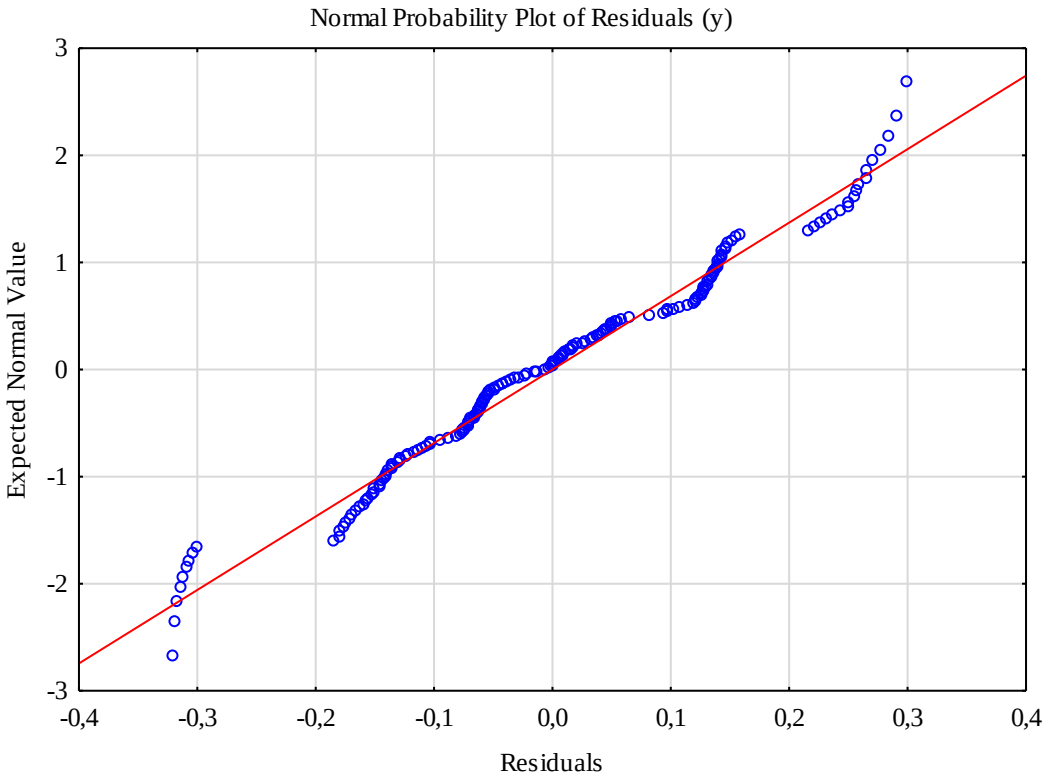

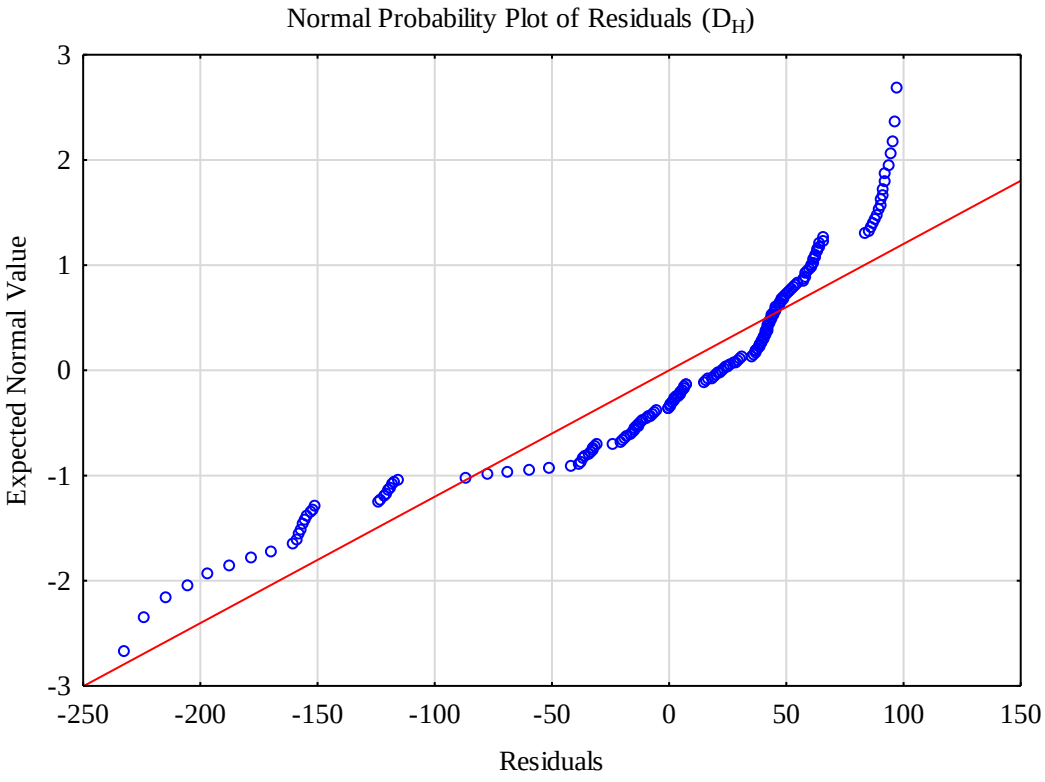

Figure 34 - Normal probability plots of residuals of dependent variables y and D_H

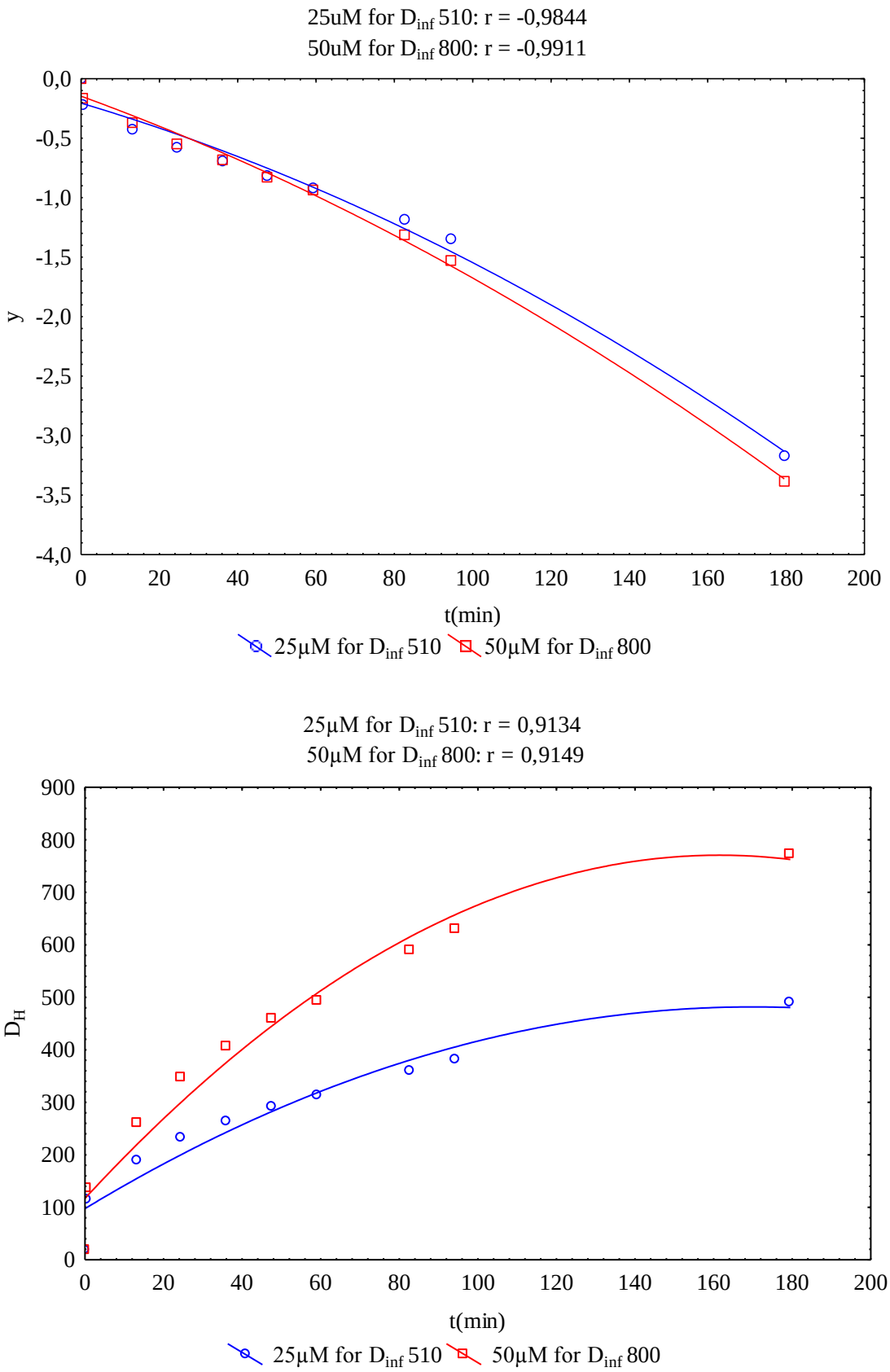

Figure 35 - Polynomial relationships of y and D_H versus t at D_0 20 (nm) in relation to concentrations *c* 25 µm of D_{inf} 510 and *c* 50 µm of D_{inf} 800

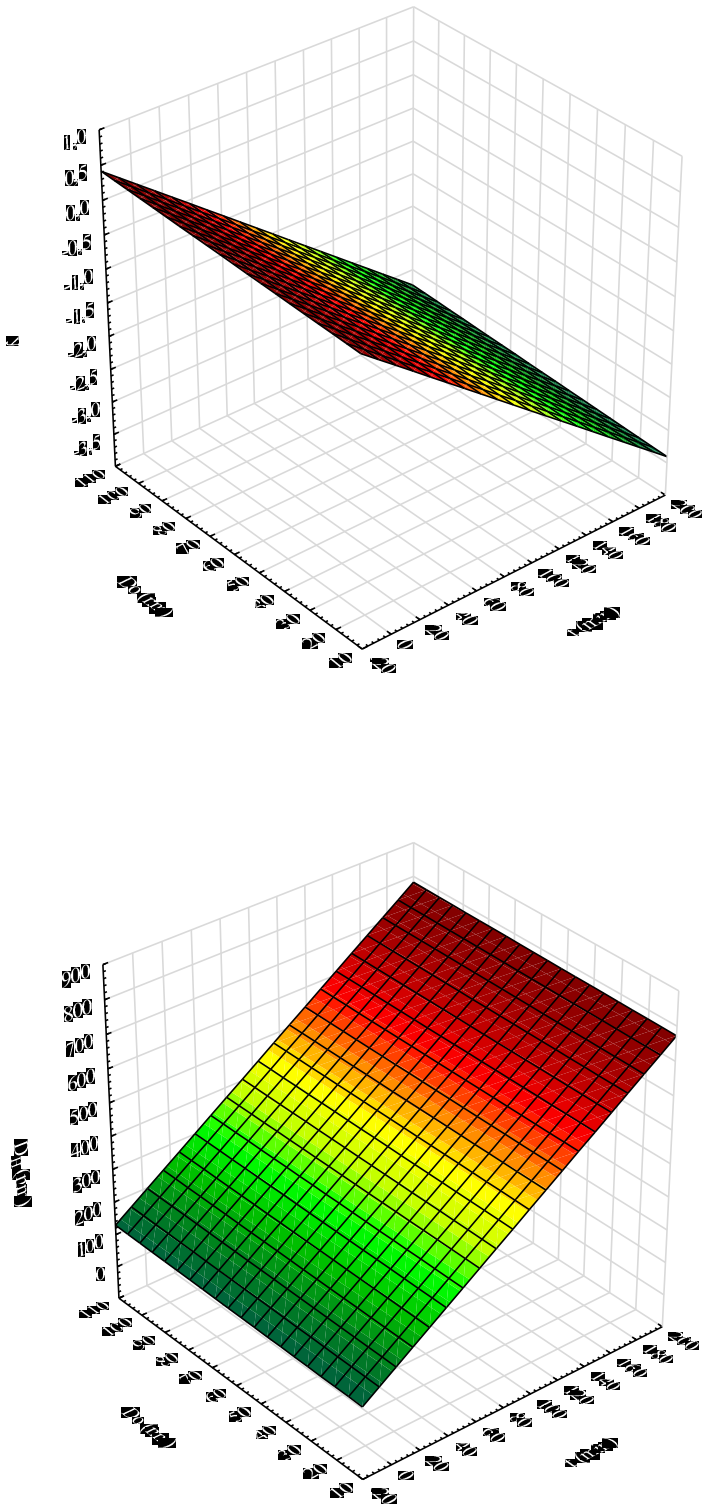

Figure 36 - 3D surface plots of y and D_H versus t (min) and D_0 (nm) using a linear fit method

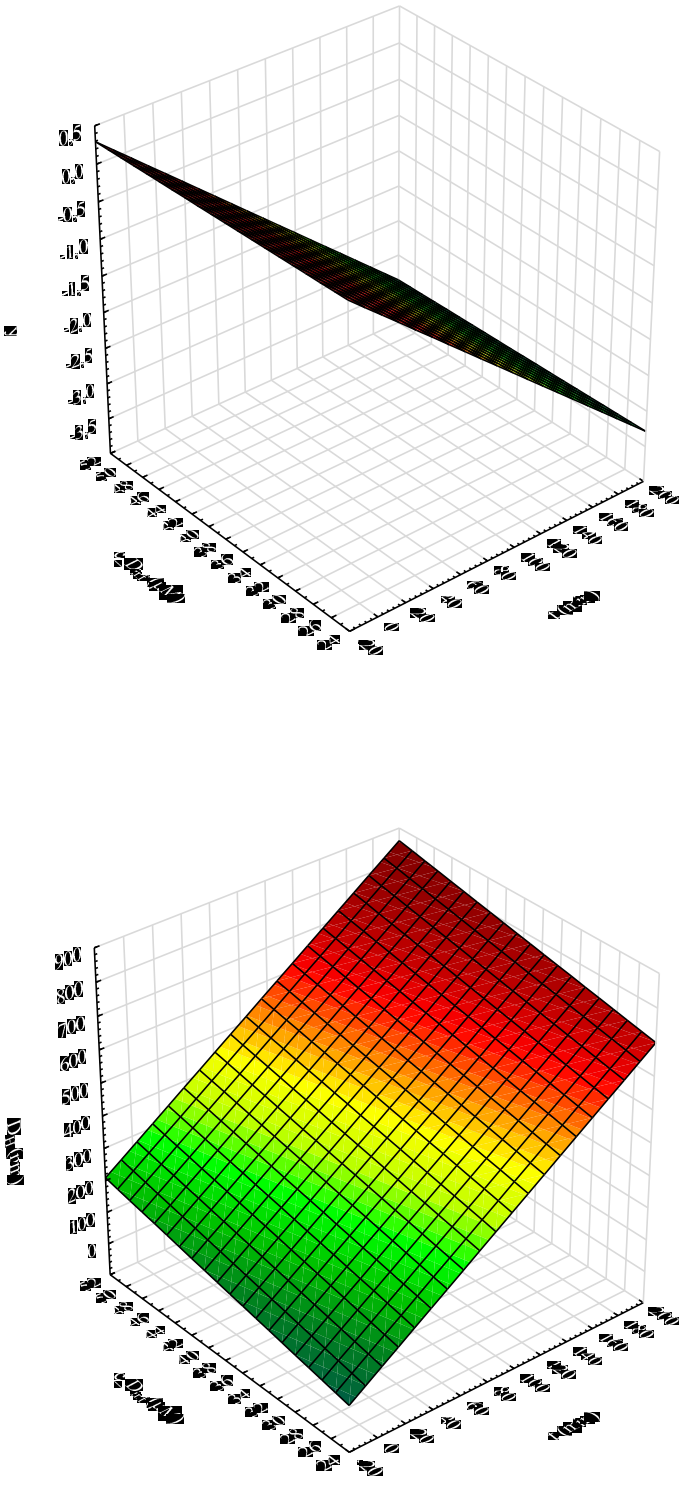

Figure 37 - 3D surface plots of y and D_H versus t (min) and c_D_{inf} (μM) using a linear fit method

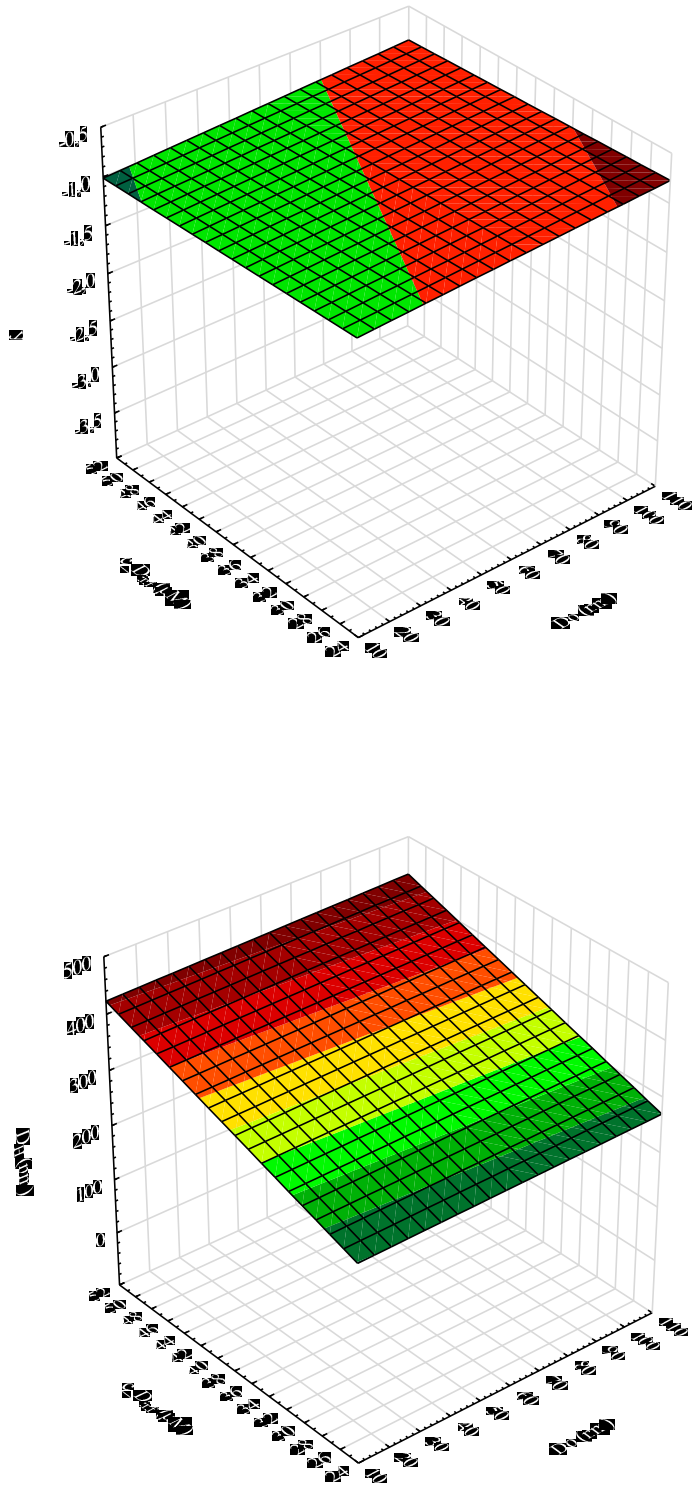

Figure 38 - 3D surface plots of y and D_H versus D_0 (nm) and c_D_{inf} (μM) using a linear fit method

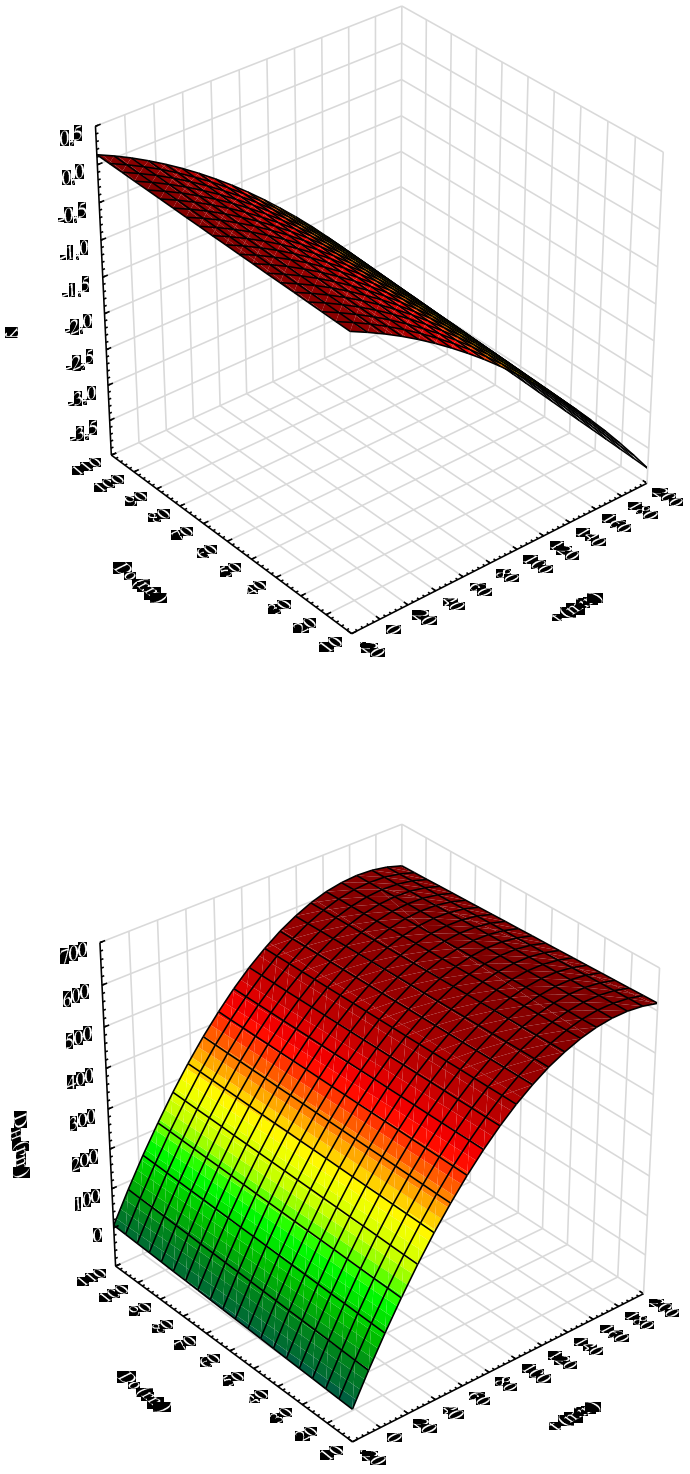

Figure 39 - 3D surface plots of y and D_H versus t (min) and D_0 (nm) using a quadratic fit method

y = Fit not drawn because of invalid range of values

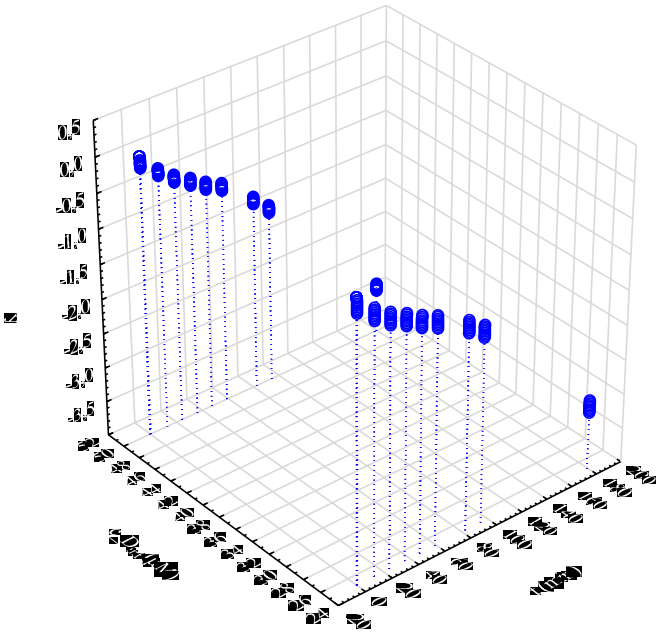

D_H (nm) = Fit not drawn because of invalid range of values

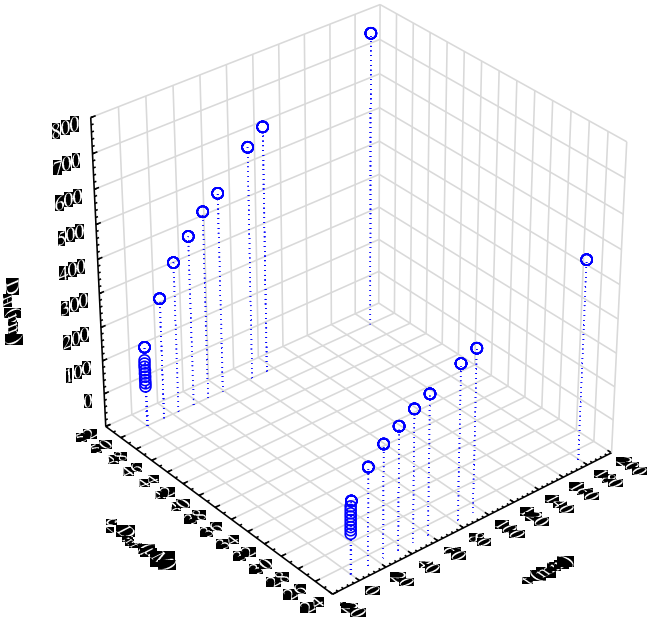

Figure 40 - 3D surface plots of y and D_H versus t (min) and c_D_{inf} (µM) using a quadratic fit method

y = Fit not drawn because of invalid range of values

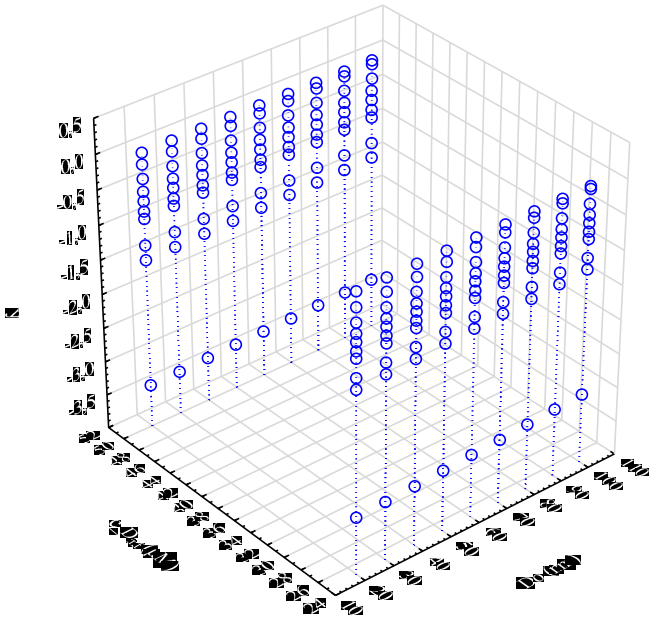

D_H (nm) = Fit not drawn because of invalid range of values

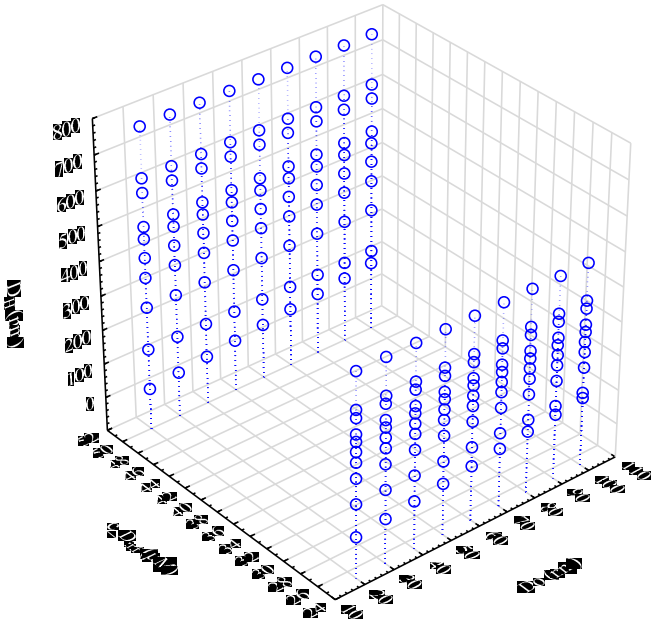

Figure 41 - 3D surface plots of y and D_H versus D_0 (nm) and c_D_{inf} (μM) using a quadratic fit method

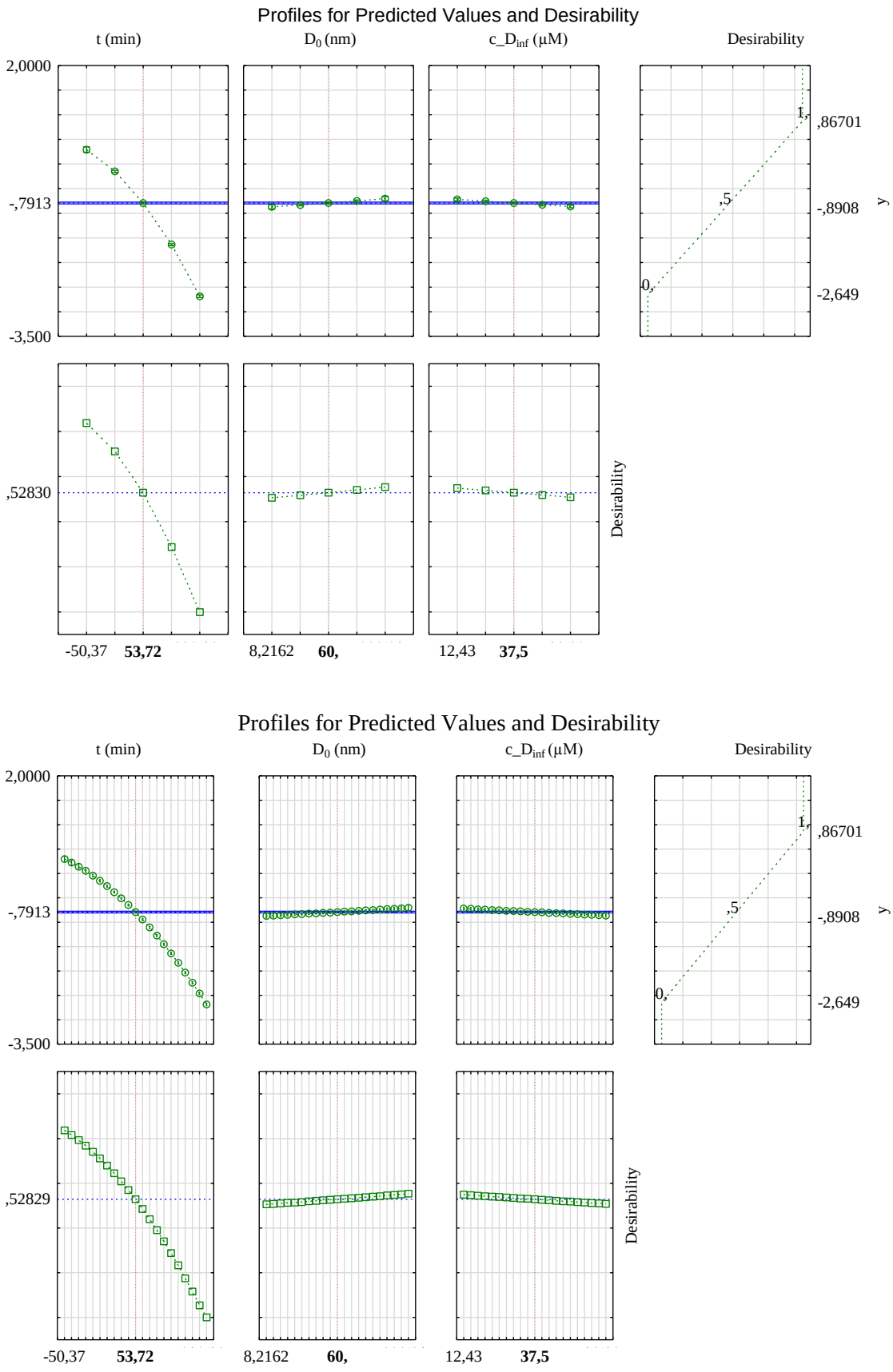

Figure 42 - Profiles for predicted values and desirability (mean) of the dependent variable, y at specific factor grids

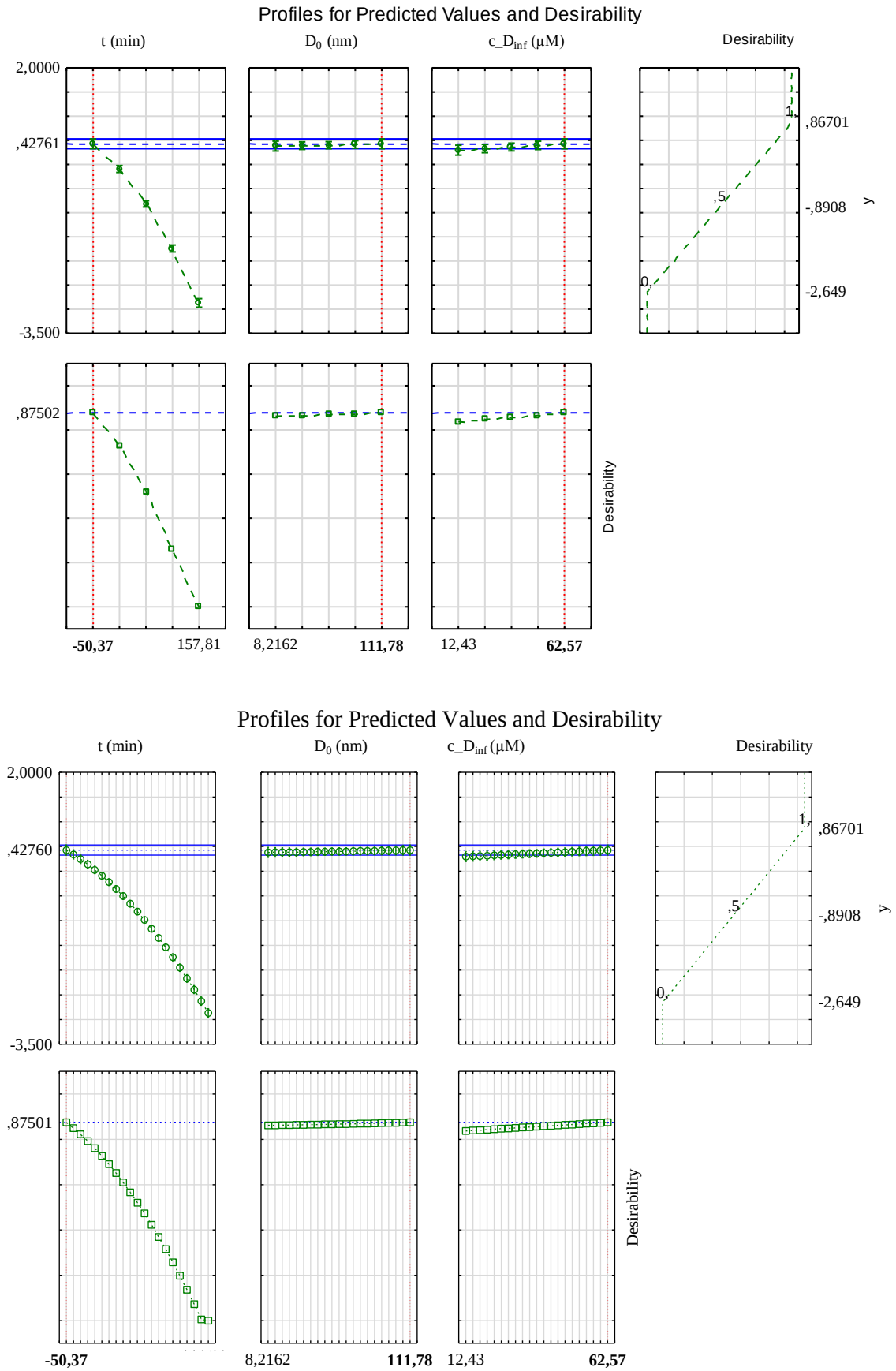

Figure 43 - Profiles for predicted values and desirability (optimum) of the dependent variable, y at specific factor grid

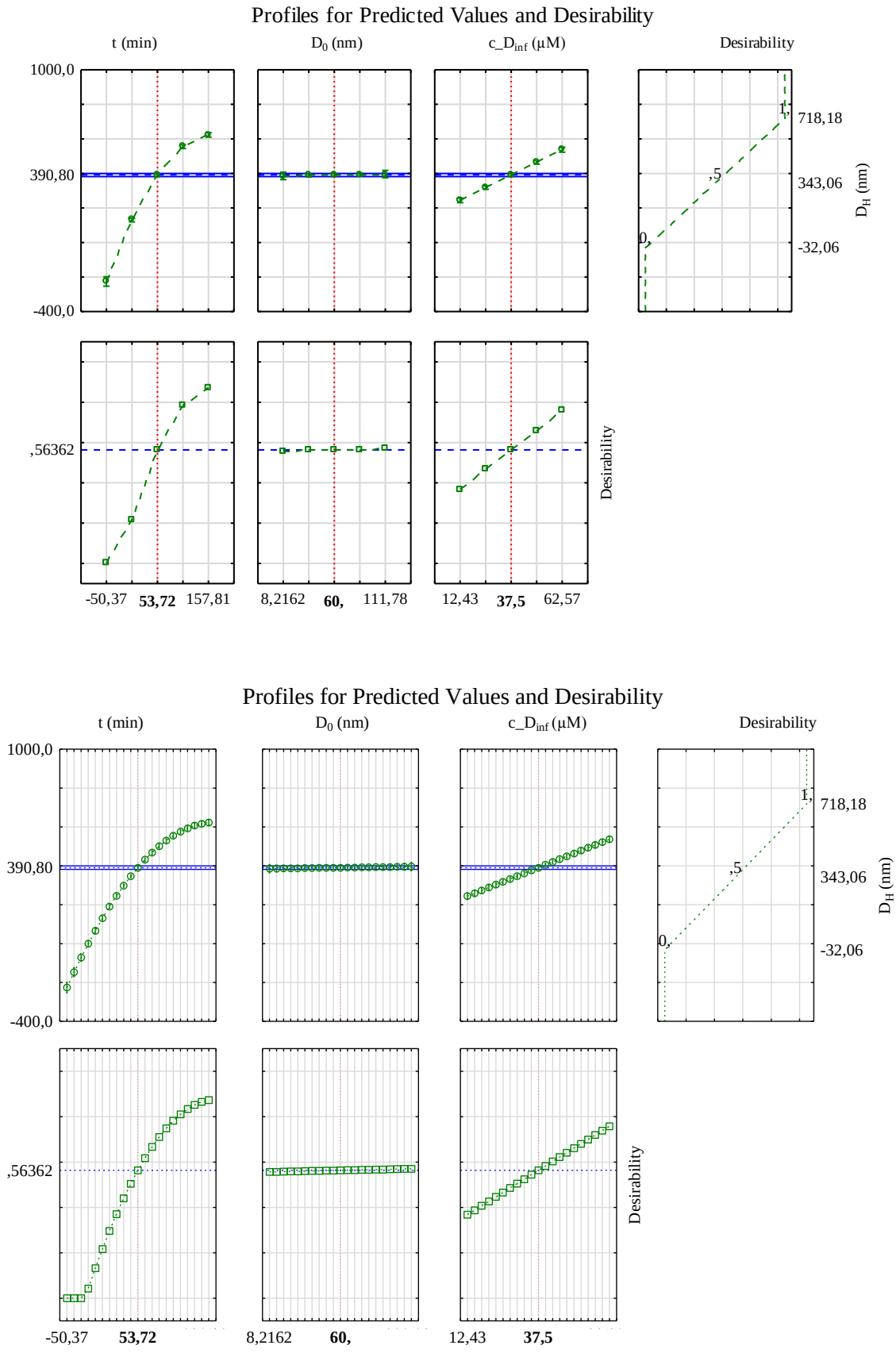

Figure 44 - Profiles for predicted values and desirability (mean) of the dependent variable, D_H (nm) at specific factor grids

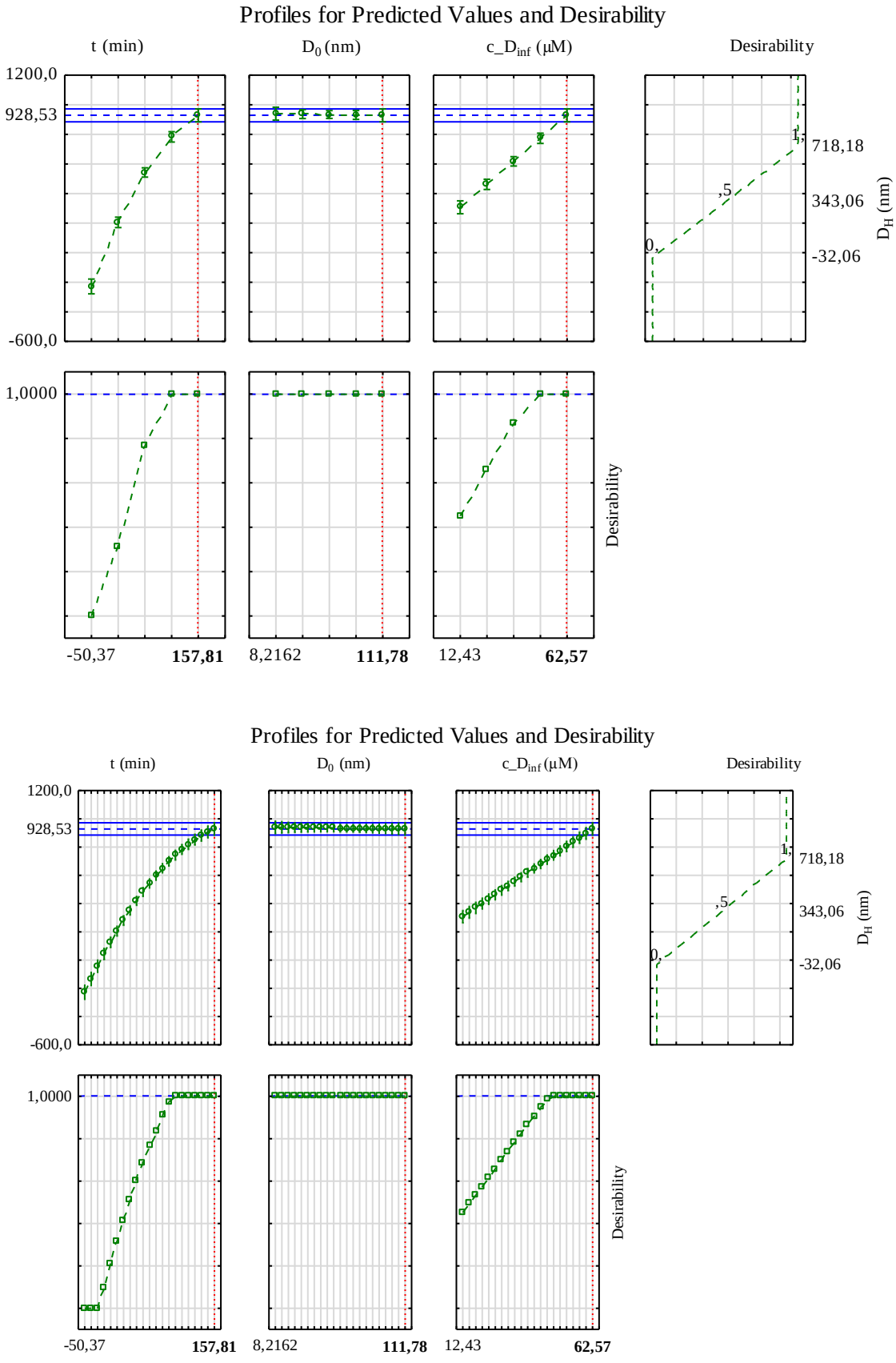

Figure 45 - Profiles for predicted values and desirability (optimum) of the dependent variable, D_H (nm) at specific factor grids

8. PRINTOUT OF PUBLISHED/ACCEPTED PAPERS

(See Literature 20–23 or Publication Activities – Papers, 1–4)